CZECH TECHNICAL UNIVERSITY IN PRAGUE

Faculty of Civil Engineering

Department of Architectural Engineering

INTERACTION OF TEXTILE REINFORCEMENT AND HIGH PERFORMANCE CONCRETE MATRIX

DOCTORAL THESIS

Tomáš Vlach

Doctoral study programme: Civil Engineering

Branch of study: Building Engineering

Doctoral thesis tutor: prof. Ing. Petr Hájek, CSc., FEng.

Prague, 2021

CZECH TECHNICAL UNIVERSITY IN PRAGUE
Faculty of Civil Engineering
Thákurova 7, 166 29 Praha 6

DECLARATION

Ph.D. student's name:
Ing. Tomáš Vlach

Title of the doctoral thesis:
Interaction of Textile Reinforcement and High Performance Concrete Matrix

I hereby declare that this doctoral thesis is my own work and effort written under the guidance of the tutor prof. Ing. Petr Hajek, CSc., FEng.
All sources and other materials used have been quoted in the list of references.

The doctoral thesis was written in connection with research on the project:

- GACR P104 13-12676S - Advanced research of UHPC matrix for ultra thin elements.
- TACR TA03010501 - Optimised subtile concrete skeleton for energy efficient buildings.
- CZ.01.1.02/0.0/0.0/15_019/0004908 - Advanced concrete elements with woven reinforcement.
- CZ.07.1.02/0.0/0.0/16_040/0000364 - Smart solar bench.
- TACR TJ02000119 - Development of concrete lightweight columns with carbon reinforcement as an element for load-bearing structures with loading and fire test.
- SGS14/116/OHK1/2T/11 - Optimization of mix UHPC composition and alternative types of reinforcement.
- SGS16/131/OHK1/2T/11 - Experimental Facade Panels from UHPC as a Base for LED Display.
- SGS18/110/OHK1/2T/11 - Thin Large Format Panels Made of TRC with Profiled Cross-Section for Environmentally Efficient.
- SGS21/095/OHK1/2T/11 - Cantilever Ultrathin Staircase Made of Textile Reinforced Concrete.

In Prague on 12.8.2021 Tomáš Vlach

signature

Acknowledgements

First, I would like to express here my great gratitude to my dissertation thesis supervisor, prof. Ing. Petr Hájek, CSc., Feng. He has been a constant source of encouragement and insight during my research and helped me with problems and professional advancements.

Special thanks also go to doc. Ing. Vladimír Žďára, CSc. and Ing. Magdaléna Novotná, PhD. for enabling work in the laboratory and opening the way to the Department of Architectural Engineering. Special thanks also go to Ing. Pavel Kokeš for the support and testing of materials in the lab.

Further thanks belong to the Department of Architectural Engineering, Faculty of Civil Engineering CTU in Prague and to the University Centre for Energy Efficient Buildings of CTU in Prague for background, willingness, and financial support.

Finally, my greatest thanks go to my family members, for their infinite patience and care.

Abstract in Czech

Tato práce je zaměřena na vzájemné spolupůsobení textilní výztuže impregnované epoxidovou pryskyřicí s matricí z vysoko-hodnotného betonu. Zabývá se možností snadného experimentálního stanovení podmínek spolupůsobení a jeho zlepšení, modelováním chování takto vyztužené konstrukce na základě těchto experimentů pomocí softwaru pro nelineární analýzu betonových konstrukcí ATENA Engineering. Kromě samotné zkoušky spolupůsobení a jejího modelování je v práci uvedeno několik příkladů modelů na zkoušku ohybové pevnosti zkušebních desek z textilního betonu v porovnání s výsledky experimentálních zkoušek. Navazuje na výsledky diplomové práce předložené autorem v roce 2014. Od této doby začal sběr dat o textilních betonech s výztuží sycenou epoxidovou pryskyřicí, měření jejich veškerých materiálových parametrů pro následné numerické modelování a vývoj dalších podkladů pro přesnější a jednoduchý návrh konstrukcí z textilních betonů.

Keywords in Czech

textilní beton, textilní výztuž, technické textilie, vysokohodnotný beton, soudržnost, roving, epoxidová pryskyřice, numerické modelováni

Abstract in English

This work is focused on the interaction of textile reinforcement impregnated with epoxy resin with a matrix of high-performance concrete. It deals with the possibility of easy experimental determination of the interaction conditions of these materials and its improvement, as well as modeling of the behavior of these both materials based on the experiments using software for nonlinear analysis of concrete and reinforced concrete structures ATENA Engineering. In addition to the interaction pull-out test itself and its modeling, the work presents several examples of models for testing of flexural strength of textile reinforced concrete slabs in comparison with the results of experimental tests. It follows the results of the diploma thesis submitted by the author in 2014. Since then, it began the collection of data on textile reinforced concretes with impregnated alkali-resistant glass roving, measurement of all material parameters for subsequent numerical modeling and development of process for more accurate and simple design of textile reinforced concrete structures.

Keywords in English

textile reinforced concrete, textile reinforcement, technical textiles, high-performance concrete, cohesion, roving, epoxy resin, numerical modeling

List of Acronyms

Abbreviation	Expression
CTU	Czech Technical University in Prague
FCE	Faculty of Civil Engineering
FEM	Finite Element Method
FRC	Fiber Reinforced Concrete
FRP	Fiber Reinforced Polymer
HPC	High Performance Concrete
OC	Ordinary Concrete
PP	Poly Propylene
PVA	Poly Vinyl Alcohol
RPC	Reactive Powder Concrete
SR	Steel Reinforcement
TF	Technical Fabrics
TRC	Textile Reinforced Concrete
TR	Textile Reinforcement
TT	Technical textiles
UHPC	Ultra High Performance Concrete

Table of Content

1 Motivation and goals of the thesis

Concrete with traditional steel reinforcement is one of the most used materials in building practice due to its availability and advantageous combination mechanical properties of both materials. The general idea is the high compressive strength of concrete and the high tensile strength of steel, which was patented by Joseph Monier (1823-1906) in 1867. He was the flower-pot manufacturer in Paris. Currently TRC becomes more and more popular in the field of design furniture and in the field of subtle structural elements with reinforcement from different types of technical textiles made of different materials of roving. Architects love these TRC subtle elements and constructions. Research institutes and universities of all over the world are interested about this young material. There are currently many research projects about TRC. [1], [2].

Development of light and very subtle concrete building constructions and elements and demand for extremely thin elements in design are inter alia reason for the development of non-traditional composite materials as reinforcement. Composite materials are used in the form of fiber reinforced polymer bars similar to the traditional steel reinforcement bars or in the form of technical textiles. Unprotected traditional steel reinforcement is not chemically resistant, does not last long in the external environment and cannot withstand the expected lifetime of the structure element. This fact limits the thickness design especially in the combination with high-performance concrete due to standards required concrete cover for passivation of steel reinforcement in a strongly alkaline concrete environment. This fact gave rise to high-performance concrete construction reinforced by technical textiles which is usually called textile reinforced concrete construction. textile reinforced concrete is currently very popular and modern material in architecture and material very often under research. Composite reinforcement from high amounts of filaments homogenized by epoxy resin matrix is free from corrosion. Composite reinforcement combined with fine-grained high-performance concrete enables a significant reduction of thickness of the various elements and thus achieves considerable materials and raw saving. Therefore, textile reinforced concrete material is also interesting in environmental contexts. This material in general is also examined at the Department of Building Structures at the Faculty of Civil Engineering, Czech Technical University in Prague. This thesis is especially focused on the interaction of textile reinforcement in high-performance concrete matrix and its easy determination and improvement for the purpose of design and modeling the behavior using software for non-linear analysis of concrete and reinforced concrete structures ATENA Engineering. This issue is relatively thoroughly dealt in the case of fiber reinforced polymer reinforcement with conventional diameters. Interaction and methods for its improvement are already successfully proposed and measured. There are numbers of articles and standards all over the world. Penetrated technical textiles using epoxy resin for homogenization is basically fiber reinforced polymer with considerably smaller diameter, but standards for elements design and the effect of interaction with the cement matrix have not yet been issued. There is also no standard with defined procedure to measure the interaction conditions. There is no mention about possibility to improve the textile reinforcement and high-performance concrete interaction in the similar way like

for fiber reinforced polymer, about the effect of surface treatment on the reinforcement parameters and the overall textile reinforced concrete element behavior. This thesis follows the results of diploma thesis submitted by the author in 2014. From this time started the interest in textile reinforced concrete elements, measurement of its material parameters for numerical modeling of tasks and development of precise design of textile reinforced concrete elements.

My personal motivation was my interest in concrete and reinforced concrete structures in general. The material of artificial stone is always different, it can be shaped in an original way. I was fascinated by the constants of the subtle stair constructions. I gradually found out more and more information, so I discovered the material of high-quality concrete. During further study, I discovered just the advantage of combining with technical textiles. A non-impregnated fabric is used, which behaves similarly to fiber-reinforced concrete with a high consumption of reinforcing material, which is expensive. With the impregnated homogenized fabric, the expensive reinforcing material can be used effectively. I wanted to learn to master and understand this material in depth so that I would be able to design and implement economical design elements from textile concrete.

The main goal of this work is experimental determination of interaction conditions between the textile reinforcement made of alkali-resistant single glass roving impregnated with epoxy resin and the cementitious matrix made of high-performance concrete. A numerical model of the experiment is created with defined bond parameters from the measured values using the ATENA Engineering program. The experiment is complemented by the possibility of improving of interaction between these both materials. The functionality and accuracy of the model and the effectiveness of improving of interaction conditions are subsequently verified by the testing of flexural strength of textile reinforced concrete specimens. These main goals of the work were supplemented by numbers of other accompanying experiments.

2 Introduction

2.1 Materials of TRC in general

2.1.1 Technical textiles

TT is a summary designation for textile materials and products whose main purpose is the fulfillment of some technical function. Their aesthetic or decorative properties are in this case usually less important. During choosing a suitable material for TT its physical and chemical properties are almost exclusively decisive. In addition to almost all kinds of common made fibers also specially modified fibers are also used for technical purposes such as aramids, carbon fibers, micro and nanofibers, ceramic fibers, metallic fibers, etc. From natural fibers are often used for TT for example jute and cotton (wraps), hemp (ropes) and silk (parachutes).

All high-strength materials with high elasticity modulus are suitable as a concrete reinforcement. Modulus of elasticity of fiber should be higher in comparison with the modulus of elasticity of concrete. These conditions meet and for concrete reinforcement are most often used alkali – resistant glass fibers, basalt, and carbon fibers. Filaments (fibers) and roving (bundles containing several hundred to several thousand fibers) of these materials are processed into the fabric with lattice structure - grids. Grids should be 3-4 times larger than the maximum grain dimension in the cement matrix. The commonly used are fabrics in a perlink form, warp knitted fabric (or spaced) or knitted mats. These textiles are very often for these applications impregnated for load-bearing capacity improving using a suitable polymer. Impregnation (usually up to 20 % by volume) is carried out on finished textiles or sometimes directly during fabrication using machines with appropriate equipment.

2.1.2 High performance concrete

The development of efficient plasticizing and super-plasticizing additives has given rise to new concrete technology and new types of concretes, which have significantly different properties compared to conventional concrete. Previously the workability of the concrete mixture was affected only by the amount of mixing water. Improving workability by increasing the amount of water, it means increasing the water cement ratio, however, results in a significant deterioration of the concrete mechanical and other parameters. The potential of cement grains is not used. The theorem known for more than a hundred years says: The less water, the stronger the concrete.

There occur numbers of positive and negative electrostatic charges on the surface of cement grains during grinding cement in the production process. Of course, these positive and negative electrostatic charges are attracted to each other, and it leads to the formation of clusters. These clusters are called flocs. These flocs can form cavities in which water is unusable for better workability and next additional water has to be added to the mixture. Then there is much more water in the concrete mixture than is needed for the hydration reaction of all cement grains. Cement grains are more distant from each other. Cement crystals do not fit together properly and therefore the strength of the resulting

concrete is reduced. However, it is not only about the strength. The concrete has also lower bulk density and logically higher porosity which leads to a significant reduction in the durability. Resulting concrete is relatively permeable to the water and aggressive agents causing the concrete degradation can easily get into the structure through the water. Thus these additives dispersing individual cement grains allow to the water cement ratio reducing and also allow to approach the minimum amount of water required to the cement grains hydration. They prevent cement grains flocculation in general due to the fact that certain molecules can neutralize the charge on the cement grains surface. In terms of charge, these plasticizers molecules can have negative and positive charge, but they can also be neutral. The gradual development of plasticizers allowed to achieve a significant strength and improve other important concrete properties.

Concretes with very high strength over 150 MPa and extremely low porosity are developed since the 80s of the last century. They are becoming more and more used and popular especially in the last two decades also thanks to the nanotechnologies development. Another less commonly used name for HPC with a similar meaning is the Reactive Powder Concrete (RPC). But for the preparation of HPC with very high strength and other parameters is no longer sufficient use only effective plasticizing or super-plasticizing additives. Also used material typical for HPC are silica flour (finely ground quartz), fly ash and bottom ash, slag, silica fume (microsilica). These are very fine components often able to participate in the concrete reaction with crystals that are smaller than the size of the cement grain. Concrete with very high strength is usually also reinforced by small fibers and microfibers of different materials and it also ranks HPC and UHPC into the category of composite materials [1]–[4].

2.2 Interaction of TR and HPC cementitious matrix

2.2.1 The state of the art

This thesis is focused on the interaction of impregnated textile reinforcement in HPC matrix and its easy determination using originally modified pull-out test. In addition, this experiment was supplemented by the bending test performed on thin slabs to further verify and test the different amounts of reinforcement in cross-sectional area. This issue is relatively thoroughly dealt with in the case of FRP reinforcement with conventional diameters. Testing methods, interaction and methods for its improvement were already successfully proposed and measured. There are numbers of articles and standards all around the world. Impregnated technical textiles using epoxy resin for homogenization are basically also FRP material with considerably smaller diameter, but standards for element design and the effect of interaction with the cement matrix have not yet been issued. There is also no standard with defined procedures to measure the interaction conditions [5].

Some general information about the material parameters are mentioned for example in general publication from RILEM [6] or for example in current study from 2021 [7].

Some articles about the interaction conditions of textile reinforcement were already published. This article is focused only on impregnated technical textiles. Portal [8] states that there is no standard methodology for measurement and evaluation of the TRC pull-out test. The pull-out test was set by the Krüger [9] and Lorenz and Ortlepp [10] asymmetric test. In their experiment samples of 400 x 100 x 15 mm were reinforced using one layer of TT. Various anchoring lengths were selected for the characterization of interaction conditions and also the moment of breaking point of TR in the sample [5], [6].

Banholzer [11] developed a one-sided test that is used for detecting of broken light-fiber filaments. In the form is manufactured the sample with a dimensions 10 x 10 mm and length 30 mm using the epoxy resin with a bundle of fibers in the middle of this prism. So, the fibers inside are sufficiently protected against the steel jaws of testing machine. The sample with epoxy prism is then embedded into the concrete matrix with dimensions 50 x 50 mm and length also 30 mm. Sample of reinforcement is during the testing procedure pulled out of the concrete part using supported steel plate with displacement speed of 0.1 mm/min until the maximum displacement of 1.7 mm [5].

Very interesting testing methodology is also described in [6] with a whole fabrics, not single roving. In this case is also included the effect of PP and PVA fibers that are used during the process of TT weaving for yarn joining. These fibrils connect the whole fabric before the process of impregnation. The principle is analogous to previous described testing methodology with single roving. A portion of TT is inserted into the HPC specimen during the concreting with free fabric length for fixing into the testing machine. Free fabric length fixed into the testing machine is pulled out from the concrete specimen using steel frame as a support for the concrete part [5].

Already it is important, that some studies were carried out on the surface treatment of impregnated textile reinforcement. Very positive is also, that the company Solidian already use the surface modification in product Solidian ANTICRACK from the year 2020. They use similar silica sand (the method) like is presented in this thesis and was measured and published much before. Previously Solidian used only the product GRID with smooth surface, where the interaction conditions were bad and concrete cover had to bee to high. It leads to the higher consumption of materials. Author of these thesis also published some articles about this GRID product [12], [13].

It will probably be other articles and materials that are not listed here in this thesis. The most important sources have been listed in this thesis and other materials will be mentioned later in the text of the thesis.

2.2.2 Standards closely related to the TR and its design in HPC matrix

Unfortunately, the Czech standards in the case of these both new modern materials are not all clear. Standards for exactly determining of interaction conditions of TR and HPC matrix have not been found at the time of thesis processing. Combinations of existing most relevant standards and their parts must be used with respect to the available laboratory test equipment, individual samples and to the possibilities of samples production. Basic Czech commonly used standard CSN 73 1328 "Determination of

adhesion of steel to the concrete" could be used for inspiration during the design of test methodology and samples. But this standard deals with traditional steel reinforcement bars in OC. Since the thesis concerns fragile composite reinforcement it is necessary to protect the end of composite reinforcement for the purpose of the testing procedure. Reinforcement must be gripped to the steel jaws (self-locking mechanism) of the mechanical testing machine without any damaging. Inspiration can be taken even at first glance beyond the field of studies. For example, part of the standard CSN EN 2561 „Aerospace series - Carbon fibre reinforced plastics - Unidirectional laminates - Tensile test parallel to the fibre direction". Another possible inspiration is described in standard CSN EN ISO 9163 "Textile glass - Rovings - Manufacture of test specimens and determination of tensile strength of impregnated rovings" and similarly CSN EN ISO 10618 "Carbon fibre - Determination of tensile properties of resin impregnated yarn".

Foreign standards are more numerous to the solved topic. A very good source and inspiration would be the American standard for testing of FRP reinforcements ACI 440.3R-03 „Guide test methods for fiber reinforced polymers (FRPs) for reinforcing or strengthening concrete structures". This US standard for testing of FRP reinforcements is maybe closest to TR with its content although it is intended for composite FRP bar reinforcements with similar diameters as traditional commercially most often used SR. Very similar thesis issues are also mentioned in ISO 10406-1 „Fibre-reinforced polymer (FRP) reinforcement of concrete – Test methods – Part 1: FRP bars and grids".

However, problem and complication in the experiments design according to the standard remains the same - very small diameters of impregnated single rovings separated from the warp of TT. These small diameters are not directly included and mentioned in standards. However it was developed from 2009 to 2014 currently probably the best integrated approach to the test methods and design of TRC material called TRC RILEM TC 232-TDT [6] where interaction in general is mentioned in its own subchapter. In the publication are clearly explained the basic principles of interaction conditions and difference of TR in comparison with other types of reinforcement as FRP bars and homogenous traditional SR. Besides the problems in the interface between cement matrix and the surface of TR there is next problem of interaction between individual roving filaments in epoxy resin matrix. Most of filaments are activated by transferring of shear forces through the polymer matrix between filaments as mentioned above. The publication also describes these principles and measurement methodology of individual fibrils interaction in polymer matrix as well as the interaction of TR in general with HPC cementitious matrix.

3 Experimental part

3.1 Materials used for experimental part

3.1.1 HPC matrix

HPC mixture has been developed at the Faculty of Civil Engineering Czech Technical University in Prague (FCE CTU) for different applications [14]. Mixture has been designed using especially local sources of raw materials. It is a self-compacting fine-grained concrete containing the following materials: cement CEM I 42.5 R, technical silica sand, silica flour (ground quartz), silica fume (micro-silica) and polycarboxylate super-plasticizer. The mixture of HPC that was used in this experiment was without any types of fibers. This only one mixture with recipe presented in Tab. 1 was used for all specimens due to the possibility of mutual comparison and easy data calibration in numerical model. Water cement ratio was 0.25 and water binder ratio was 0.20 for this developed mixture. All commonly used mechanical experiments were carried out according to Czech standards and results are presented in the next chapter 3.3. The same HPC recipe has been also used for several applications and research activities at the FCE CTU like waffle and solid experimental facade elements [15] or in [16], [17].

Tab. 1: Mix design of HPC [15].

Component	Unit	HPC
Cement I 42.5R	[kg/m^3]	680
Technical silica sand	[kg/m^3]	960
Silica flour	[kg/m^3]	325
Silica fume	[kg/m^3]	175
Superplasticizers	[kg/m^3]	29
Water (12°C)	[kg/m^3]	171
Total	[kg/m^3]	2340

3.1.2 AR Glass roving

Only AR glass fibers were chosen as a roving material type for composite textile reinforcement in polymer matrix due to lower E modulus and more visible interaction conditions and also due to economic aspects. For the TRC application AR glass roving has relatively low price with good mechanical properties in comparison to other fibers such as carbon or aramid [17]. Used roving was from the company Cem-FIL® with a length weight (titer) of 2400 g/km (= 2400 tex), specific gravity of material 2680 kg/m^3, tensile strength 1700 MPa and modulus of elasticity 72 GPa according to the technical data sheet [15].

3.1.3 Epoxy resin for roving impregnation

Larger quantity of epoxy resin of low viscosity, around 65 % in cross sectional area, was due to experimental manual production in the lab and surface modification. As an epoxy

resin was used in all experiments mentioned in thesis SikaFloor 156 from the company Sika® [15]. Basic parameters of pure resin are tensile strength in bending 15 MPa and modulus of elasticity 2.0 GPa. Specific gravity of material is 1100 kg/m^3 according to the technical data sheet.

3.2 Specimen production

3.2.1 Concrete specimens

The first it is important the preparation and mixing of the reference HPC mixture. Dry constituents of HPC were mixed in two parts. The first part was technical silica sand and silica fume and it was mixed for 4 minutes in 1-speed mixing machine Filamos M80 or M180 for larger amount of concrete, compulsory mixer with 47 revolutions per minute to break the lumps in silica fume. For lower amount of HPC was used standard mixing machine for cement mortars. After that, other dry components (cement and silica flour) were added and mixed for 4 minutes. Water and superplasticizer were mixed together just before they were added to the HPC dry mixture. After the concrete mixture became uniform, it was mixed for the next 5 minutes.

All specimens were then casted in molds. Molds for pure HPC specimens were traditional steel molds used for OC or cement mortar with applied demolding oil on the contact surface just before casting. The mixture of reference HPC as mentioned above was self-consolidating, so it was not necessary to use a frequency vibrator or vibrating table. The concrete had to be casted quickly in the mold because the processing time was limited by the effectiveness of super plasticizer. After casting in molds specimens were covered with a thin polyethylene sheet and kept at the laboratory temperature and in the dark for 1 day before taking them out of the molds. After demolding all specimens were kept in a water tank for 27 days to assure constant temperature and humidity conditions during the process of hardening according to the standard. The temperature in the dark room was constant 22.0 °C and the humidity was also constant around 60 % thanks to the air conditioning. Then specimen dimensions and weight were measured and the last steps were mechanical loading test performed after 28 days in the sum and calculations results evaluation.

Fig. 1: More types of specimen just after the concreting and casting, pure HPC prism 40 x 40 x 40 mm, prisms 100 x 100 x 400 mm, cubes 100 x 100 x 100 mm, specimens for pull-out test 100 x 100 x 20 mm and façade TRC elements.

This procedure of concreting was similar for the pure HPC and for the TRC specimens mentioned in next chapter 3.2.3 and several groups of different specimens were prepared. Dimensions of pure HPC specimens were prisms 40 x 40 x 160 mm for the tensile test, cubes with edge length 100 mm for the compression test, prisms 100 x 100 x 400 mm for the determination of static elasticity modulus and dog-bone shape with cross section 30 x 30 mm for the uniaxial tensile test. TRC specimens were small slabs 100 x 100 x 20 mm for the cohesion test and plates 100 x 360 x 18 mm for the four-point bending test as mentioned in chapter 3.3, also some bigger slabs were concretes as mentioned in Fig. 1.

3.2.2 Textile reinforcement

Textile reinforcement was produced by our self from mentioned combination of AR-glass roving and epoxy resin because of required specific grid spacing and possibility to design surface treatment. Larger quantity of epoxy resin of low viscosity 65 % in cross sectional area was due to experimental manual production in the lab and this amount also allows the surface modification in order to improve the interaction conditions.

First specimens for the basic material parameters testing had to be carried out. It means impregnated single roving for the tensile test and similar procedure for the cohesion test. For the single roving tensioning was used a simple steel or wooden frame. The length of roving was about 700 mm. For roving impregnation was successfully used a painting foam roller as presented in Fig. 2. This procedure prevented to the damage and pulling out of individual fibrils and provided sufficient amount of epoxy resin in cross sectional area for individual fibrils interaction. The procedure of impregnation was identical for singe roving and for the TR as a whole.

Fig. 2: View on the process of impregnation of own made textile reinforcement using epoxy resin and painting foam roller.

In order to improve the parameters of composite TR, partial research was also carried out with different types of fillers added to the polymer matrix. These fillers were easily mixed with epoxy resin in different concentrations and roving was impregnated using the same procedure like without fillers. The samples were also cured at room temperature for one day. For this experiment were used two basic types of fillers. The first type were nanoparticles with extremely small particle size and it was achieved great results of composite material parameters. No more information about these fillers is presented in this thesis. Fillers does not affect the interaction of reinforcement and concrete, but it affect the interaction of individual fibrils in the composite reinforcement, which is not directly the subject of this thesis. But results of this experiment are presented completely in [18]. Basic mechanical parameters were demonstrably improved, but nanoparticles and these developed composite materials are very expensive in comparison with the pure epoxy one without filler. It was a reason for other interesting research activities using cheaper fillers with larger particle size like sika "Stellmittel T" or silica flour [19]. Microscopic view on the fillers in epoxy matrix between single filaments is presented in Fig. 3. Some of silica flour parts have similar diameter in comparison with diameter of AR glass filament. Results of the tensile tests of single roving with short description is presented in chapter 3.2.2. Medium grain size of silica flour was 0.06 mm.

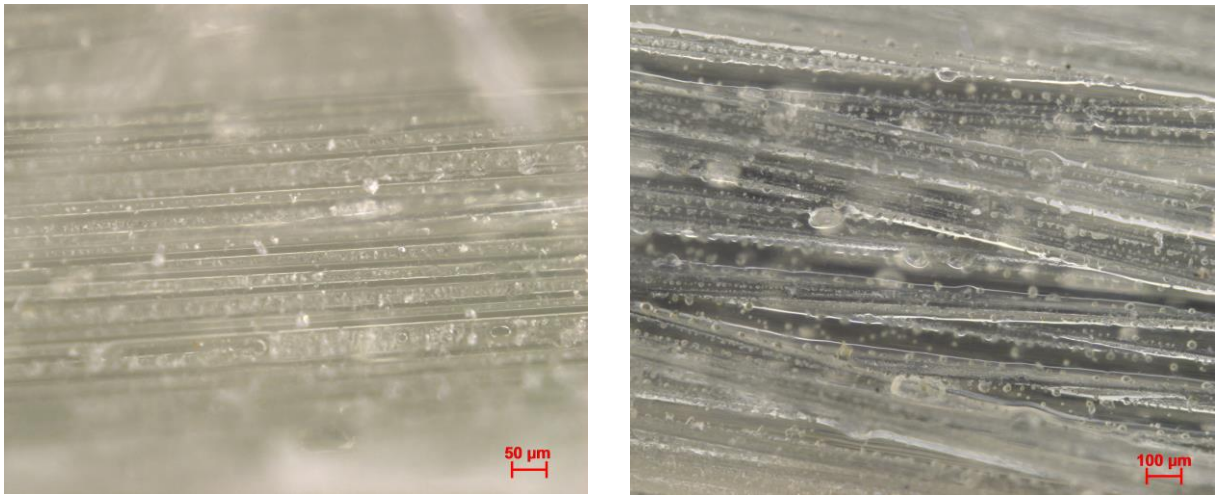

Fig. 3: Detailed microscopic views on the filaments with fillers in epoxy impregnation, magnification 200 times, Sika filler (left), and quartz powder filler (right) [19].

The surface modification had to be processed just after the process of impregnation before hardening of epoxy resin. The same components were used for the surface treatments like for the HPC mixture. It means silica flour and technical silica sands with different grain size, which were easily available. Material was loosely sprinkled on the surface of the impregnated roving without any external force. Unused material could be reused again without any rest. The procedure of surface treatment was also identical for singe roving and for the TR as a whole. Detailed view on impregnated single roving is presented in Fig. 4. Specimens are without surface modification on the left side and with surface modification on the right side using fine grain silica sand with maximum.

Fig. 4: Detailed view on impregnated single rovings without surface modification (left) and with surface modification using fine grain silica sand (right).

The process of hardening lasted minimally for one day based in the room temperature. Next day impregnated single roving reinforcements could be removed from the steel or wooden frame for the next steps and it was application of sleeves. Sleeves were necessary for the fixing of specimens into the testing machine using its steel jaws. Composite impregnated single roving is very brittle for the direct installation. Sleeve was applied only on the one end of composite reinforcement in the case of cohesion test and on both ends of specimens in the case of tensile test.

One or both ends of specimens were fitted into sleeves using the same epoxy resin like for impregnation. Two types of sleeves were done during research. First type was steel sleeve according to ACI 440.3R-03 standard with modified dimensions for single impregnated roving. The length of the specimen between steel sleeves in the case of tensile test specimens was 300 mm and the length of each steel sleeve with diameter 20 mm was 150 mm. Specimen preparation was very demanding and fragile during preparation and installation and specimens were very susceptible to damage because of the large weight of steel sleeves in comparison with rigidity of impregnated single roving. It was the reason that the test procedure modification was found. Another method for specimen preparation [20] has been originally developed for the tensile testing of single roving without polymer matrix, but these method was also used also for presented impregnated single roving. Both ends of specimens were fixed to the small epoxy prims 8 x 8 x 80 mm without steel sleeves. For the epoxy prisms casting was used prepared silicon mold. The distance between prisms was the same 300 mm like for steel sleeves [21].

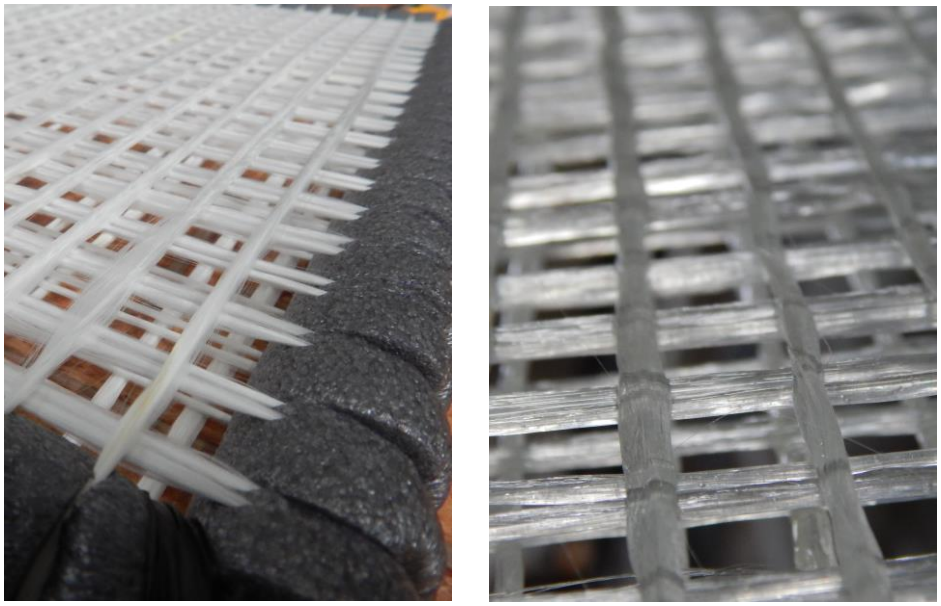

Fig. 5: Detailed view on installed rovings for TR before impregnation process (left) and detailed view on impregnated part of own made grid (right).

TRC plates were designed with specific dimensions 100 x 360 x 18 mm for the four-point bending test and it was also the reason for own made TR grids with own developed impregnation and surface modification with individual grid spacing. Grids were prepared

without polyester or any other binding, fabric retained shape only thanks to the impregnation. Rovings were first wrapped up the prepared steel frame in the transverse direction, then all also all in the longitudinal direction without any interlacing, perlink binding, warping and etc. During one wrapping procedure two layers of TR were produced. Impregnation and surface modification process were done by the same procedure as for single roving. View on the own made TR is presented in Fig. 5. The day after impregnation procedure was TR divided and cut to the desired dimensions and it was the final step in own made TR preparation for the concreting.

3.2.3 Textile reinforced concrete

Concreting was done for two types of material testing performed for the purpose of this thesis. First experiment for determination of basic material parameters was a pull-out test with impregnated single roving with and without surface treatment in two modifications. Second test was a four-point bending test performed especially for the validation of all material parameters of previous testing.

HPC mixture content and mixing process has been described in previous chapter as well as hand-made production of individual TR. As a material for presented thesis was used only AR-glass roving. Mold for all TRC specimens were prepared individual using system of laminated chipboards. One mold for TRC plates for four-point bending test was made for three identical plates and one mold for pull out test was prepared for five identical specimens. Panels joining were ensured by steel self-tapping screws.

Pull out test was performed in two modifications. The first was inspired by [10] with an unsymmetrical anchoring length. This pull-out test method was performed for the comparison of developed own testing methodology. On one side of the specimen a penetrated roving pull-out was secured using the short length 20 mm. On the opposite side penetrated roving was anchored along the remaining length of the HPC specimen. The HPC plate with dimensions of 60 x 278 mm has a thickness of only 6 mm. The only one penetrated roving using epoxy resin with or without surface modification was embedded in HPC specimen matrix in its axis. Five pieces were created for each set of specimens.

The second type of pull-out test was originally inspired by American standard for testing of FRP reinforcements ACI 440.3R-03 "Guide test methods for fiber reinforced polymers (FRPs) for reinforcing or strengthening concrete structures" with modified specimen dimensions. The same single penetrated roving as in previous pull-out method has been fixed in the middle of mold before the concreting of HPC part. Sleeve was installed only on one side of single roving because of fixing to the testing machine. Concrete part has a constant dimensions 100 x 100 mm and variable thickness according to the single roving diameter. First experiments were performed with the thickness closed to the standard with respect to ratios with other two dimensions, so the first thickness was 100 mm [22]. Especially in the case single penetrated roving with the surface treatment the single composite roving was usually broken before the start of slipping along the from the cementitious matrix. It leads to the thickness optimization using software ATENA Engineering. Resulted optimal thickness of specimens for used AR-glass roving 2400 tex

was calculated to 20 mm, where was calculated pulling out with perfect bonding conditions and reached tensile stress of reinforcement approximately 80 % of tensile strength.

A small cone made from silicone was installed on the side of mold with steel sleeve against the pulling of a shear cone from HPC part. This HPS shear cone would negatively affect results. Mold was not provided with a demolding oil to prevent the contamination of the surface of single composite reinforcement. Laminated chipboards are very smooth and thanks to that demolding process of specimens was without any problem. The developed epoxy sleeve replaced by the steel one made the preparation process of specimen much easier.

Process of panel's preparation for the four-point bending test procedure was quite simple in comparison with specimens for pull out test. TR was cut to the specimen dimensions 100 x 360 mm. It means a few millimeters smaller on each side for easier installation inside the wooden mold from chipboards. During the concreting process were used no spacers. Casting process was done layer after layer. It means the layer of HPC, then the TR was inserted, then the middle part of HPC, next TR and the upper part of HPC. In the case of 4 TR layers designed for one plate, all TR layers were inserted in same time. The concrete cover has been designed only 4 millimeters and it has been secured with the controlled thickness of HPC layers. Specimen was not vibrated to prevent the flooding of TR on the HPC surface. Fortunately vibrating was not required for no described specimen thanks to the used self-consolidating HPC mixture.

After the casting process in molds specimens were treated in the same way as described in 3.2.1. One day after the concreting and demolding all specimens were kept in a water tank for next 27 days with the constant temperature in the dark room 22.0 °C and also the constant humidity around 60 % thanks to the air conditioning. Only specimens made for the pull-out test with sleeves were not inserted into the water because of their fragility but they were kept in the same air-conditioned room, like other groups. Specimens for the pull out test according were modified [10] The anchoring length approximately 20 mm was secured using transverse very short saw-cut through the penetrated roving just below the steel part for the installation into the test machine and controlled crack at the required distance from the upper saw-cut. Double-side saw-cut was used for the predetermined breaking point – controlled crack and this point was also the border of unsymmetrical anchoring length. The length approximately 230 mm in the bottom part was certainly sufficient for the anchoring securing. Then all necessary TRC specimen dimensions and weight were measured before the testing procedure after 28 days in the sum.

3.3 Experiments

Several experiments were done during the research in order to obtain basic material parameters of pure materials and also TRC composites. Chapters are divided to the experiments with HPC without any reinforcement, measurement of TR and finally

experiments with combination of both materials TR and HPC. Subchapters are further broken down into individual experiments.

3.3.1 Mechanical parameters of pure HPC

3.3.1.1 Compression test

Testing procedure respected the CSN EN 12390-3 standard using the INOVA DSM 2500 electrohydraulic testing machine. Uniaxial compression test was performed on the cubes with an edge length of 100 mm due to high strength of HPC and maximal loading force 2500 kN of using machine. These samples were loaded with the constant speed of 0.2 mm/min. Typical curve from the testing procedure is presented in Fig. 6. Average experimental compressive strength of used HPC was 144.5 MPa. General view on damaged concrete specimen is presented in Fig. 7.

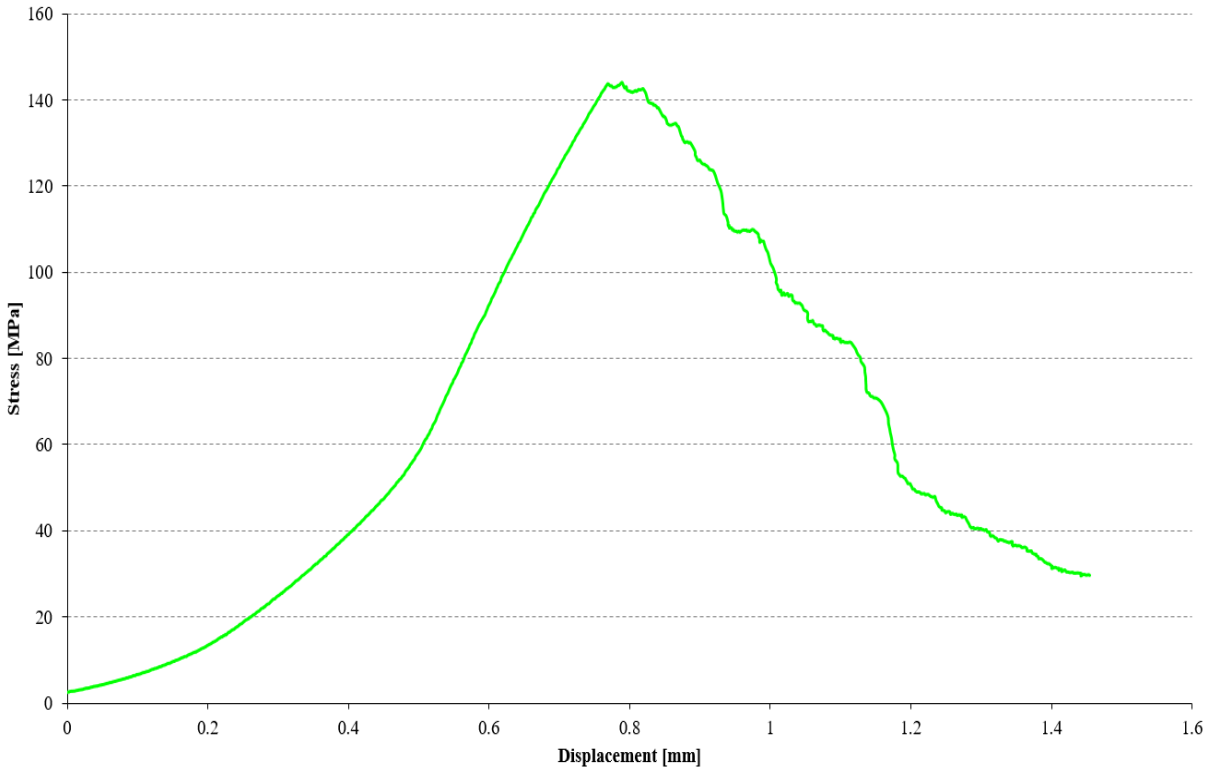

Fig. 6: Typical experimental curve from the testing procedure for compression test.

Fig. 7: Concrete cube with edge length 100 mm after the testing procedure.

3.3.1.2 Three-point bending test

MTS 100 testing machine with maximal load force 100 kN and Dewetron 500 data acquisition system was used for the bending test. The three-point bending test procedure was in respect with CSN EN 1015-11 standard. Groups of minimally three specimens were produced for this standard test with cross sectional dimensions of 40 x 40 mm and a length of 160 mm. The distance between supports was 100 mm and the loading support was placed in the middle of these bottom supports. View on the specimen just before testing placed in steel mechanism is presented in Fig. 8. Average experimental flexural strength of used HPC was 10.4 MPa.

Fig. 8: Concrete prism with dimensions 40 x 40 x 160 mm just before testing procedure.

3.3.1.3 Direct tensile test

Tensile strength of used HPC was performed using again MTS 100 testing machine with maximal load force 100 kN and Dewetron 500 data acquisition system. Testing procedure was performed in laboratories of Experimental Center CTU in Prague. Tensile strength testing procedure respected the CSN 73 1318 standard. Eight specimens in the sum were produced for this testing because of the difficulty of the test and only two specimens were damaged correctly in the middle part of dog-bone. The dog-bone shaped specimens, installed specimen in testing machine and specimen's dimensions are presented in Fig. 10. Expanded parts of the specimens were mechanically fixed in the steel jaws using screws and nuts without any use of epoxy resin. Linear strain was measured by a pair of strain gauges. The loading speed of the specimens was 0.2 mm/min - constant throughout the experiment until failure. For the strain calculations has been used average output from both strain gauges. Average experimental direct tensile strength of used HPC was 6.78 MPa. This strength was similar for all tested specimens correctly and also incorrectly damaged in the expanded concrete part.

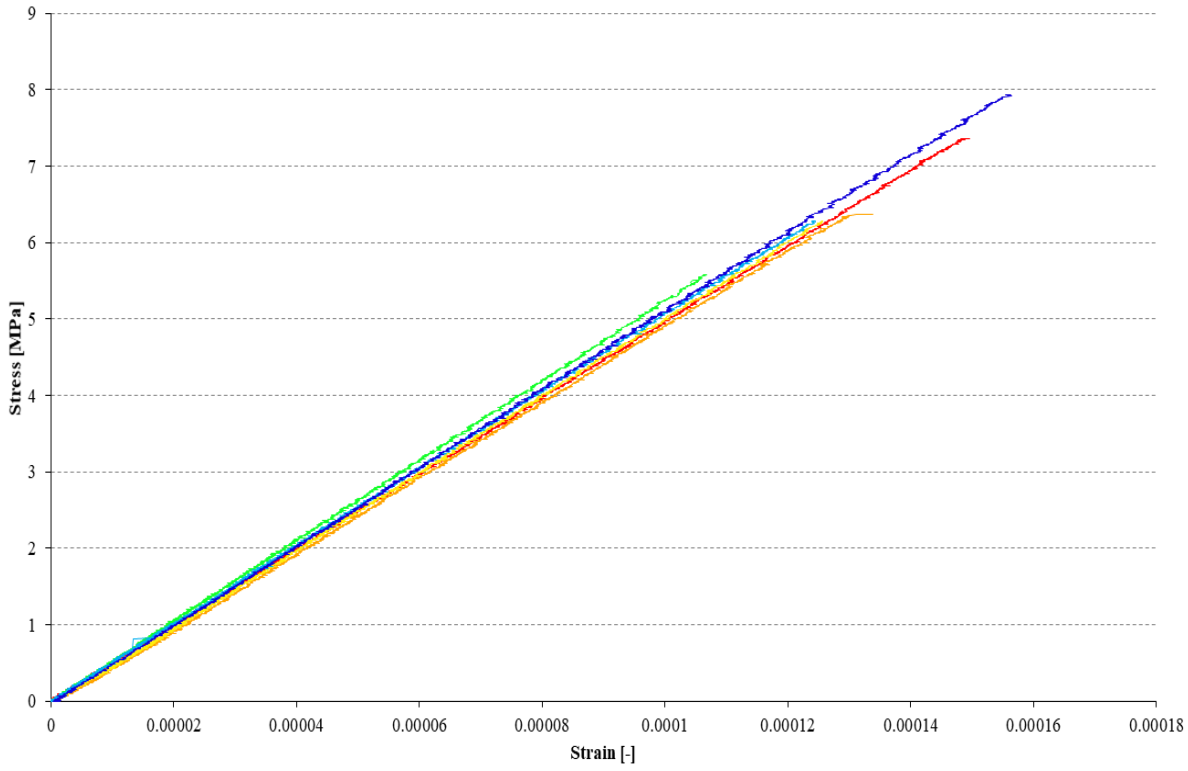

Fig. 9: Typical linear average curve from the testing procedure for tensile using calculated average output from both strain gauges.

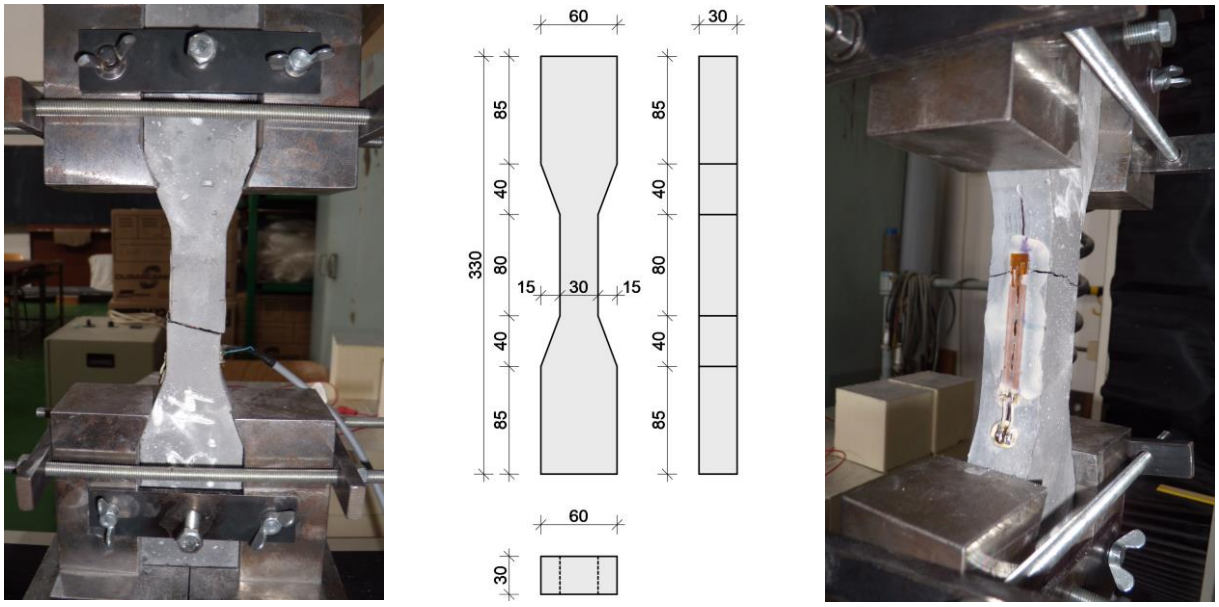

Fig. 10: Concrete specimen after the testing procedure with correct damage, dog bone specimen dimensions and view one the strain gauge.

3.3.1.4 Young's modulus

Testing procedure respected the CSN ISO 6784 standard. This test was performed using the EU 40 test machine with HBM D1 sensors. Specimens used for this experiment were prisms with dimensions 100 x 100 x 400 mm. Average static modulus of elasticity in compression of used HPC was 49.5 GPa measured on three concrete specimens.

Dynamic modulus of elasticity for comparison was performed according to the CSN 73 1371 standard as a second nondestructive test method [23], [24]. Specimen dimensions were the same 100 x 100 x 400 mm. Average dynamic modulus of elasticity of used same HPC was 49.6 GPa. It means almost the same value in the comparison with static modulus of elasticity. Table of results is presented in Tab. 2. Time of etalon and measured time of etalon was 32.4 μs, Nominal frequency of probe was 15 kHz, wavelength was calculated 32.2 mm and coefficient of dimensionality was considered 1.054. All specimens were tested in the age 28 days.

Tab. 2: Calculation of dynamic modulus of elasticity.

Spec	m	d_1	d_2	l	V	ρ	length	t_L	E	Ø E
	[kg]	[mm]	[mm]	[mm]	[m^3]	[kg×m^3]	[mm]	[μs]	[MPa]	[GPa]
1	9,207	100,0	98,1	400,0	0,003926	2345	100,0	20,7	49297	50,0
							100,0	20,4	50758	
							100,0	20,4	50758	
							100,0	20,5	50264	
							400,0	83,1	48913	
2	9,225	100,5	100,4	400,0	0,004034	2287	100,5	20,4	49926	49,2

							100,5	20,4	49926	
							100,5	20,4	49926	
							100,5	20,5	49440	
							400,00	83,9	46791	
3	9,383	100,3	101,0	400,0	0,004054	2315	100,34	20,7	48954	49,6
							100,34	20,3	50902	
							100,34	20,4	50404	
							100,34	20,5	49913	
							400,00	83,4	47928	
Ø	9,272	100,3	99,8	400,0	0,004004	2316	-	-	49607	49,6

View on the specimen is presented in Fig. 11 during both testing procedures. Testing set up of statis modulus of elasticity is presented in the left side and dynamic modulus of elasticity is presented on the right side with visible measuring points thanks to the trace after the application of gel.

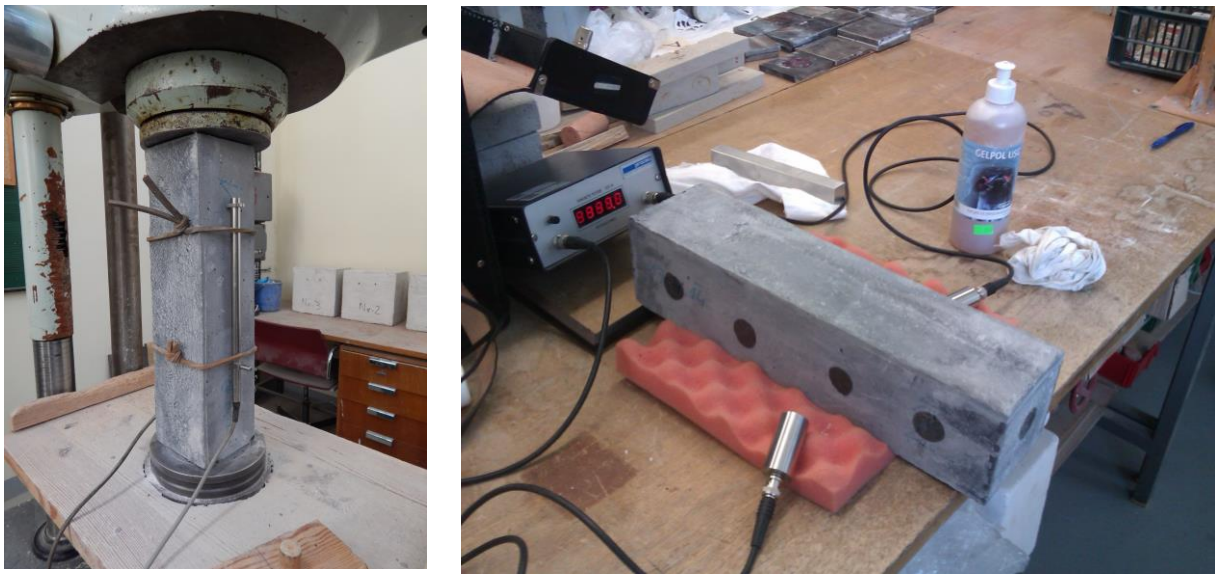

Fig. 11: Testing set up of static modulus of elasticity (left) and dynamic modulus of elasticity (right), both nondestructive tests.

3.3.2 Textile reinforcement

3.3.2.1 Determination of cross-sectional area

Cross sectional area is a very important input used as boundary conditions for next experiments, calculations and also numerical modeling. Composite textile reinforcement made from single roving has a very irregular shape of the cross-sectional area. In the initial experiments the area was determined by a sliding gauge as it is done with the composite or traditional steel reinforcement of conventional dimensions. But the scattering of the values was too large. Calculated results were not constant and predicted

results were not achieved during follow up experiments. It was necessary to change the measurement procedure.

The purpose was to keep it simple method with relevant results. An advantage was the technical data sheet of the manufacturer roving. Due to the linear and specific density it is possible to simply calculate the theoretical cross-sectional area of single roving. If we measure the weight of known length of the impregnated single roving, we can also simply calculate the theoretical weight of the single roving of known length. If the values are subtracted, it is known the weight and amount of impregnation consumed and it is possible again simply calculate the cross-sectional area of the impregnation itself thanks to the impregnation manufacturer's technical data sheet – specific gravity. The sum of calculated single roving area and area of impregnation gives the desired cross-sectional area of the single TR [6], [25].

3.3.2.2 Tensile test and determination of elasticity modulus

Accurate determination of both parameters, tensile strength and tensile static modulus of elasticity is very important for elements designing and numerical modeling. Some types of testing are not clearly prescribed in standards. For this research about basic tensile parameters was chosen and adapted the procedure according to ACI 440.3R-04 about the test methods for FRP for reinforcing or strengthening concrete structures. This adapting was because this standard describes the same material, but with a significantly larger cross-sectional area. Steel sleeves were installed on both ends of specimens using epoxy resin.

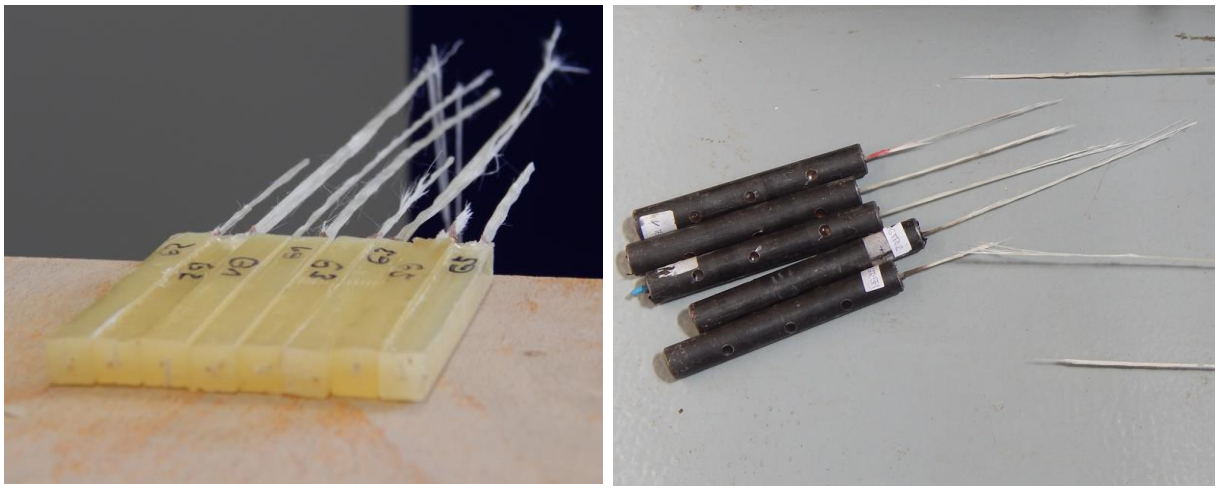

Fig. 12: View on the broken specimens in sleeves made from epoxy prisms 8 x 8 x 80 mm (left) and in the massive steel sleeves 20/2.5 x 120 mm with epoxy inside (right) [21].

Because specimen preparation is very demanding and fragile during preparation and installation and specimens are susceptible to damage, so the test procedure modification has been found. The method is described in [20], [26] and has been originally developed for the tensile testing of single rovings without polymer matrix [27]. Similar testing procedure was applied for the tensile testing of single rovings with polymer epoxy

matrix. Measured and calculated mechanical properties were the tensile strength and static elastic modulus using method [21], [25], [26], [28]. View on both types of sleeves epoxy and steel for fixing in testing machine is presented in Fig. 12. Pictures were taken after the loading test procedure.

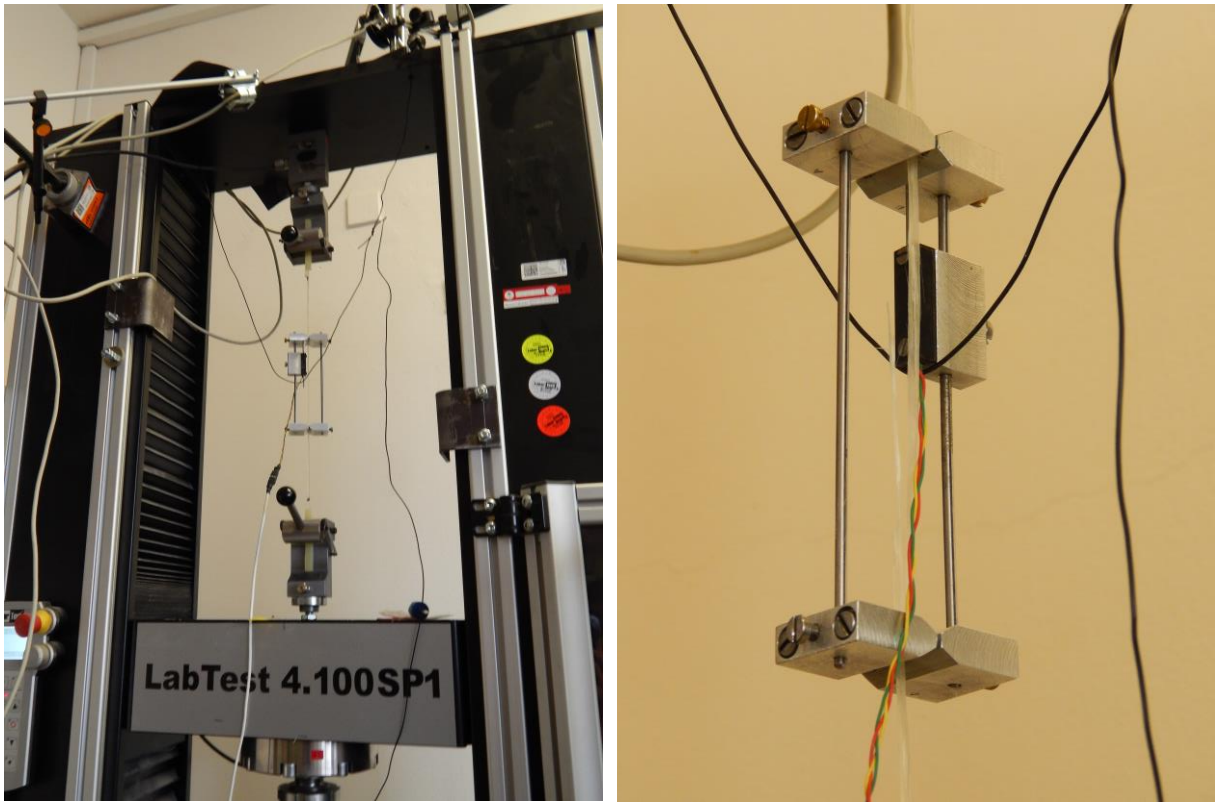

Fig. 13: View of the specimen in sleeves made from epoxy prisms installed in the testing machine before testing (left) and detailed view on small potentiometer (right) [21].

Testing of specimens was performed in LabTest 100 testing machine. This testing machine was additionally provided with data acquisition system using external card because of using small external potentiometer for elongation measurement. The speed of loading was 2.0 mm/min. It corresponds approximately to the increase of stress 2.0 MPa/s. Specimens were loaded with this constant speed until the failure. The views on small potentiometer are presented in Fig. 13, both for the case of epoxy prisms 8 x 8 x 80 mm as sleeve for fixing. The course of the test was monitored using data acquisition system that monitored the relationship of the acted force to the time of the test and deformation course. Graphical outputs were made from the courses of the tests. Force – displacement curves and stress – strain curves are presented in Fig. 15 and. Curves are very similar for each group of specimens [20], [21]. In Fig. 14 is presented also microscopic detail view on the damaged specimen after the testing procedure. It is visible that specimen was filly impregnated by epoxy resin.

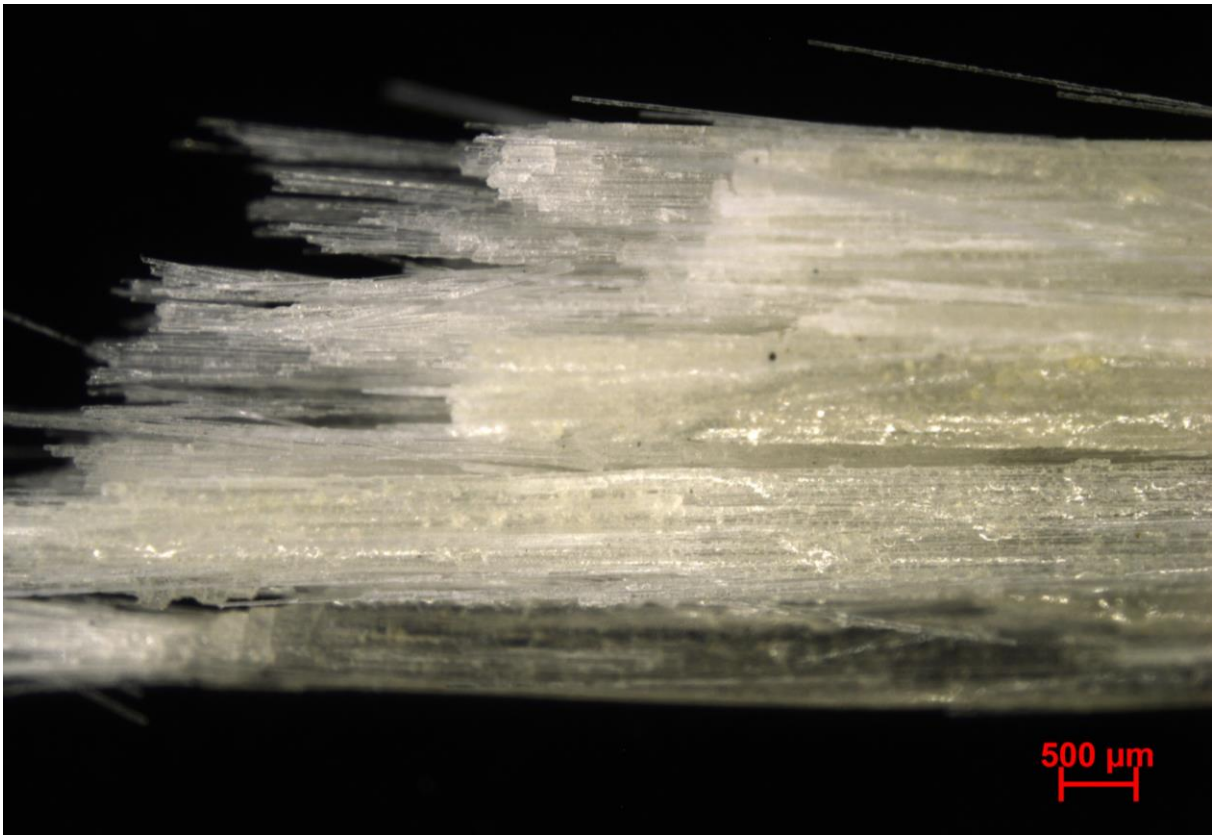

Fig. 14: Microscopic view on the composite reinforcement surface – contact area between HPC part and composite reinforcement without (left) and with the surface treatment (right).

Fig. 15 shows that specimens with epoxy prisms have higher values of elongation and also higher values of maximal force. This is due to lower rigidity of the small epoxy prisms compared to the steel sleeves. Specimens with epoxy prisms also achieved higher maximum force just before damage. This may be due to bad sample with steel sleeves handling. They are heavy and fragile and they can be easily damaged before testing. Damage of specimens may not be visible. Prisms are lightweight and handling is much easier. Results and higher tensile strength indicates that use of the epoxy prisms gives more accurate results compared to the steel sleeves [21]. Results of this experimental test was used as boundary conditions for numerical modeling in next chapters. Results using steel and especially epoxy sleeve were also compared with values determined theoretically by using Mori-Tanaka method. Theoretical and experimental results were almost identical and it indicates the correctness of developed experimental procedure and calculations [25].

Tab. 3: Results and calculations of tensile test, cross sectional area, maximum tensile force and strength, static elastic modulus [21].

spec. [mm]	E 1	E 2	E 3	E 4	E 5	aver.	S 1	S 2	S 3	S 4	S 5	aver.
m [g]	0.385	0.386	0.407	0.417	0.440	0.407	0.398	0.405	0.405	0.428	0.420	0.411
m_e [-]	0.145	0.146	0.167	0.177	0.200	0.167	0.158	0.165	0.165	0.188	0.180	0.171
A [mm^2]	2.191	2.195	2.286	2.327	2.417	2.283	2.248	2.277	2.277	2.371	2.339	2.302
A_e [mm^2]	1.296	1.300	1.390	1.431	1.522	1.388	1.352	1.382	1.382	1.475	1.443	1.407
F_{max} [N]	1374	1205	1462	1283	1342	1333	1087	1262	1104	1132	1280	1173
f_t [MPa]	627	549	640	551	555	584	484	554	485	478	547	509
ε [-]	4.234 $\cdot 10^{-3}$	4.821 $\cdot 10^{-3}$	4.066 $\cdot 10^{-3}$	4.486 $\cdot 10^{-3}$	4.678 $\cdot 10^{-3}$	4.457 $\cdot 10^{-3}$	3.255 $\cdot 10^{-3}$	2.842 $\cdot 10^{-3}$	2.913 $\cdot 10^{-3}$	3.003 $\cdot 10^{-3}$	2.739 $\cdot 10^{-3}$	2.951 $\cdot 10^{-3}$
ΔF [N]	299.9	307.2	300.0	300.0	300.0	301.4	200.4	199.4	199.8	200.0	198.1	199.5
E [GPa]	32.3	29.0	32.3	28.7	26.5	29.8	27.4	30.8	30.1	28.1	30.9	29.5

Basis tensile parameters of used composite reinforcement were calculated from all measured values. All calculated results are presented in Tab. 3. Specimens with epoxy prisms have indication *E* and specimens with steel sleeves and epoxy inside have indication *S*. Symbol m in the Tab. 3 means the weight of specimens with length 100 mm and m_e means the calculated weight of pure epoxy, because it is known the weight of pure roving from defined length weight 2400 tex using technical data sheet. Symbol *A* and A_e mean the calculated cross-sectional area of composite and pure epoxy resin using specific gravity of materials from technical data sheets. F_{max} is maximum measured tensile force just before breaking of specimen and f_t is calculated tensile strength using cross sectional area *A*. Elongation *ε* was measured using small external potentiometer monitoring the distance change between two edges of sensor with base of 130 mm. Elongation was monitored in the range of forces *ΔF*. Based on these results and calculations could be calculated also the modulus of elasticity *E* using basic Hooke's law [21].

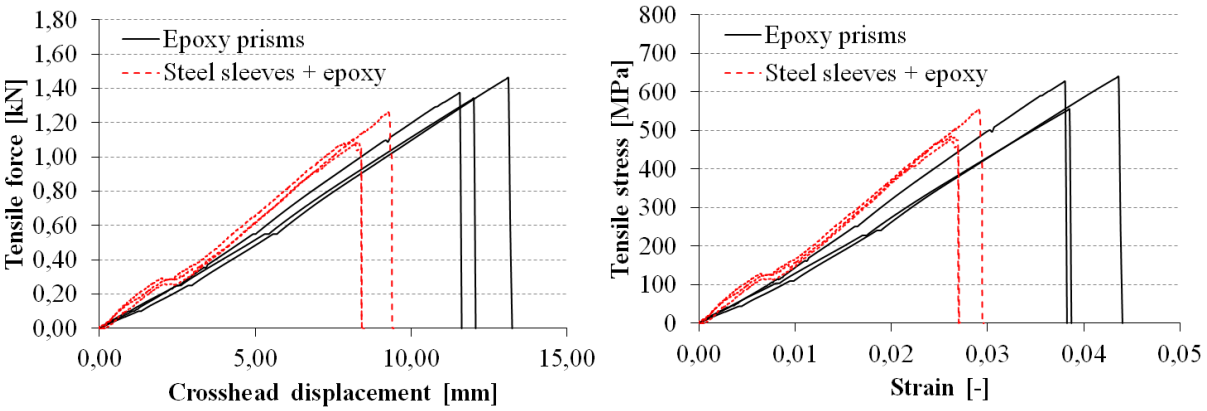

Fig. 15: Force – displacement (left) and stress – strain (right) curves using data from the testing machine, specimens with epoxy prisms and steel sleeves with epoxy resin inside.

It is also very interesting to compare the two approaches to the calculation and interpretation of the modulus of elasticity. AR glass roving is homogenized using epoxy resin as a basic assumption of this thesis. But it is a composite material where its mechanical parameters are determined mainly by fibers. Therefore, if we consider only the area of glass fibers without epoxy as area of reinforcement in the calculations of the modulus of elasticity, with good homogenization it should be approximately similar result of modulus to the theoretical value given in the manufacturer's technical sheet. May be slightly lower value due to imperfections, minor damage and so on. The same idea can be applied to strength. Results from the next measurement already only with epoxy sleeves are presented in Tab. 4. Values with considered cross-sectional area of roving have indication *R* and values considered cross-sectional area of composite (roving + epoxy resin) have indication *C*.

Tab. 4: Results and calculations of tensile test, maximum tensile force, tensile strength, static elastic modulus, considered on the cross-sectional area of the pure roving in comparison with cross-sectional area of the composite.

F_{max} [N]	f_{tr} [MPa]	f_{tc} [MPa]	E_r [MPa]	E_c [MPa]
1374	1534	627,1	66642	27238
1205	1346	548,9	80949	33018
1462	1633	639,7	76269	29880
1283	1433	551,3	74200	28557
1342	1499	555,3	77983	28893
1333	1489	584,5	75209	29517

Theoretical values of used AR glass roving from the technical data sheet are the maximal tensile strength 1700 MPa and tensile modulus of elasticity 72 GPa. The tensile strength and tensile modulus of elasticity related to the theoretical cross-sectional area of the pure roving in Tab. 4 are very similar, and it can therefore be said that the cross-section was well homogenized with used epoxy resin. If it were possible to prove that the composite reinforcement with surface treatment has a substantially perfect interaction conditions with the cement matrix, it would be possible to simplify the calculation of the TRC structures if the condition of good homogenization of the reinforcement is met. Textile reinforced concrete with fully impregnated rovings could be designed for the parameters of the reinforcement material. However, this simplification cannot be applied when considering interaction between reinforcement and cementitious matrix.

As mentioned in chapter 3.2.2 also fillers in epoxy matrix and its influence on the tensile strength, filler Sika "Stellmittel T" and silica flour. Results of the tensile test are presented in Fig. 16 and Fig. 17. All results are in the graph compared with the pure version without any filler. Results of this experiment are interesting. Influence of Sika filler is positive in both cases – it means with this type of filler was increased the tensile strength and the elastic tensile modulus. Contrast effect had quartz powder filler in the case of tensile

strength. It decreased with increasing concentration of quartz powder filler. In the case of elasticity modulus there was a slight increase of values due to stiffer matrix. This experiment shows it is possible to find cheaper alternative filler with similar influence on mechanical properties like with expensive nanoparticles presented in [18]. It is important to take into account that mechanical properties can be easily worsened using filler material. Mutual particle size must respect individual reinforcing fibers of composite [19].

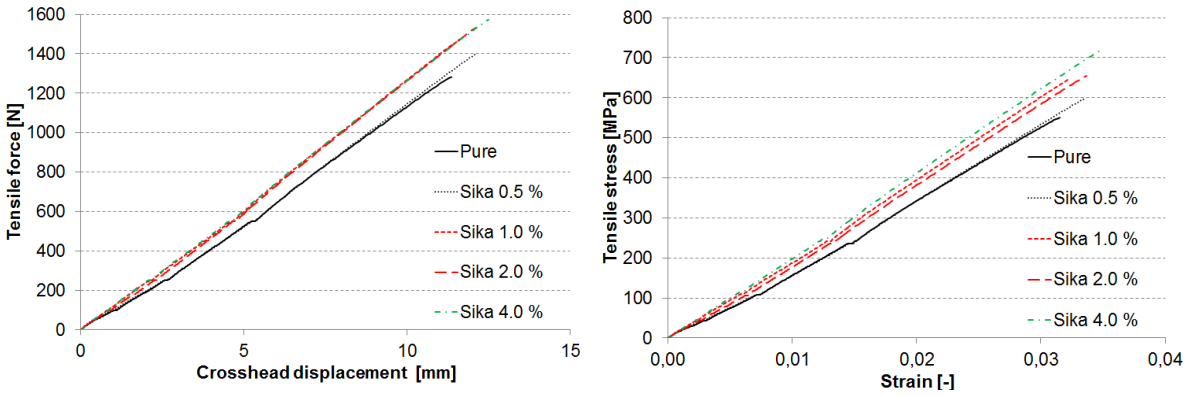

Fig. 16: Force – displacement (left) and stress – strain (right) curves using data from the testing machine, specimens with filler in epoxy Sika "Stellmittel T" [19].

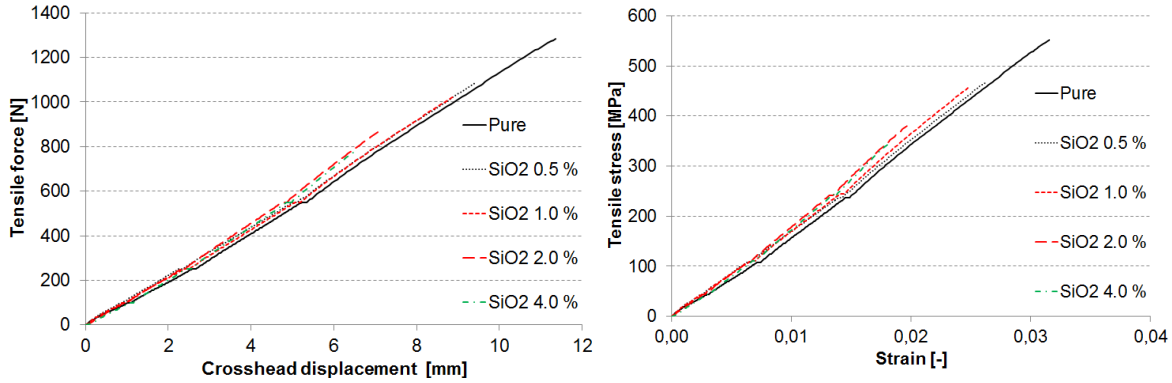

Fig. 17: Force – displacement (left) and stress – strain (right) curves using data from the testing machine, specimens with filler in epoxy silica powder (flower) [19].

3.3.3 Textile reinforced concrete

This chapter provides the most valuable and aggregate data. In the first subchapter two used different pull-out test methods are described for the determination of bond behavior between single roving CR and HPC cementitious matrix. Bond behavior was one of the main topics of this thesis as a basic parameter for the description and design of TRC construction. Four-point bending test presented in the second chapter was selected for the validation of numerical modeling and easy presentation of surface modification positive influence. Flexural stress is also the basic load of TRC construction in practice.

3.3.3.1 Pull out test inspired by method from Dresden

As mentioned in previous chapters, the first pull out test method was inspired by [10] and was performed for the comparison of developed own testing methodology. The HPC plate with dimensions of 60 x 278 mm has a thickness of 6 mm and single penetrated roving was anchored along the whole length of the HPC specimen. This roving with or without surface modification was embedded in HPC specimen matrix in its axis. Five pieces were created for each set of specimens. This thesis presents only results of pure penetrated roving without surface modification and with the surface treatment by silica sand with particle size 0.1 – 0.6 mm based on previous results. The anchoring length 20 mm was secured using transverse very short saw-cut through the single penetrated roving just below the steel part for the installation into the test machine and controlled crack at the required distance from the upper saw-cut. Double-side saw-cut was used for the predetermined breaking point – controlled crack and this point was also the border of unsymmetrical anchoring length. The length approximately 230 mm in the bottom part was certainly sufficient for the anchoring, ten times longer than controlled length. Both ends of specimen were fixed in the testing machine using prepared steel parts in combinations with steel screws for easier installation. View on the testing set up is presented in Fig. 18.

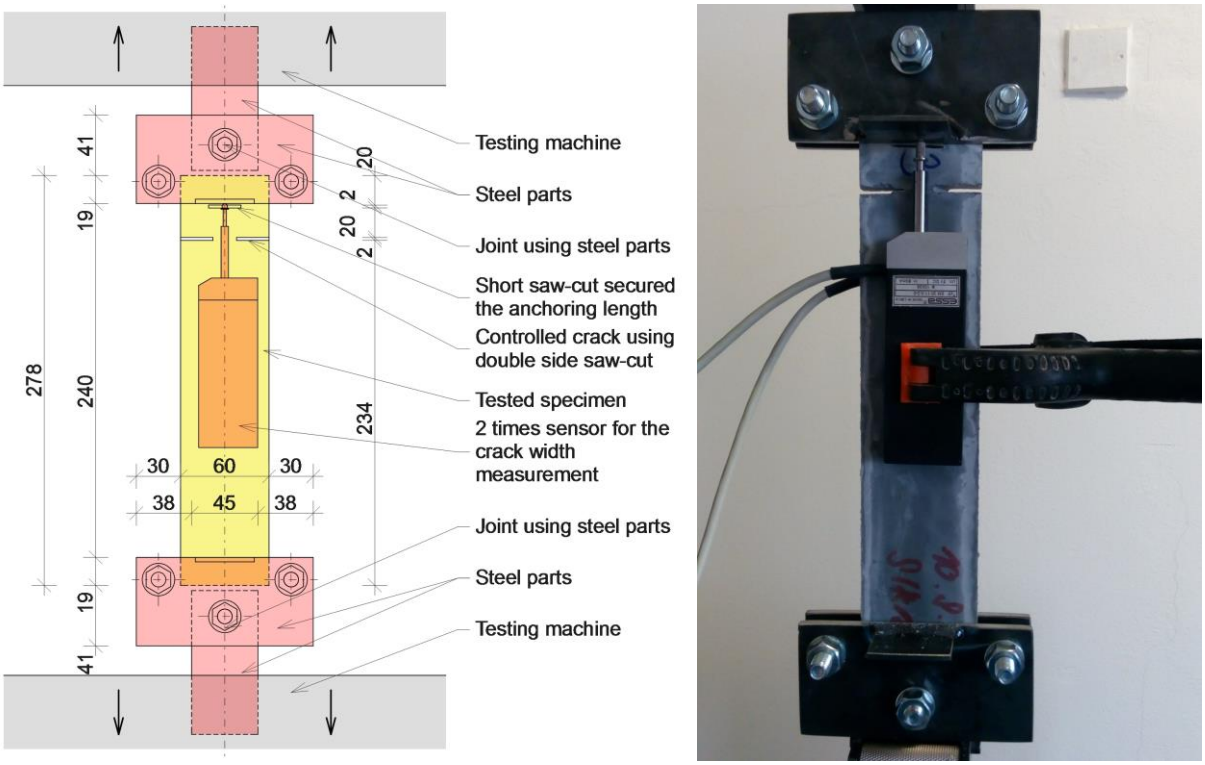

Fig. 18: Basic scheme of the pull out test inspired by [10].

During the test procedure for determination of bond behavior were measured time, force, crosshead displacement and development of the crack width using two external potentiometers to obtain accurate values in the axis of specimen where the impregnated single roving is located. The speed of loading was 2.0 mm/min according to prescribed

tensile stress increasing approximately 2.0 MPa/s in ACI 440.3R-03 standard. Results are presented in Fig. 19 in the form of two graphs. Crack width is identical for both graphs. Stress mentioned in the first graph is calculated to the contact area of composite reinforcement and cement matrix considering the ideal cylindrical surface using the cross-sectional area data and anchoring length. Stress mentioned in the second graph was calculated to the cross-sectional area of roving with epoxy polymer matrix according to the chapter 3.3.2.1and 3.3.2.2. Therefore, the maximum tensile strength of roving with influence of polymer matrix is approximately 600 MPa but for no specimen was damaged the reinforcement. The HPC was always damaged due to its small cross-sectional area in comparison with reinforcement and transverse stresses initiation due to the location of the saw-cuts.

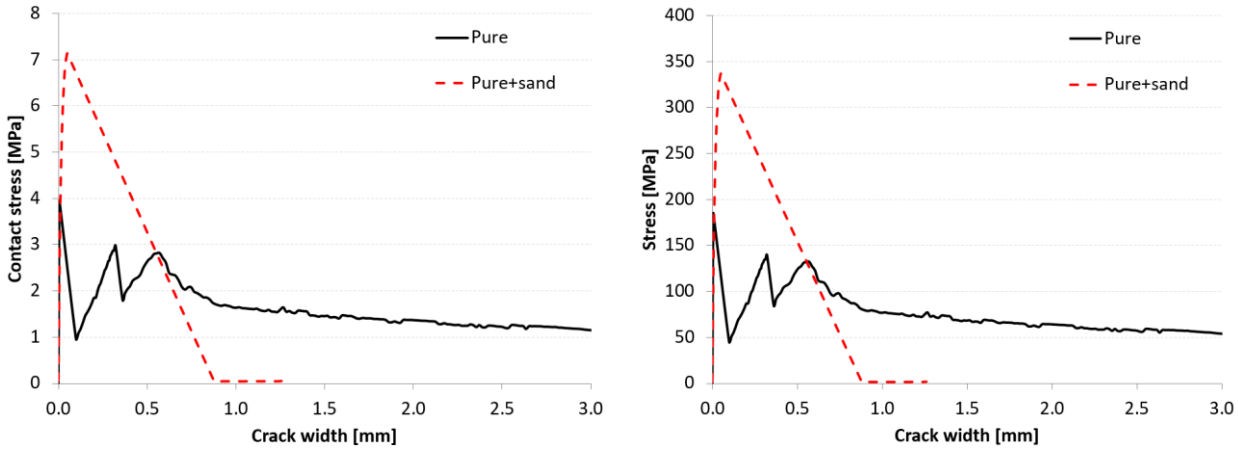

Fig. 19: Contact stress – crack width (left) and reinforcement tensile stress – crack width (right) representative curves from the reference pull out test using data from the testing machine and two external potentiometers.

So this method negatively affects the results and it is not possible to examine the bond behavior until the moment when reinforcement is broken. More information is presented in next chapter 4.3.1 about the numerical modeling. But it is good visible in Fig. 19 the rapid difference between specimens with and without surface treatment. The black full line representing the sample without surface treatment shows gradual pulling-out of reinforcement from the HPC sample. After the controlled crack initiation there is significant decrease of force during the loading process because of bad interaction of materials and the need for a large contact area (large reinforcement length) for reinforcement activation. Area in the contact with concrete after the controlled crack formation is reduced during pulling out and therefore there is evident a decrease of force until the end of testing procedure. The red dashed line representing the sample with surface modification. Controlled crack initiation was in the similar moment, but force continued to grow up thanks to the very good interaction conditions. In a short time after the first crack formation and minimal crack opening occurred concrete failure without expressive slipping of composite reinforcement and without violation of composite reinforcement. Maximum forces measured in this type of experiment were more characteristic for different breaking points of concrete but the slope of the curve after the

crack initiations indicated the bond behavior of the impregnated single roving in HPC cementitious matrix.

In Fig. 20 is presented view on the damaged specimen, where is very good visible the described problem of concrete failure much before the reinforcement damage. Cracks logically occur in places of the highest tensile stresses in the concrete part, which will be confirmed by a numerical model. Smooth roving on the left and in the middle had usually one typical horizontal crack or vertical, usually not both during the process of pull out. Roving with surface treatment on the right side had both typical vertical and horizontal crack thanks to the better interaction conditions. First was usually vertical crack and thanks to the rotation od small two concrete part closed to this initiated crack, it leaded to the horizontal crack initiation, because of concentration of higher tensile stress at the edges of the hole.

Fig. 20: View on the damaged specimens, smooth roving with typical vertical crack (left), smooth roving with typical horizontal crack (middle), roving with surface treatment and typical both vertical and horizontal crack (right).

In the last Fig. 21 in this chapter is presented more curves with more representative options and specimens, but in the same way like in the Fig. 19. It is visible similar curves trend. The higher contact stress was reached with surface treatment using silica fine grain sand for red lines and blue lines. Surprisingly, a positive effect was also observed for the green lines with filler Sika (Sika "Stellmittel T" material in concentration 2 % weight of epoxy – the best results from the tensile test of reinforcement) without any surface treatment.

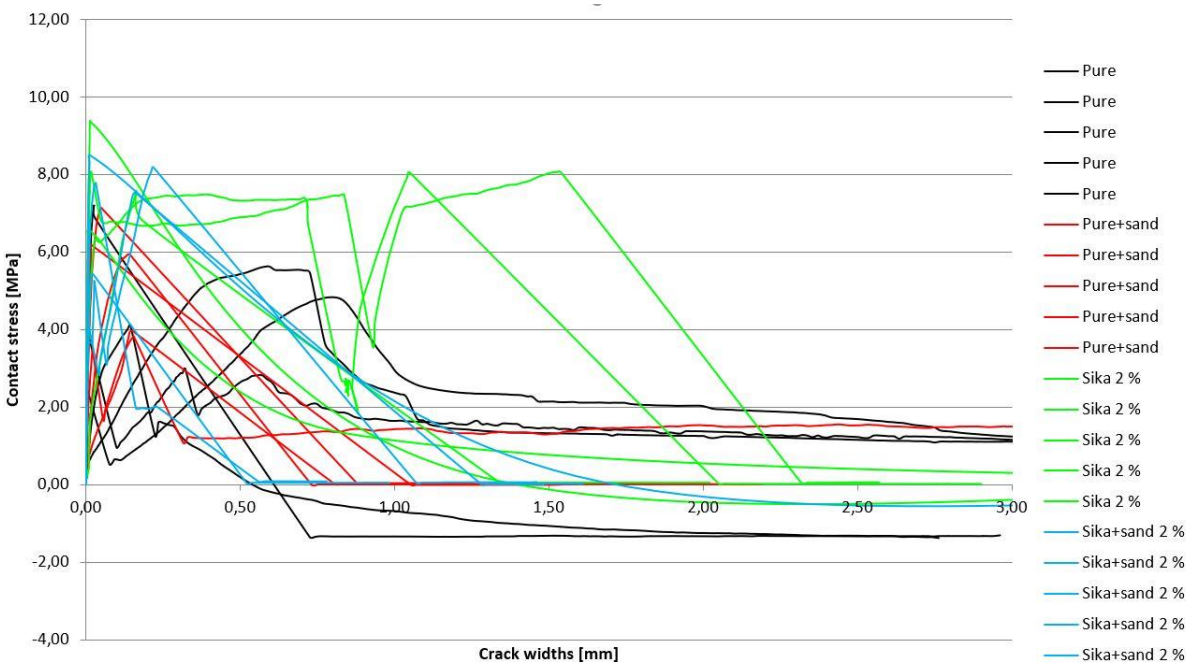

Fig. 21: Contact stress – crack width diagram presented on more types of specimens. Visible effect of surface treatment, but low contact stress due to the concrete part failure.

3.3.3.2 Pull out test according to the ACI standard

The second pull out method was focused on complete curve of bond behavior with a simple interpretation and application of results in the field of science as well as in the field of engineering and structures designing. As mentioned above method was inspired by the ACI 440.3R-03 standard, but specimen dimensions were originally modified due to small cross-sectional area of composite reinforcement. It is similar and work also with only one impregnated single roving. Verified epoxy sleeve was installed only on one side of single roving because of safe fixing to the testing machine without damaging the impregnated yarn. Presented concrete part has a constant dimensions 100 x 100 mm and optimized thickness for presented single AR-glass impregnated roving. First experiments were performed with the thickness closed to the standard with respect to ratios with other two dimensions, so the first thickness was 100 mm [22]. Especially in the case single penetrated roving with the surface treatment the single composite roving was usually broken before the start of slipping along the from the cementitious matrix. This unsuccessful first experiments lead to the thickness optimization using software ATENA Engineering. Resulted optimal thickness of specimens for used roving 2400 tex was calculated to 20 mm. View on the own developed testing set up inspired by ACI standard is presented in Fig. 22.

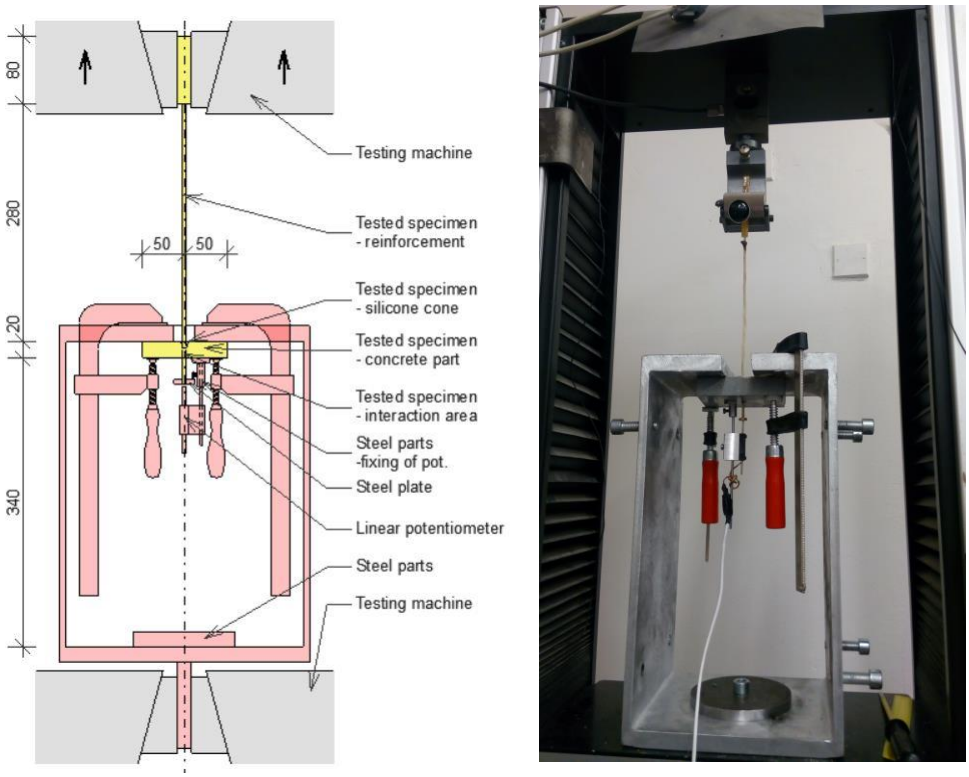

Fig. 22: Basic scheme of own developed pull out test method inspired by ACI standard and picture of the actual setup adapted to the dimensions (parameters) of the reinforcement.

Fig. 23: Detailed view of bottom part of concrete specimen with installed potentiometer and supported constructions for the pull out values measurement

During the test procedure inspired by the ACI standard for easy determination of bond behavior were measured time, force, crosshead displacement and pulling out on the end

of specimens using one small potentiometer. It was always fixed using small bolt into the small steel part treated by exact lathe. Steel part was firmly attached to the concrete surface by epoxy resin. A piece of rigid circular steel plate was attached at the end of composite reinforcement using also epoxy resin. The potentiometer touched the free end of the reinforcement with steel plate, which exceeded the concrete sample by approximately 20 mm. So, the theoretical maximal value of pulling out was approximately 15 mm included the circle plate thickness. Detailed view of potentiometer and its fixing on the HPC part is presented in Fig. 23. The speed of loading was also 2.0 mm/min according to prescribed tensile stress increasing approximately 2.0 MPa/s in ACI 440.3R-03 standard.

Results are presented in Fig. 24 and Fig. 25 in the form of two graphs similarly as in previous method. Pull out is identical for both graphs. Stress mentioned in the first graph is also calculated to the contact area of composite reinforcement and HPC cementitious considering the ideal cylindrical surface using the cross-sectional area data and anchoring length. The anchoring length was measured on the samples before the concreting process. It was the height of sample without a silicon cone made on the edge of the HPC. All samples were damaged by breaking of the reinforcement – impregnated single roving. It was broken after slipping thanks to the surface treatment – silica sand, so by damaging of fibrils at the surface. In the case of smooth reinforcement, this reinforcement was broken on the same principle, usually after a longer time, by the unevenness of the concrete in contact area. This is caused by small changes in the cross-sectional area of roving, which is in contact with the concrete. The impregnated roving has never an ideally round shape.

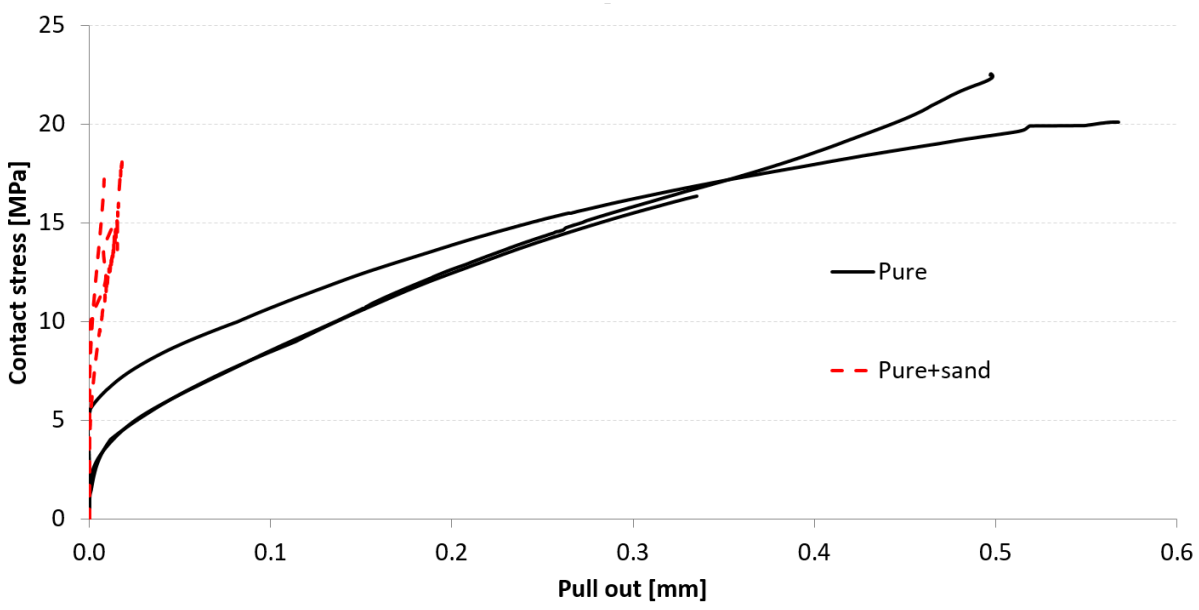

Fig. 24: Contact stress – pull-out curves from the own developed pull-out test inspired by ACI standard using data from the testing machine and potentiometer.

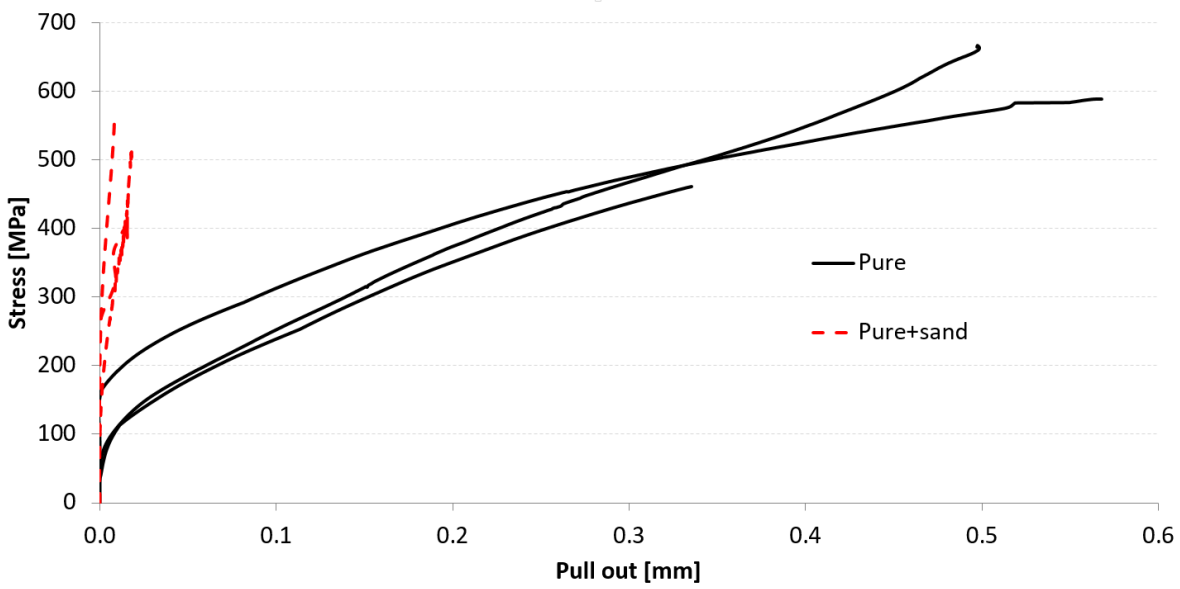

Fig. 25: Reinforcement stress – pull-out curves from the own developed pull-out test inspired by ACI standard using data from the testing machine and potentiometer.

Based on the results of tensile test described in 3.3.2.2 it is known the tensile strength of roving with influence of polymer matrix approximately 600 MPa. During the testing procedure of own developed pull-out test method, the reinforcement was damaged for all specimens with the values of maximum tensile stress in composite reinforcement corresponding with presented results of tensile test. Impregnated single roving was in most cases damaged inside of the HPC prism due to the reinforcement surface is pressed by the irregular internal surface of HPC that surrounds the part of composite reinforcement during the process of reinforcement activation. With higher tensile stress the fibers near of the surface may be damaged and it leads to creation of weakened cross sectional area. This weakened place is also usually the place where the composite reinforcement is broken. However, epoxy impregnation of the single roving provides sufficient protection in HPC specimen against its premature damage in addition to other benefits as results in this chapter present. HPC part of specimens was without any visible damage on both surfaces.

It is also very good visible in Fig. 24 and Fig. 25 the rapid difference between specimens with and without surface treatment like in the previous described case. The black full lines representing typical samples without surface treatment show very fast pulling out of reinforcement from the HPC part of sample. After the reinforcement activation in its length, it is very slow increase of force during the loading process because of bad interaction of both materials. This result is not so positive, because a big anchoring length of composite reinforcement will be required for the transfer of load in TRC element. For the considered flexural load of TRC element there will be also massive crack opening. The red dashed lines representing typical samples with surface modification provide much better results with higher stiffness of contact. Surface modification is without higher

negative influence on the tensile strength of impregnated single roving. Silica sand particles do not allow almost any slipping due to the large roughness of the surface.

Area in the contact with concrete is in this testing method constant thanks to the free end of composite reinforcement behind the HPC part of specimen. Pulling out is recorded after the reinforcement activation in its entire length due to the location of potentiometer on the opposite side of the concrete part. This beginning point of pull-out is sometimes called the cohesion.

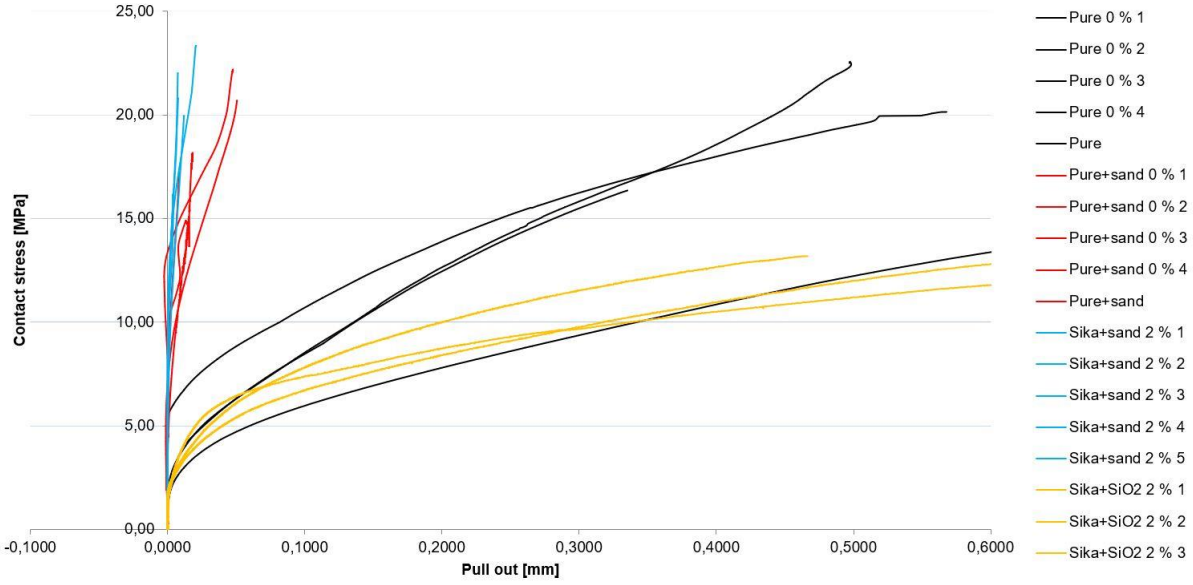

Fig. 26: Contact stress – pull-out curves from the own developed pull-out test inspired by ACI standard presented on more types of specimens.

In the last Fig. 26 in this chapter about the mechanical testing of bond behavior using own developed method is presented more results of pull-out test – selected interesting material variants. Other materials and especially different grain size of surface treatment were also tested and only the most important or typical variants are given in this work. In general, it can be stated that silica sand with grain size 0.1 – 0.6 mm had the best results without any negative influence on the tensile strength of reinforcement. Fillers in epoxy matrix, not as a surface treatment, had logically almost no influence on the pull-out test procedure. It is also visible in Fig. 26. Yellow line with SiO2 (silica flour, selected the variant with concentration 2 % by weight of resin with best results in tensile test) and black line pure, both without surface treatment have similar curves. Similarly, the comparison of red line and blue line, both with surface treatment using silica fine grain sand. This figure is also presented in chapter 4.3.2 about the numerical modeling for the comparison of experimental results with results of numerical model.

3.3.3.3 Four-point bending test

Small slabs with dimensions 100 x 360 mm were created for the four-point bending test procedure. Their thickness was constant 18 mm. The concrete cover for all variants of reinforcement was designed constant only 4 millimeters and it has been secured with

the controlled thickness of HPC layers. Specimens were not vibrated to prevent the flooding of TR on the HPC surface due to its lower density. One HPC mixture was used for all specimens as mentioned above. One group of minimally three specimens was created for the same designed amount of reinforcement. Six sets of samples were prepared in the sum.

Three sets were with the surface treatment and three sets were without the surface treatment with identical TR. The first group was made of two identical layers of pre-prepared TR. Each layer had 5 impregnated rovings in longitudinal direction with grid spacing 22 mm. Grid spacing in transverse direction was 24 mm. The second group was also made of two identical layers of pre-prepared TR from 10 impregnated roving in longitudinal direction and grid spacing approximately 9 mm. Grid spacing in transverse direction was also 24 mm. The last third set of specimens was made of four layers with 10 impregnated rovings in longitudinal direction like in previous case. This combination of 4 layers and 10 roving in one layer was maximal possible amount of composite reinforcement for this specimen dimensions and composite reinforcement production technology, especially for the specimens with surface treatment. View on the testing set up and typical first crack is presented in Fig. 27.

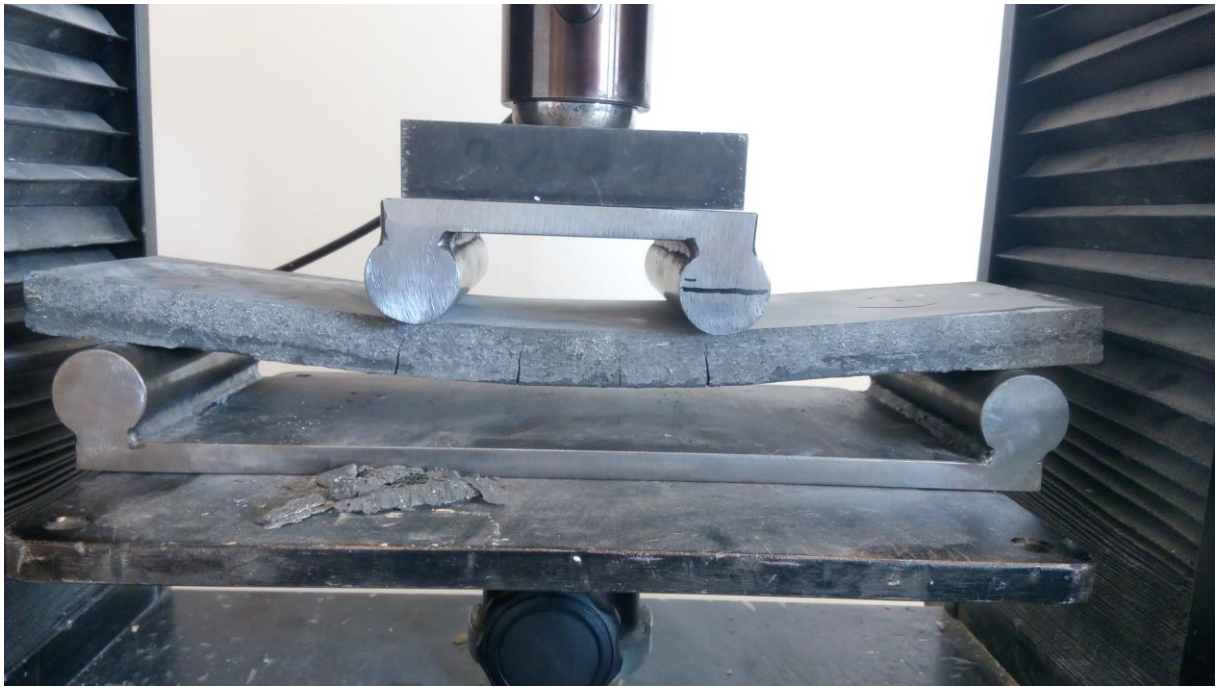

Fig. 27: View on the loaded specimens during the four-point bending test on slabs with dimensions 100 x 360 x 18 mm with 2x5 impregnated rovings with surface treatment.

During testing the distance between centers of support was standard for a four-point bending test 300 mm and 100 mm between centers of loading supports. The 15 mm radius of curvature was used for all supports. Monitored parameters during testing procedure were magnitude of the reaction on the load cell and displacement of crosshead of the testing machine. Four-point bending test was performed on MTS 100 testing machine with controlled load speed 2.0 mm per minute [29]–[31].

Results are presented in Fig. 28 in the form of force – displacement graph. It is because presentation of flexural stress on the y axis in HPC part is not exact after the first crack initiation, despite the fact that it is commonly used for result presentation. All specimens with surface modification have the same color, like specimens without surface modification with the same amount of TR in cross sectional area, but darker. Only two layers of TR with five rovings in each layer behaves like a slightly reinforced concrete construction element with very wide cracks, especially in the case of TR without surface treatment. It leads to the formation of plastic joints and the crack opening effect is clearly visible. For experimental results are characteristic two cracks under the loading supports and their opening sometimes until the specimen collapses in the cases of lower amount of TR or in the cases without surface modification and bad interaction of HPC and TR. Sometimes only one crack also could be initiated. This happened due to more facts: incorrect position of reinforcement and different concrete cover, variable thickness of specimen, very bad interaction between composite reinforcement and cementitious matrix and small amount of reinforcement in cross-sectional area of specimen. On the other side, especially in the case of good materials interaction and increasing amount of reinforcement in cross sectional HPC area, reinforcement pulling out is not so significant and it leads to the next cracks initiation and multiple cracking [29], [31].

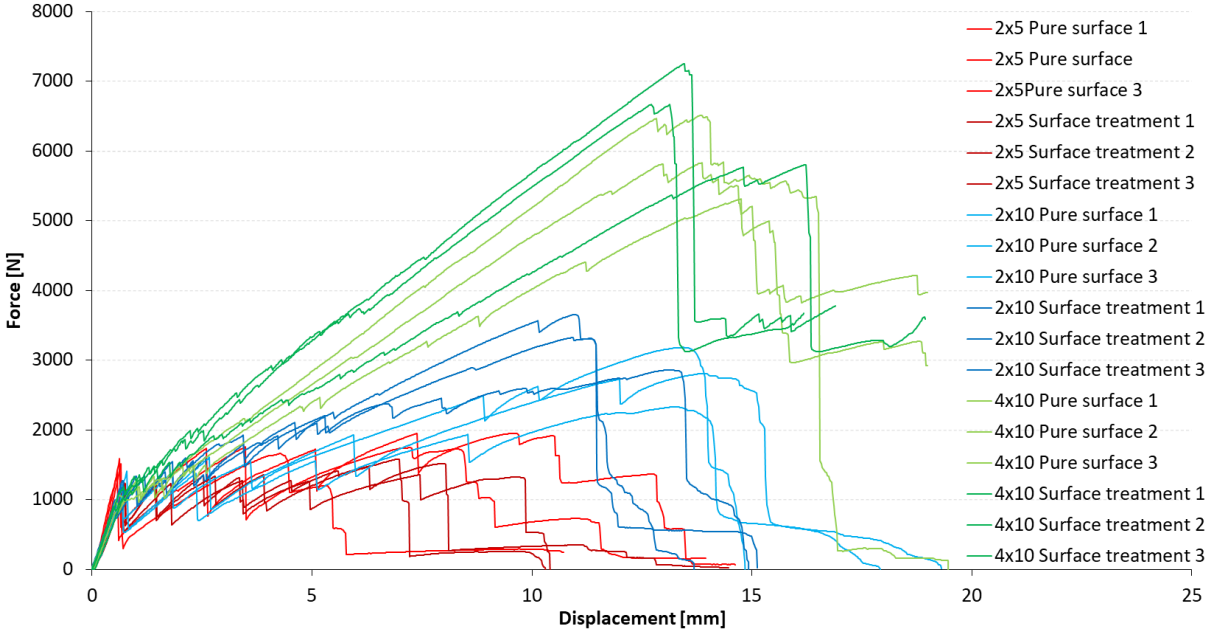

Fig. 28: Force – displacement curves from the four-point bending test with different amount of TR, with and without surface modification using data from the testing machine.

TR with surface modification provides significantly better results regarding the cracks formation and development. Better bonding conditions leads to the very short anchoring length for reinforcement activation without a significant decrease of force due to loading by displacement. Hand in hand with cracks also maximal force was measured larger. Visible difference between pure surface and surface modification is present in Fig. 29. Comparable results at the beginning of curve during the process of reinforcement

activation are in the case of 2x10 impregnated rovings with surface treatment and in the case of 4x10 rovings without surface treatment. Difference in maximal reached force is due to little bit different HPC cover and of course due to different cross-sectional area of reinforcement. It is also obvious from both presented Fig. 28 and Fig. 29 that with higher amount of TR can be achieved similar shape of curve like with traditional materials and diameters of reinforcement. All these curves in comparison with the numerical model are also mentioned in chapter 4.4.7.

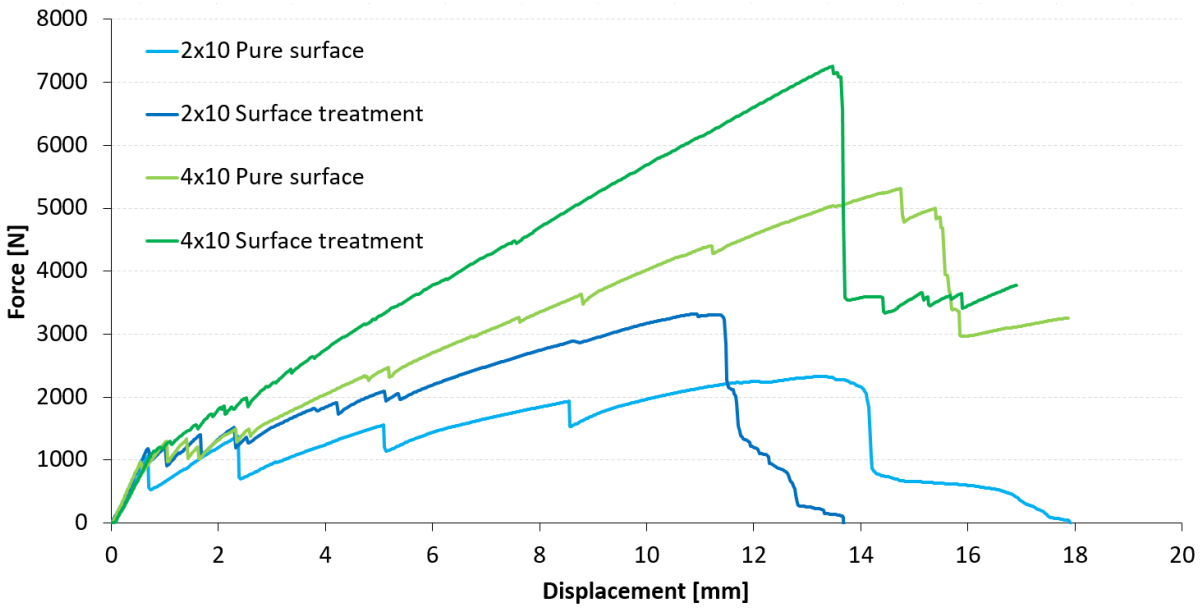

Fig. 29: Force – displacement curves from the four-point bending test, selected typical curves for the visible difference between specimens with and without surface modification.

For a better idea of the difference in the development of cracks, a view of damaged TRC specimens with different amounts of reinforcement corresponding with reinforcement presented in graphs is presented in Fig. 30 and Fig. 31. Looking at all these images, the difference is especially noticeable in the number of cracks, its width and the application of effect of multiple cracking in the case of more reinforced specimens an specimens with the surface treatment. With more and more cracks on the specimen, they are less and less wide and visible. And difference with number of cracks their opening is also visible on the surface treatment for the same amount of reinforcement. All pictures were taken approximately in the moment of slabs collapse.

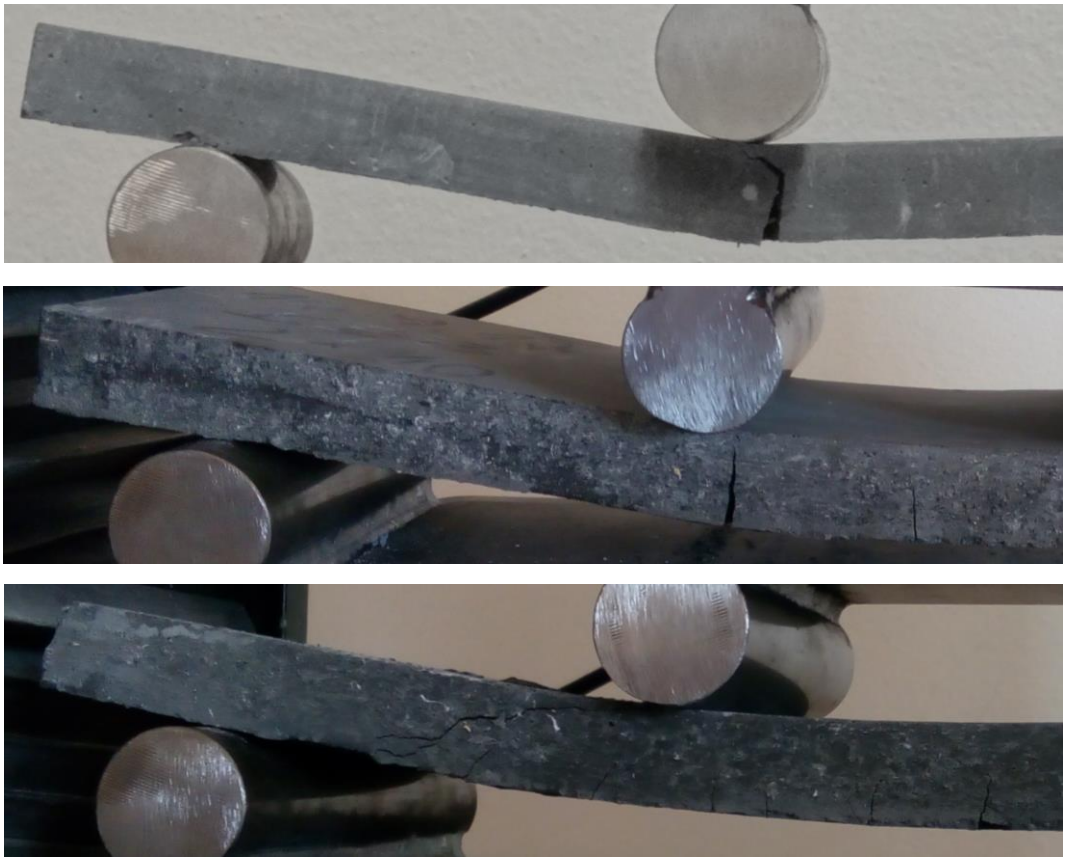

Fig. 30: View on the specimens with different amount of reinforcement before the moment of collapse, presented specimens without surface treatment. First line 2x5, second line 2x10, third line 4x10 rovings.

Important is the last picture presented in Fig. 30. Visible crack under the loading support is shear crack and indicates a shear failure in combination with bending moment. This failure was quite common with a higher value of the loading force. At the end of the experiment there was a combination of shear failure of concrete and rupture of the reinforcement due to the bending moment between supported and loading support. This phenomenon is very difficult for numerical modeling exactly after the shear crack opening. However, it is important to note that this is the end of the loading process, where the textile reinforced concrete structure (slab) is already far beyond the serviceability due to the large deformation.

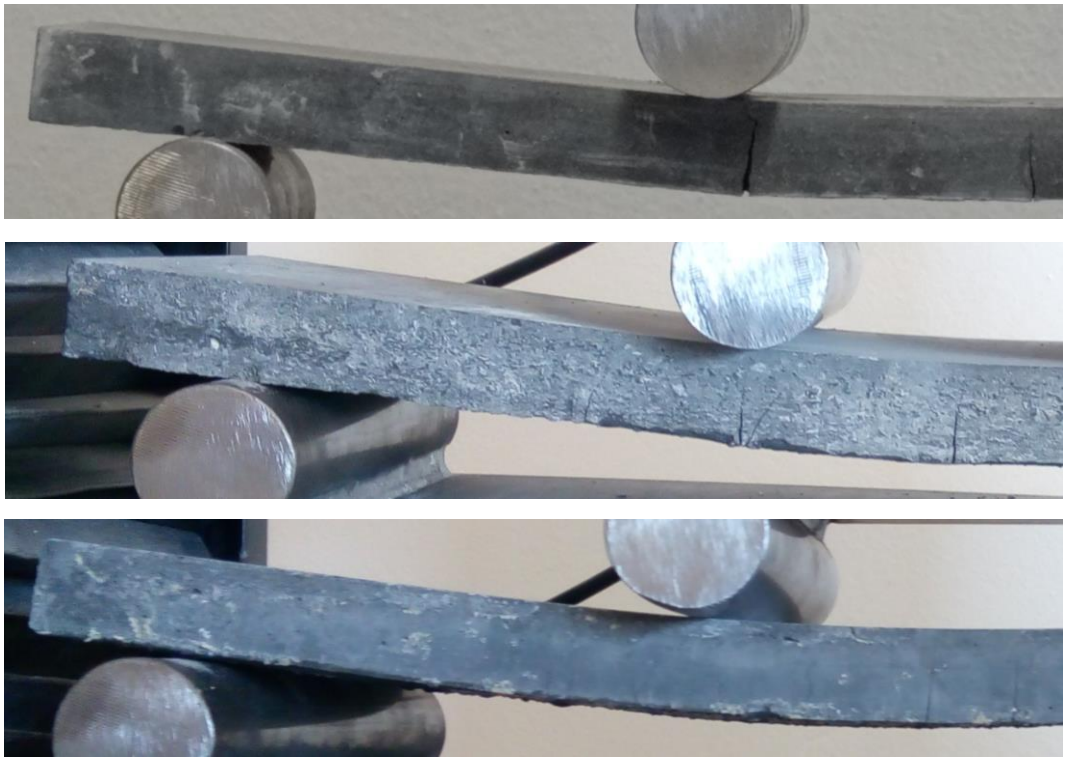

Fig. 31: View on the specimens with different amount of reinforcement before the moment of collapse, presented specimens with surface treatment using silica sand. First line 2x5, second line 2x10, third line 4x10 rovings with the best results.

4 Numerical modeling

Numerical models were created in the ATENA Engineering 2D program [32] for nonlinear analysis of concrete and reinforced concrete structures. The following chapters describe all material parameters used in the numerical model, separately chapter about calibration of bond behavior and the last chapter about validation of these used parameters on the final four-point bending test of textile reinforced concrete slabs with different amount of textile reinforcement. Numerical models were created for the smooth variant of impregnated textile reinforcement and for the reinforcement with one type of surface treatment based on the previous mechanical experiments – silica fine grain sand.

4.1 Material parameters

4.1.1 Concrete

HPC was modeled using topology tool Macro-element and the textile reinforcement was modeled using topology tool Bar reinforcement. HPC was chosen as a material type 3D non-linear Cementitious 2. Material characteristics are shown on following pictures. Concrete is usually defined by following parameters: elastic modulus E, Poison's ratio μ, compressive strength f_c, tensile strength f_t, fracture energy G_f, strain at the peak of stress ε_{cp} and plastic displacement of concrete w_d. Princip of failure law with defined curve is presented in Fig. 32. Princip of crack opening is presented in Fig. 33. Softening displacement law with defined curve is presented in Fig. 34.

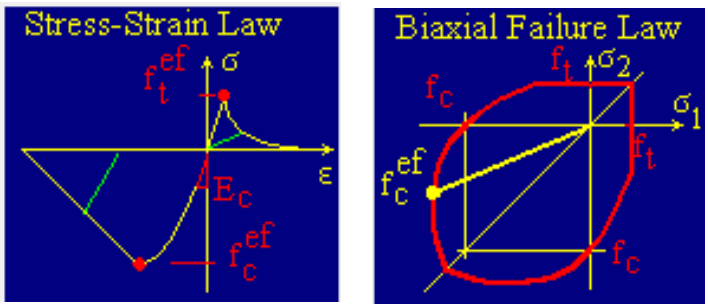

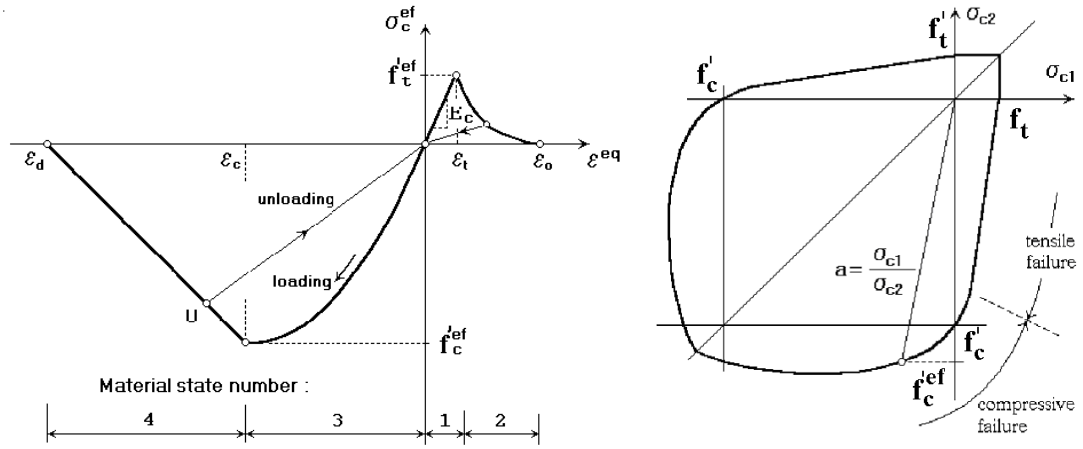

Fig. 32: Failure law of concrete in general defined by ATENA for used material in numerical model – 3D non-linear Cementitious 2 [33].

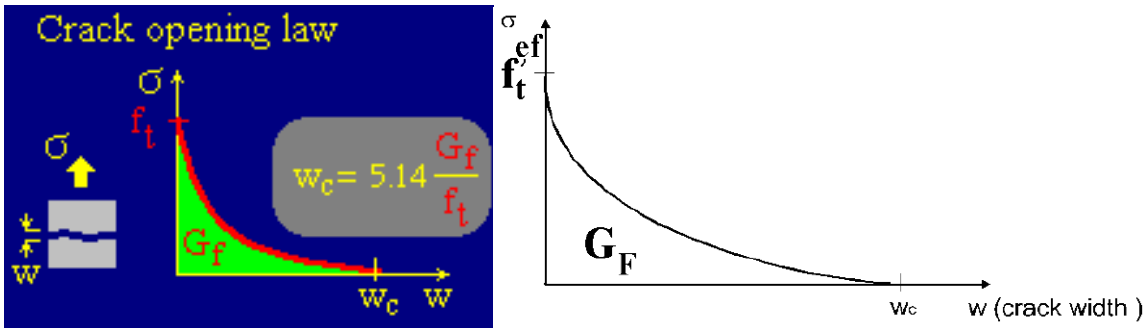

Fig. 33: Crack opening law of concrete defined in ATENA for used material in numerical model – 3D non-linear Cementitious 2 [33].

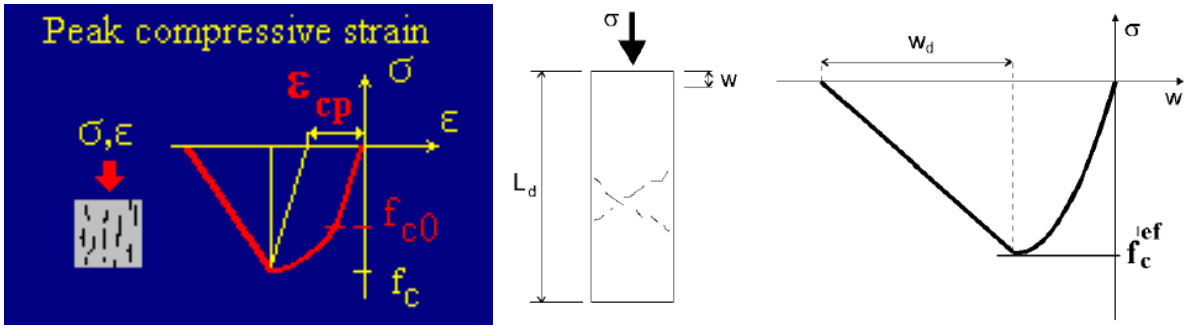

Fig. 34: Softening displacement law of concrete in compression defined by ATENA for used material in numerical model – 3D non-linear Cementitious 2 [33].

Next presented figures present specific material parameters of HPC used in numerical model. It is necessary to state that some values have been adjusted according to the results of calibrations of material parameters and therefore may not be identical with the measured values. This part of the chapter is therefore closely related to the chapter 4.2. Predefined pressure in a material type 3D non-linear Cementitious 2 was 160 MPa, little bit higher in comparison with measured values based on the previous experience and modeling in this ATENA software. This is the reason for the "HPC 160" material designation, which can be seen in the following figures.

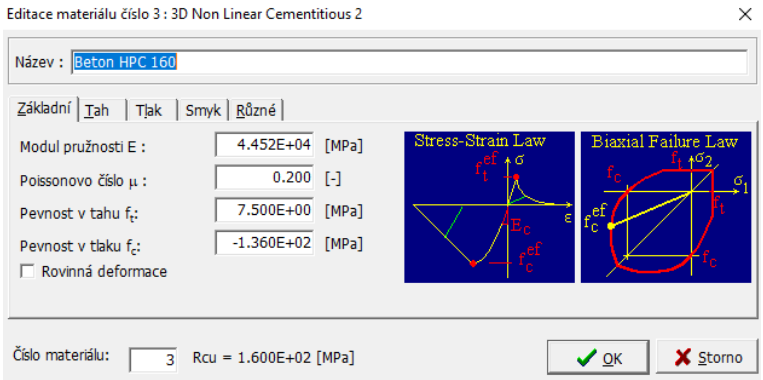

Fig. 35: Input data used in 3D non-linear Cementitious 2 as a basic material properties of HPC in model.

Subsequently automatically generated parameters were adjusted according to the measured and calculated values and according to the minor other numerical models for calibration purposes mentioned in chapter 4.2. So the following parameters were modified: Tensile strength was changed to 7.5 MPa, modulus of elasticity was 44.5 GPa, compressive strength was 136 MPa. These values are presented in Fig. 35.

Very important and big change in comparison with generated data from software was the specific fracture energy. In the case of HPC with fine grain aggregates with maximum grain size 1.2 mm is specific fracture energy almost zero in comparison with traditional concrete. It was change only to 20 N/m as visible in presented Fig. 36. It is also reason of suddenly crack opening after the crack initiation presented and very good visible for example in this thesis in Fig. 83 from the presented part of four-point bending test. Just after the crack initiation the reinforcement is very fast activated. It is also one of reasons in combination with higher amount of cement why HPC without reinforcement (fiber, textile, bar and their mutual combination) is almost not used. The last Fig. 37 present the plastic parameters of concrete in compression.

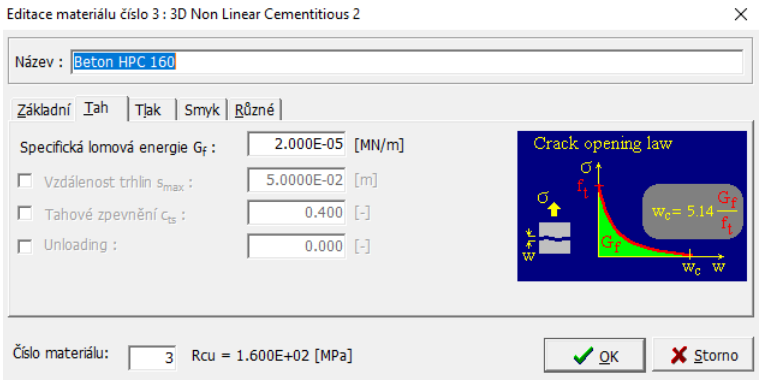

Fig. 36: Input data used in 3D non-linear Cementitious 2 as a fracture energy set into the model of HPC.

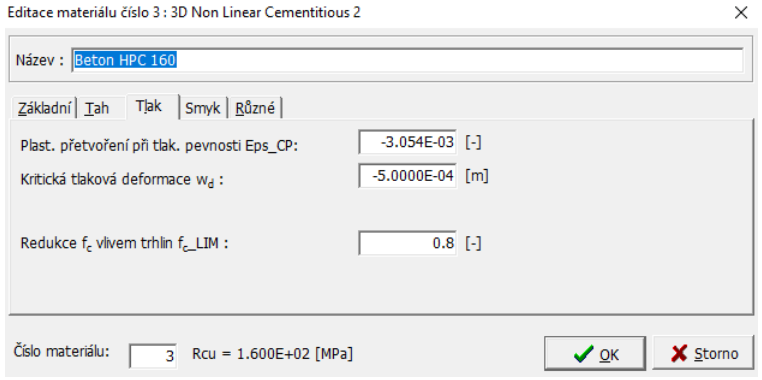

Fig. 37: Plastic parameters of the concrete in numerical model.

4.1.2 Reinforcement

Reinforcement and steel parts were modeled with the same program instrument with the selectin linear, bilinear or multilinear curve representing the material parameters. Steel parts were used in numerical simulations of experiments mainly as supports and loading supports, sometimes supporting construction. Easy principle of stress-strain law for linear curve in ATENA software is presented in Fig. 38. Poison's ratio μ was defined 0.3 and modulus of elasticity was selected 210 GPa as mentioned in Fig. 39. It was linear and ideally elastic.

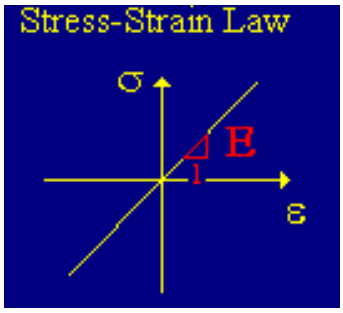

Fig. 38: Basic elastic and linear stress-strain law of steel plates.

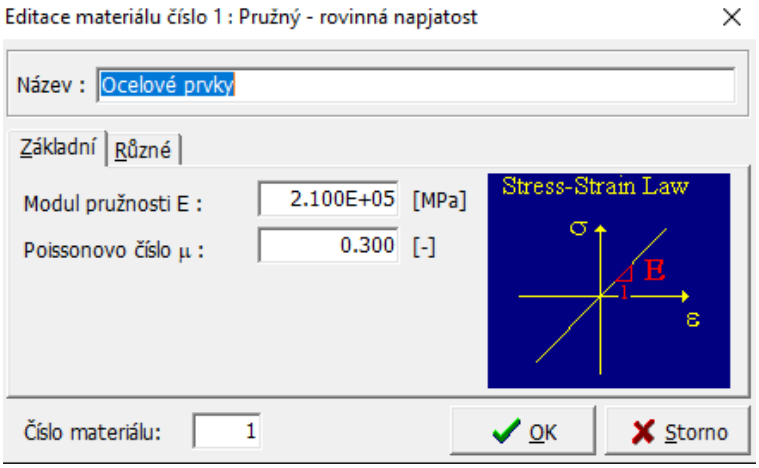

Fig. 39: Defined material parameters of steel parts in models.

Composite reinforcement was defined using two types of defined curves, bilinear and multilinear due to the definition of the moment of failure of the reinforcement. Other options have been tried, but these two methods of material modeling were the best in terms of achieved results.

Bilinear model of reinforcement was used with elasticity modulus 29.5 GPa and a yield strength 584 MPa. So composite reinforcement was simply defined for the purpose of model with perfect plasticity due to the less complexity of the computational model and good accuracy of the results. The considered material parameters of the reinforcement

correspond to the parameters of composite – impregnated single roving, see chapter 3.3.2.2 and description of Tab. 4. This curve and its values are therefore suitable for a defined cohesion of the reinforcement and this curve was also considered primarily for combination with defined coherence parameters.

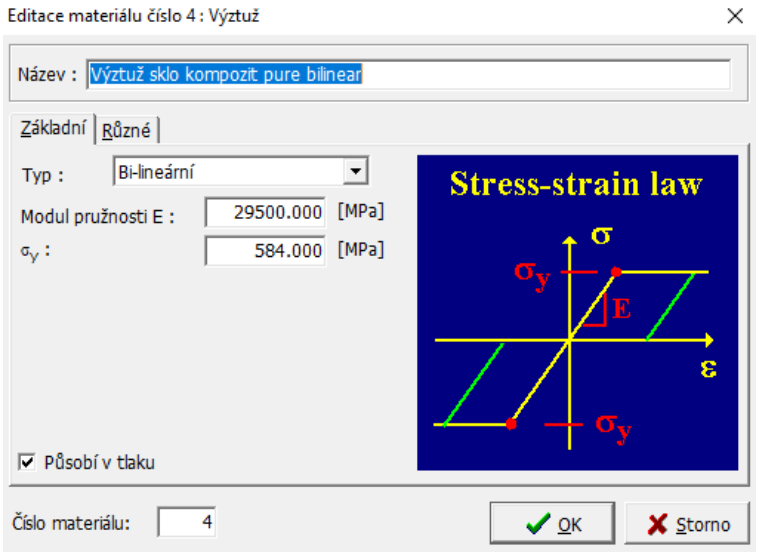

Fig. 40: Material parameters of reinforcement defined in the analysis with the best results using bilinear curve for the defined cohesion.

The multilinear curve is more suitable for perfect interaction of both materials and was used only for the perfect bonding due to the complexity of the calculation when the strength in the reinforcement decreases. Combination of both realistic curve of material and modeled cohesion is very time consuming and not so effective. Therefore, the material parameters are in presented case in Fig. 40 given in this case for pure roving according to chapter 3.3.2.2 and description of Tab. 4. Maximal tensile strength was considered 1489 MPa according to the measured and calculated value with a corresponding value of elongation. A small residue of strength is the model close to reality. It is possible more accurately model the course of the experiment during the collapse of the sample. Of course, many other variants and combinations was also tested.

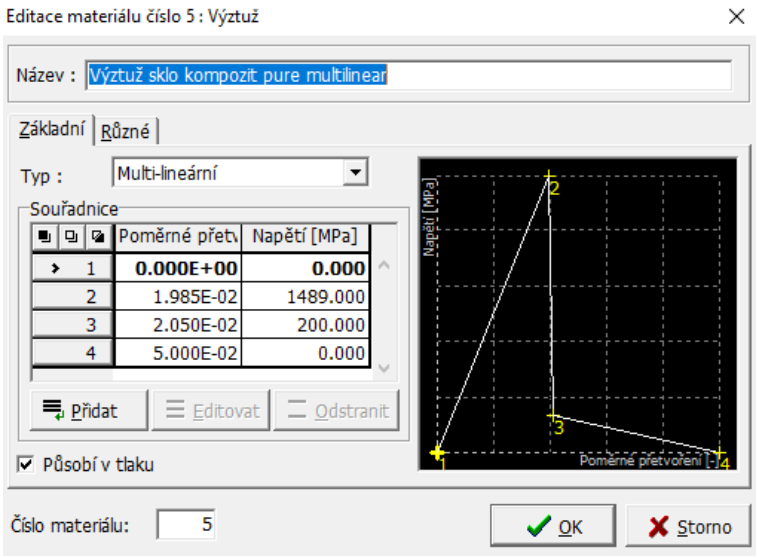

Fig. 41: Material parameters of reinforcement defined in the analysis with the best results using multilinear curve for the case of perfect bonding.

It is necessary specify after many model simulations that both curves presented in Fig. 40 and Fig. 41 are suitable for modeling of the first half of experiment without major mutual deviations, because the load-bearing capacity of the reinforcement is not achieved. Both curves can be applied to the phases of the crack development and of the crack opening. The strength and the corresponding elongation converted to the cross-sectional area of pure roving are possible when the perfect interaction is considered, and quality homogenization of the reinforcement is assumed. When cohesion between reinforcement and cementitious matrix is modeled, it is necessary to enter the strength and the corresponding elongation calculated on the cross-sectional area of the whole composite.

4.1.3 Cohesion – reinforcement bond

Interaction conditions were defined using material tool Reinforcement Bond with user-defined non-linear curve. Many curves were considered and their possible simplification, curves with the best achieved accuracy of models are presented. The most difficult was to define and debug the curves so that it works good after the first crack initiation, but also during the crack development, crack opening and before the collapse of the sample. First step in the curve specification was based on the exact measured values and shape during the pull-out test. Because the concrete samples from the pull-out test were thin, it was assumed that this could simplify the reinforcement bond modeling. Then curve was during the modeling little bit modified to test the effect on the result. As a result, this assumption was successfully confirmed, which is described in more detail in the chapter 4.3, better in part 4.3.2. It leads to the easy reinforcement bond definition based exactly and directly on the pull-out test results.

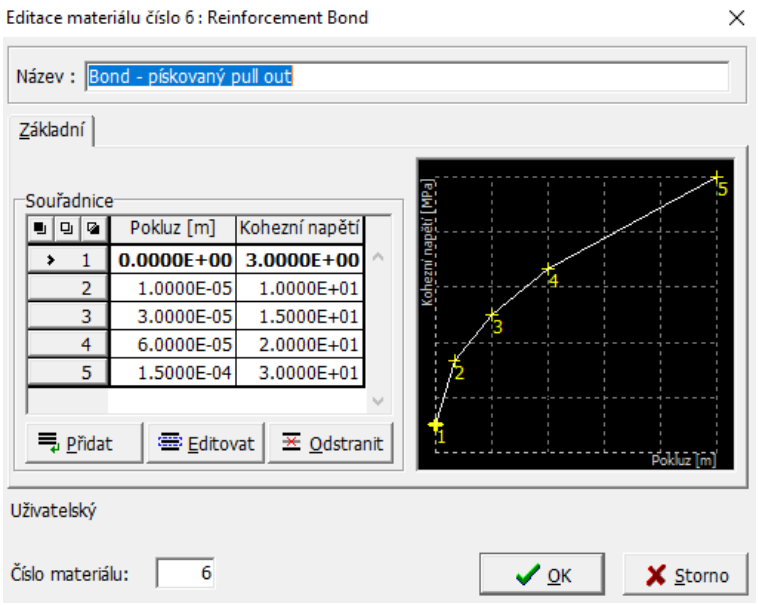

Fig. 42: Bond curve for specimens with surface treatment using silica sand.

Finally, four curves with defined cohesion – reinforcement bond were used in numerical models with different stiffness. One used curve represents specimens reinforced by impregnated rovings with the surface modification using silica sand. This bond is presented in Fig. 42. Next three curves represent smooth surface of impregnated roving without any surface modifications. Three stiffness were considered. The medium soft stiffness is presented in Fig. 44, soft stiffness in the bond area is Fig. 44 and ultra-soft stiffness represent the last curve in Fig. 45. Interaction between reinforcement and cementitious matrix for specimens with smooth surface is not constant.

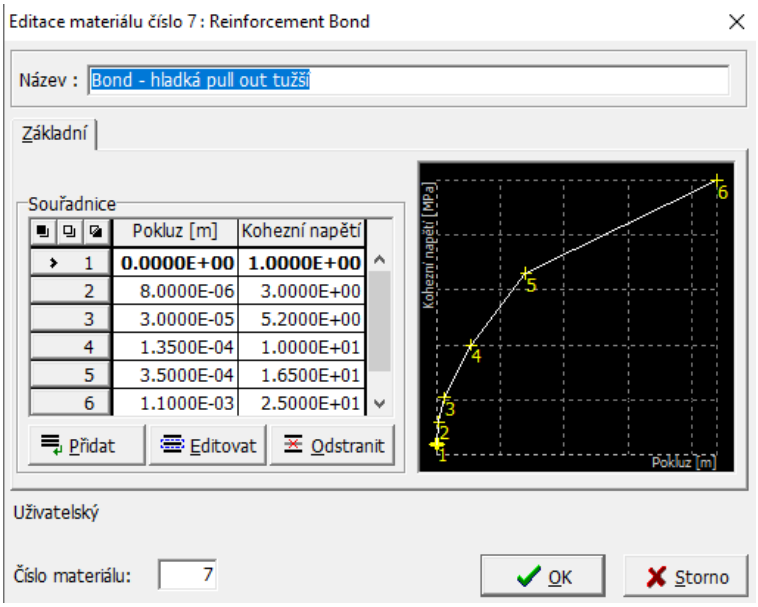

Fig. 43: Bond curve for specimens with smooth surface, medium soft version.

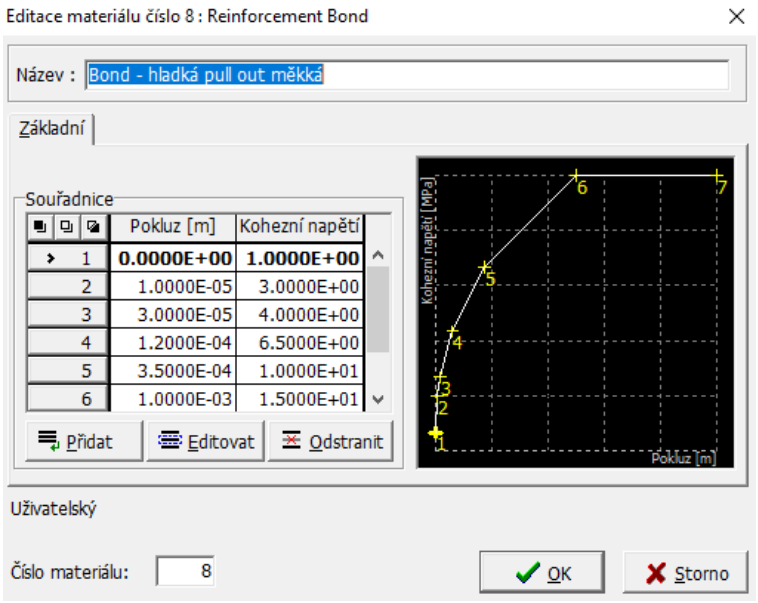

Fig. 44: Bond curve for specimens with smooth surface, soft version.

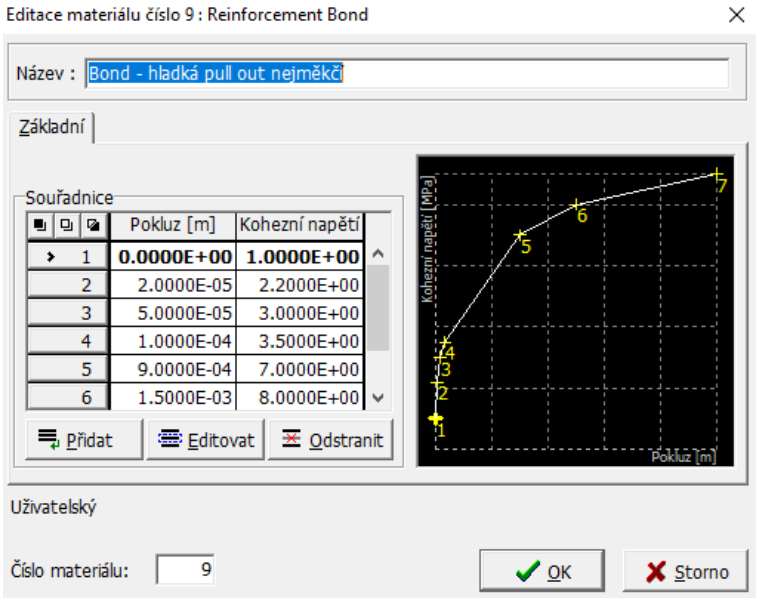

Fig. 45: Bond curve for specimens with smooth surface, ultra-soft version.

It depends on the amount of used epoxy resin, the viscosity of the epoxy resin, the time of application of the epoxy resin, the method of stretching of roving and so on. Therefore, it is necessary to define more curves according to the measured cohesion parameters from the pull-out test. Comparison of all four defined curves of cohesion (reinforcement bond) for a better idea of the considered joint stiffness is in the sum presented in Fig. 46.

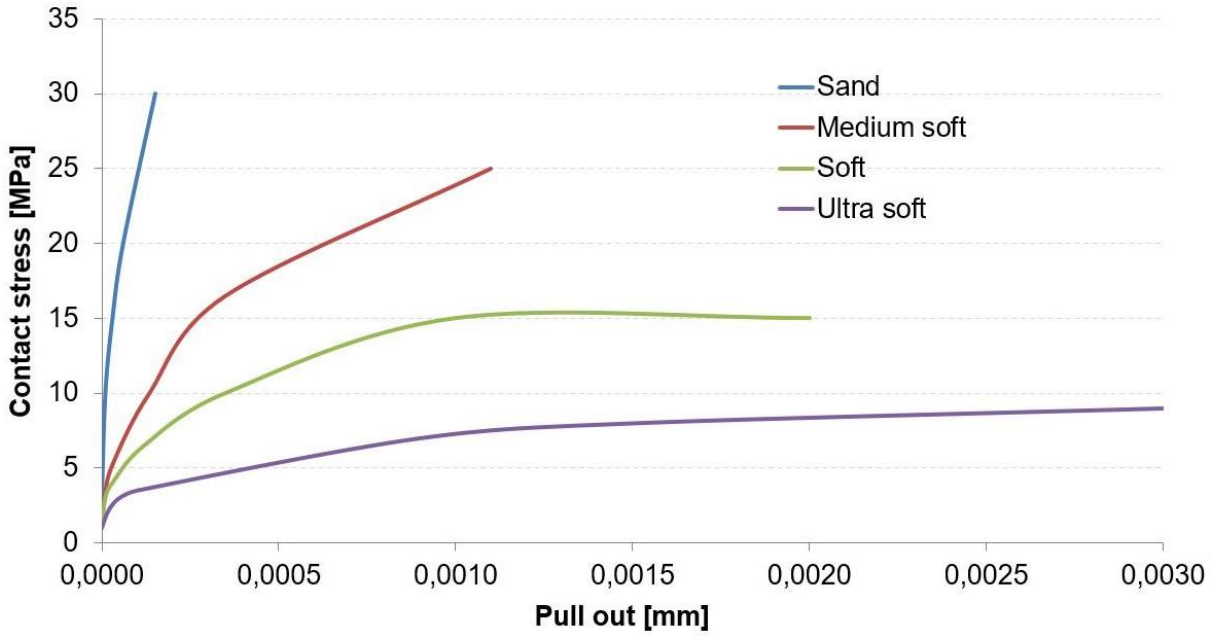

Fig. 46: Comparison of all defined curves of cohesion for a better idea of the considered joint stiffness.

4.2 Calibration of material parameters

4.2.1 Concrete – compression test model

The compression test of the pure HPC was modeled very simply using 2D programming environment by means of a concrete mass of corresponding dimensions with real experiment, into which a load was applied using two modeled solid steel plates. The model is presented below in the Fig. 47.

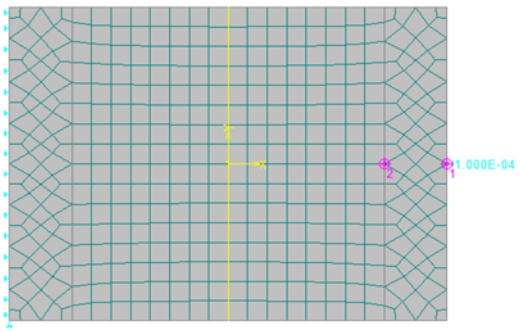

Fig. 47: 2D Model of compression test. FEM, monitors, axis and loading are shown.

The next Fig. 48 presents a view of a loaded concrete sample just before failure during the step 18. Presented value is Y displacement - perpendicular displacement from the axis of the applied load between steel supports. The numerical values of strengths and behavior are very similar to the behavior of really loaded specimens, which are described in the chapter 3.3.1.1. The selected and calculated input parameters of the HPC are correct from this point of view.

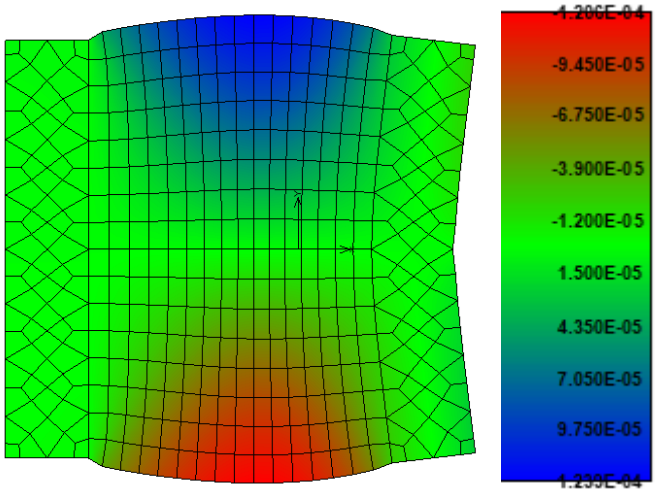

Fig. 48: Displacement Y during the concrete testing (step 18).

4.2.2 Concrete – tensile test model

The tensile test of the pure HPC without any reinforcement was modeled using ATENA 2D programming environment by means of a concrete mass of corresponding dimensions with real mechanical experiment. The concrete part is modeled from five polygons to create a regular network. One edge of the sample was fixed and the other side was defined by the prescribed edge shift in individual steps. The model is presented below in the Fig. 49.

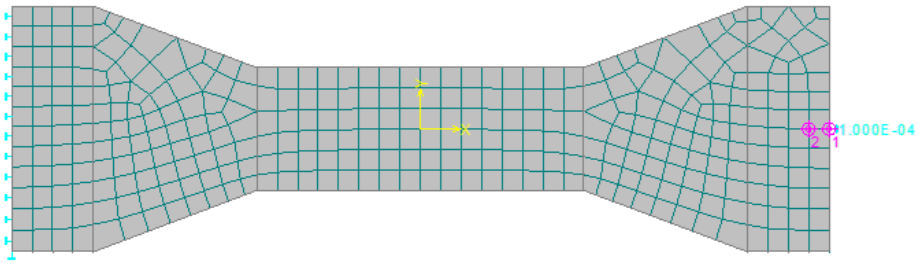

Fig. 49: Model of tensile test. FEM, monitors, axis and loading are shown.

Below in figures are presented example outputs from the program, just before the collapse of the sample and after the collapse of the sample. Prior to the collapse of the sample, the model showed a series of microcracks in the area around the change in the cross section of the sample (step 9). This was also the place where the sample subsequently collapsed (step 10). The presented quantities are displacement X in Fig. 50 and principal stress in Fig. 51.

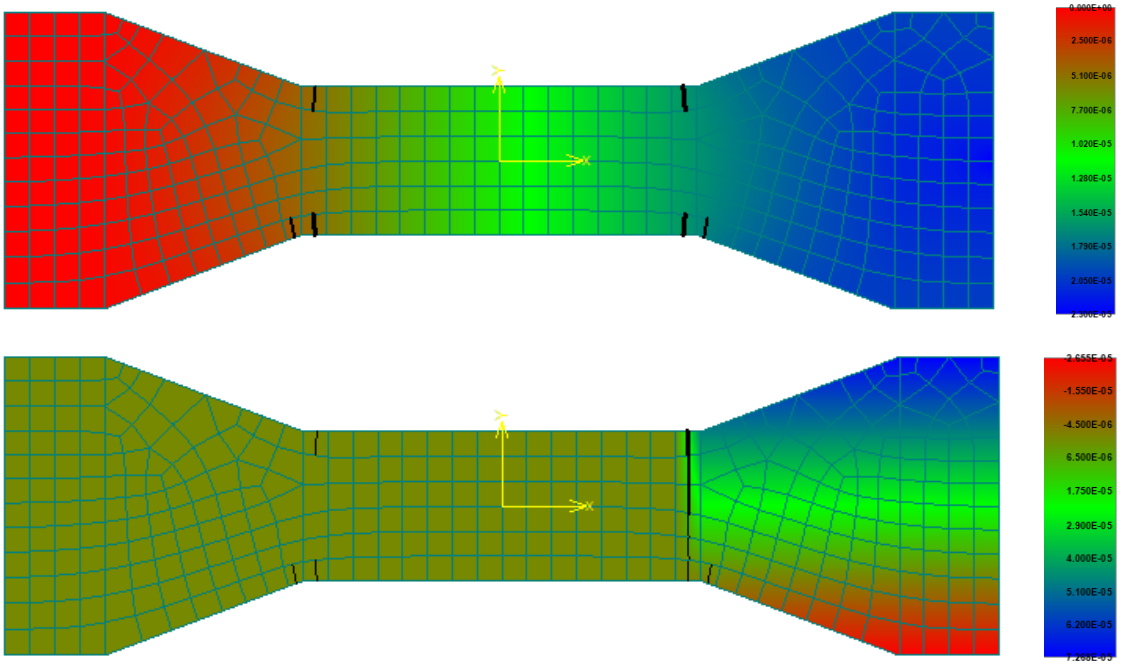

Fig. 50: Displacement X just before failure with first micro cracks (step 9) and below displacement X after cracking (step 10).

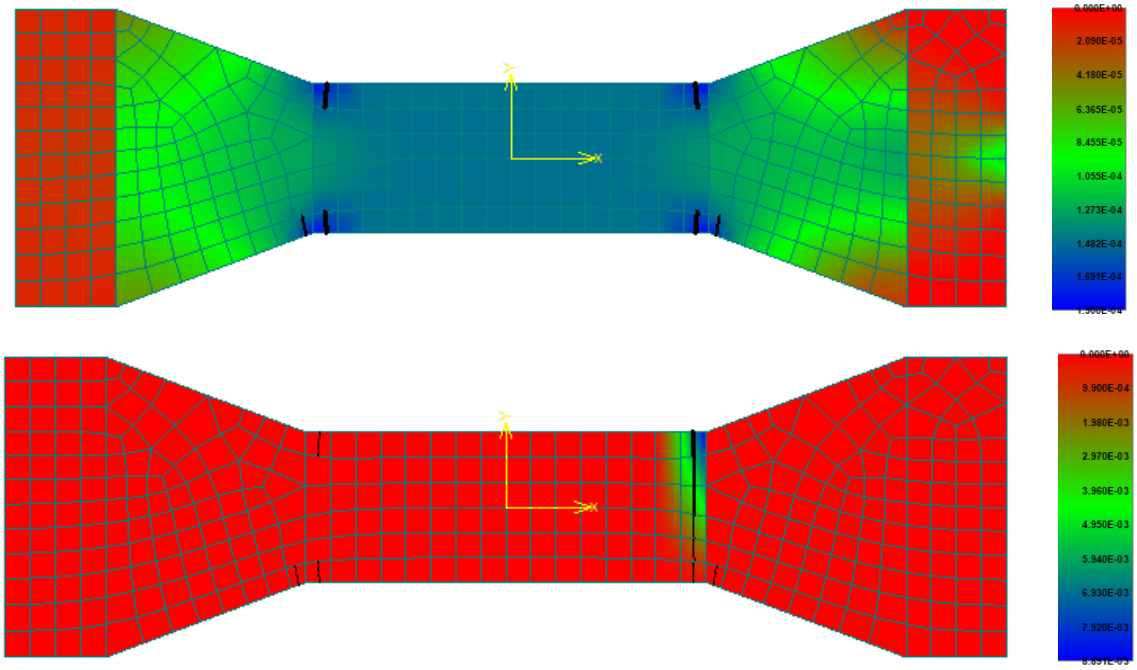

Fig. 51: Principal strain just before failure with first micro cracks (step 9) and below principal strain after cracking (step 10).

In this case of the tensile test of HPC concrete, the results of the numerical model are also identical to the results measured in a real mechanical experiment. The selected and calculated input parameters of the HPC are correct from this point of view.

4.2.3 Concrete – four-point bending test model

Model presented in Fig. 52 for basic material parameters calibration was already created using textile reinforced concrete samples. It means samples of HPC reinforced with textile reinforcement. This chapter is therefore also followed by a chapter 4.4. In is presented the basic model of four-point bending test using symmetry. The grid was gradually chosen so that it is a total of 13 points per sample thickness approximately 18 mm. This ensured sufficient accuracy of the results even with accurate micro cracks and cracks development.

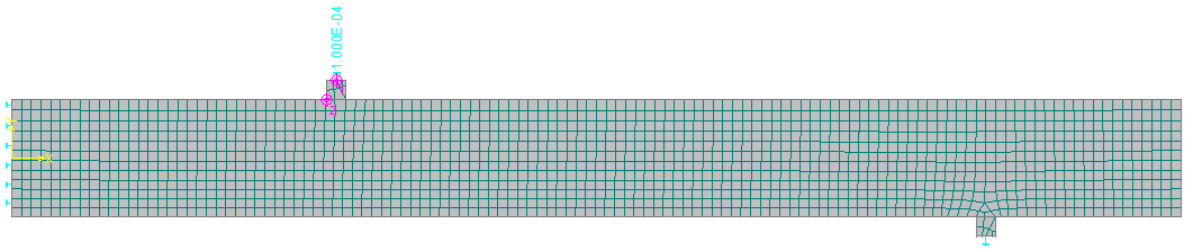

Fig. 52: Model of four-point bending test using symmetry. FEM, boundary conditions, monitors and loading are presented.

Fig. 53 and Fig. 54 present the moment at the beginning of loading process, when the slab behavior is more or less linear until the moment of the first crack initiation – opening. Thus, the cracks presented in the Fig. 53 and Fig. 54 are microcracks that are invisible to the naked eye. Principal tensile stress presented in Fig. 53 reaches the values of the defined tensile strength of concrete 7.0 MPa. In Fig. 54 is presented the principal strain before the moment of crack opening.

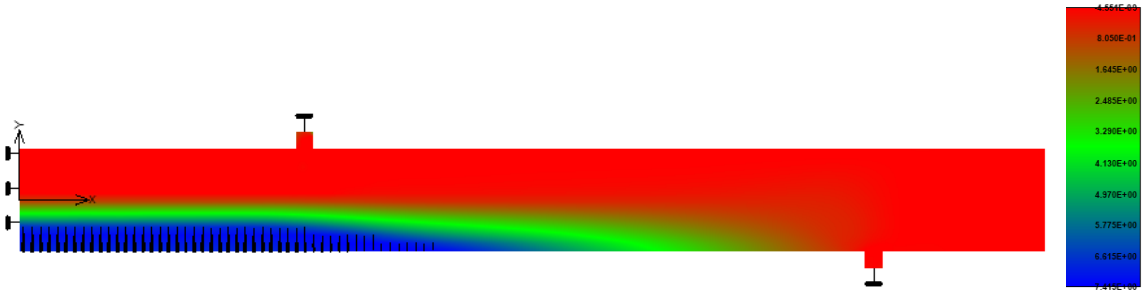

Fig. 53: Principal stress (tensile) before the moment of crack opening (step 14).

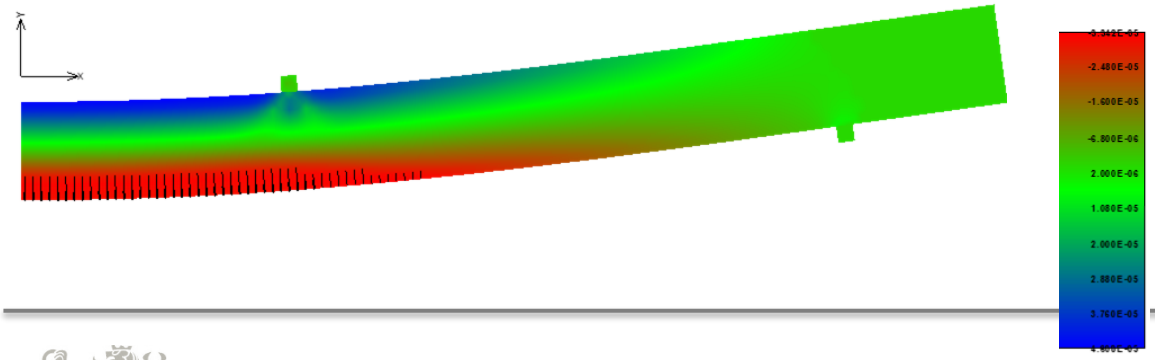

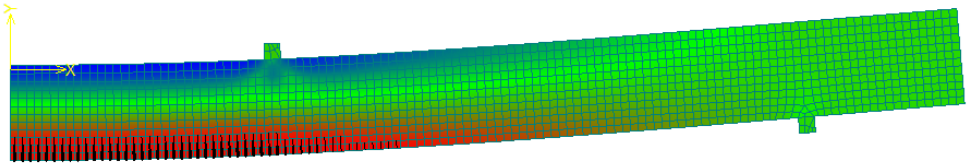

Fig. 54: Principal strain before the moment of crack opening (step 14).

Next figures represent the moment just after the first crack massive opening and reinforcement activation. In Fig. 55 is presented principal strain after the moment of the first crack opening (step 15). This first crack is typically located around the area of loading support and logically it is the dominant area of principal strain changes. In Fig. 56 is presented the crack width after the first crack opening, which is approximately according to the model $6 \cdot 10^{-6}$ m after the reinforcement activation. The load steps were modeled as an increase in deformation in steps as in the real loading test procedure.

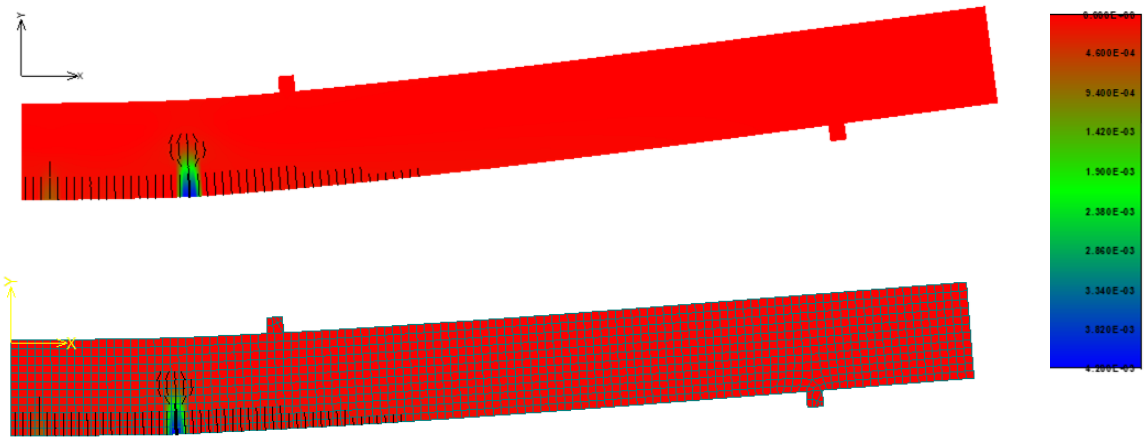

Fig. 55: Principal strain after the moment of the first crack opening (step 15) around the area of loading support.

Fig. 56: Crack width after the first crack opening (step 15).

The last Fig. 57 presents the principal strain after collapse in modeled step 28. It represents the slightly textile reinforced concrete slab presented for example in Fig. 86 with only two opened massive cracks under the loading support. So the modeled

behavior of slightly reinforced TRC slab was correct and it is possible to state that the material parameters of the model was calibrated for the next steps – cohesion parameters.

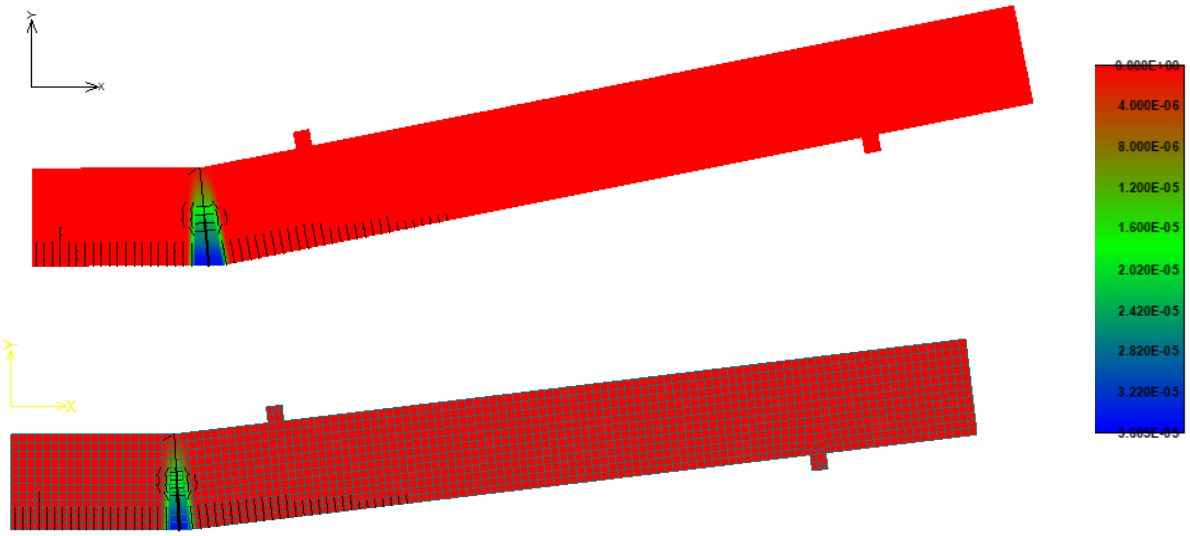

Fig. 57: Principal strain after collapse (step 28).

4.3 Calibration of bond behavior

For composite TR made from alkali resistant glass fibers and basalt fibers (basalt fibers are not included in this thesis) the modulus of elasticity decreases approximately to the values of the elastic modulus of HPC. Therefore, it is very important the knowledge of interaction conditions between both basic materials for accurately modelling of crack propagation and opening using analytical method or non-linear computational programs. This is a significant difference in comparison of technical fabrics with traditional steel reinforcement where are generally considered perfect interaction conditions in models between both materials with multiple cracking. The method will be logically applicable also to rovings made of materials with higher modulus of elasticity, typically carbon.

Two model calibrations for the two selected methods for determining the interaction conditions are described below. More attention is paid to the modified method inspired by ACI standard, which was used for validation of the final model of flexural test. It is important for verification, if measured curve from pull out test can be without major changes used directly as a reinforced bond for numerical modeling in ATENA Engineering, eventually other software.

4.3.1 Pull out test inspired by method from Dresden

As mentioned in chapter 3.3.3.1, the first pull out test method was inspired by [10] and was performed for the comparison with method according to the ACI standard. HPC plate has in the longitudinal direction one single penetrated roving with or without surface

treatment. This numerical simulation presents only results of roving without surface modification and with the surface treatment by silica sand with particle size 0.1 – 0.6 mm. It was mentioned that maximum tensile strength of roving with influence of polymer matrix was approximately 600 MPa, but the collapse was always in HPC part, reinforcement was never broken. The numerical model should confirm the unsuitability of this method and the damage in the concrete before reaching the tensile strength of the impregnated single roving. At the same time, model should also show the difference between a smooth surface and surface treatment using silica sand. In Fig. 58 is presented a view on the created numerical model with visible mesh. The mesh has a higher density of nodes in the monitored part of the reinforcement.

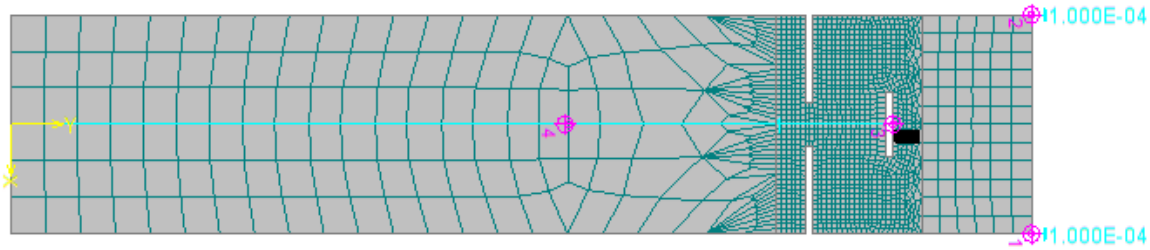

Fig. 58: Model of bond test (FEM, boundary conditions, monitors and loading are shown).

From results of experiments in chapter 3.3.3.1 it is known, it is not possible to examine the bond behavior until the moment when reinforcement is broken. Model confirmed with defined reinforcement bond that after the controlled crack initiation there is significant decrease of force during the loading process because of bad interaction of materials and the need for a large contact area for reinforcement activation. Area in the contact with concrete after the controlled crack formation is reduced during pulling out and there decrease of force until the end of testing procedure. But as mentioned in chapter 3.3.3.1, a short time after the first crack formation occurred concrete failure without higher slipping of composite reinforcement, so it would be very difficult to determine the reinforcement bond from this measurement using sophisticated analytic methods. This is the reason reinforcement bond curves from the pull-out test inspired by ACI standard were used as mentioned in chapter 4.1.3 about the reinforcement bond definition for model.

In Fig. 59 is presented model output with defined cohesion for smooth surface without any surface treatment. Left side presents model calculation step 81 just before moment of failure and right side of this picture presents model calculation step 82 just after the failure. Principal stress (a) indicates localization of collapse and it correspond with (c) displacement Y and visible modeled cracks. Stress (b) and bond slip (c) of reinforcement before the failure is also presented. In comparison of model crack development with pictures of damaged specimens presented in Fig. 20 is obvious that the model corresponds to the real course of the experiment.

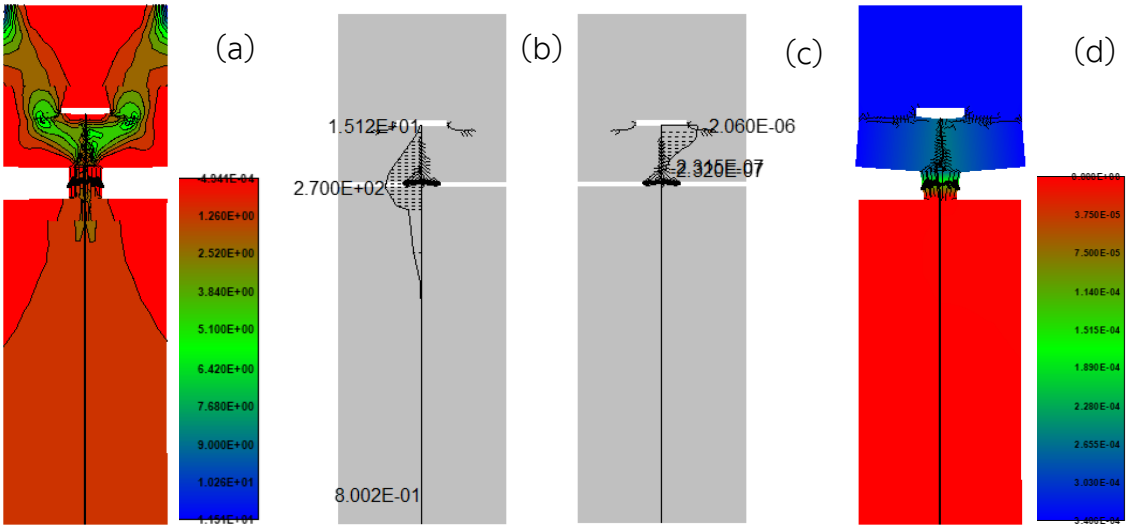

Fig. 59: Presented model with defined cohesion for smooth surface, principal stress in the step 81 just before failure (a), corresponding stress in single roving reinforcement (b) and bond slip (c), displacement Y in the step 82 after the failure around reinforcement (d).

In Fig. 60 is presented the next model output with perfect bonding. Left side presents model calculation step 78 in the moment of failure and right side presents model calculation step 10 after the first controlled crack initiation. Principal stresses are presented in (a) and (c) and corresponding reinforcement tensile stress in (b) and (d). In this case comparison of model crack development with real pictures presented in Fig. 20 also corresponds. Model is correct and for sure, this method is not suitable for determining of interaction conditions between the impregnated single roving and HPC matrix.

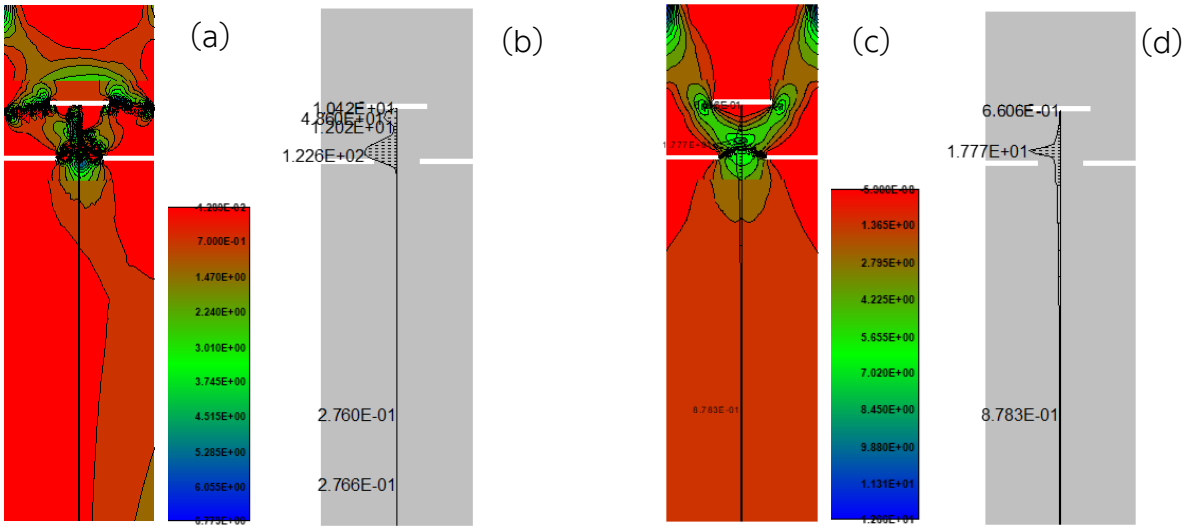

Fig. 60: Presented model with the perfect bonding, principal stress in the last step 78 (a), and corresponding stress in single roving reinforcement (b), principal stress in the step 10 (c) and corresponding stress in reinforcement (d).

Furthermore, the correction of steel part was also modeled. The small steel structure was a necessary part of the sample for its fixation to the jaws of test machine. This design could skew the measurement results compared to the model, where this design was not considered. Therefore, the model was created separately and the value of the deformation of the steel was subtracted from the slip of the reinforcement depending on the magnitude of the loading force – reaction. Model of steel part for correction of pull-out values is presented in Fig. 61, presented is principal strain and displacement.

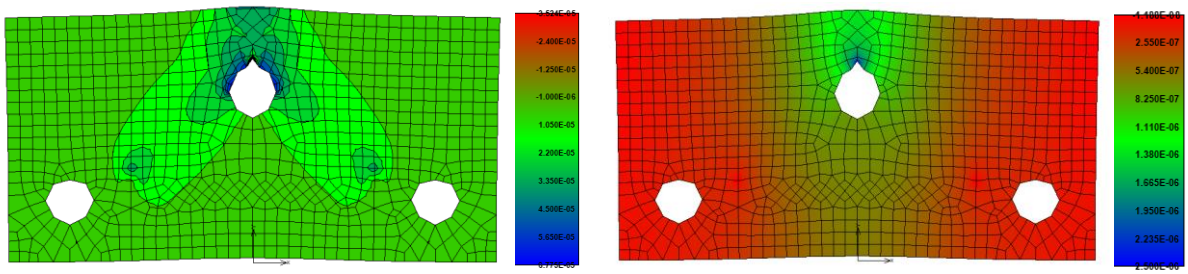

Fig. 61: Steel parts for sample fixing – curve distortion verification, principal strain in step 25 (left) and displacement Y in step 25 (right).

4.3.2 Pull out test according to the ACI standard

The second pull out method inspired by ACI standard was focused on complete curve of reinforcement bond behavior with a simple interpretation. Epoxy sleeve was installed only on one side of single roving because of the safe fixing to the testing machine jaw without damaging of the impregnated yarn. Presented concrete part has a constant dimensions 100 x 100 mm and optimized thickness for presented single AR-glass impregnated roving 20 mm. The same dimensions were used in the numerical model. The distance between epoxy sleeve and concrete part could not be modeled, because reinforcement must be placed into the macro-element. So this part of free reinforcement was not modeled and epoxy part was int contact with concrete part as visible in Fig. 62, but without any bond. Reinforcement in the epoxy sleeve was modeled with perfect bonding. Monitored parameters were the reaction in the point of loading and pull-out. Not all models and material variants are presented, only the most interesting or representative models.

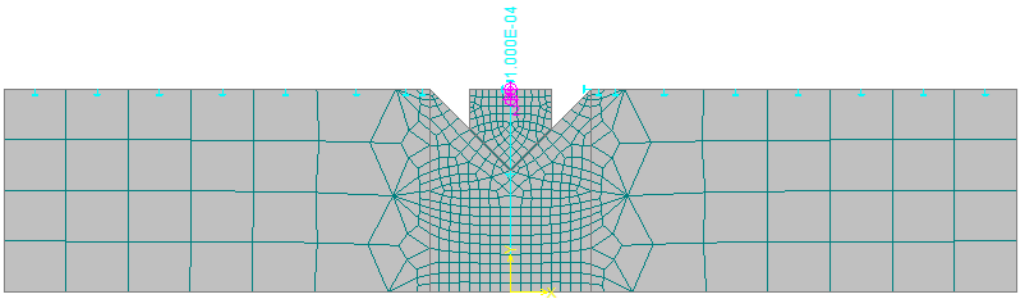

Fig. 62: Model of bond test (FEM, boundary conditions, monitors and loading are shown).

The first was modeled the linear reinforcement bond defined by two points with the stiffness of silica sand as a surface treatment. In Fig. 63, Fig. 64 and Fig. 65 are presented

gradually loading steps 15, 44 and 63. In all three figures are presented parameters compressive principal stress and reinforcement tensile stress. As visible in figures, reinforcement was gradually activated with more and more loading steps. During the loading are visible some cracks in the upper part of concrete specimens, but without bigger damage. This is the positive effect of shear cone, so the length of reinforcement in the contact with concrete is constant during the loading procedure, as confirmed by model.

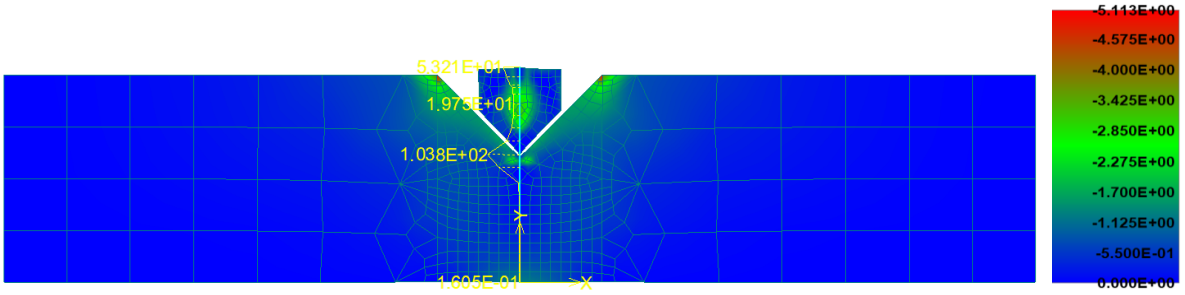

Fig. 63: Compressive principal stress [MPa] and reinforcement stress [m] (step 15).

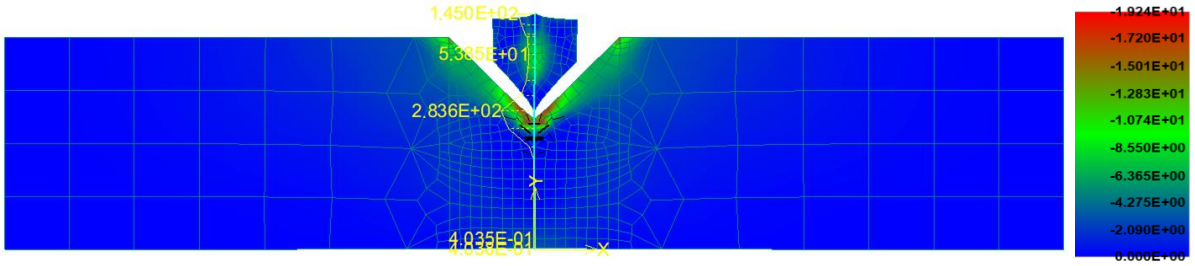

Fig. 64: Compressive principal stress [MPa] and reinforcement stress [m] (step 44).

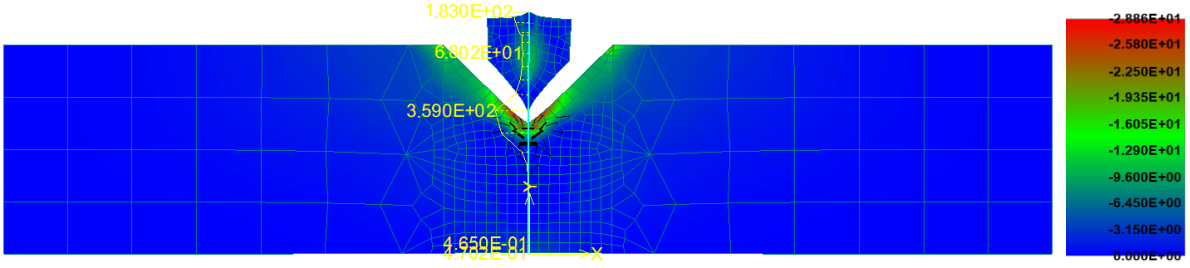

Fig. 65: Compressive principal stress [MPa] and reinforcement stress [m] (last step 63).

Next model presents results of modeled reinforcement bond "medium soft". Similarly like in previous case, in Fig. 66, Fig. 67, Fig. 68 and Fig. 69 are presented gradually loading steps 35, 160, 222 and 240. With lover stiffness of reinforcement bond more steps was done because of longer reinforcement activation. In all four figures are presented parameters compressive principal stress and reinforcement delta slip. As visible in figures, reinforcement was again gradually activated with more and more steps. Delta slip is without big differences in values on both ends, so it confirms the idea of applying the measured curve directly as a reinforcement bond to the model. During the step 222

it is visible lower delta slip around upper surface because of the crack development in this area. Model provides insight into the structure.

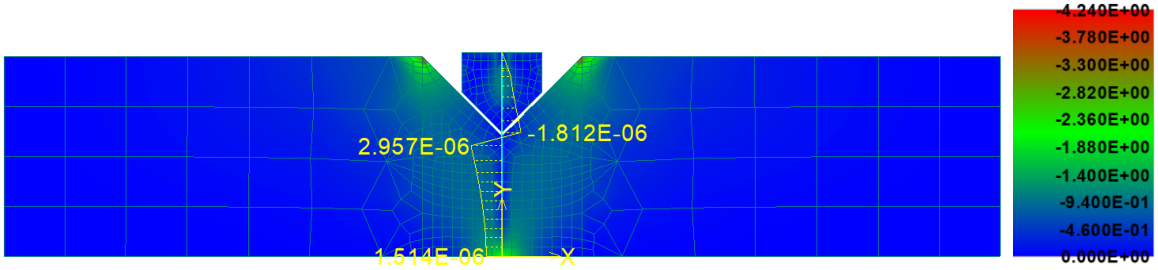

Fig. 66: Compressive principal stress [MPa] and reinforcement delta slip [m] (step 35).

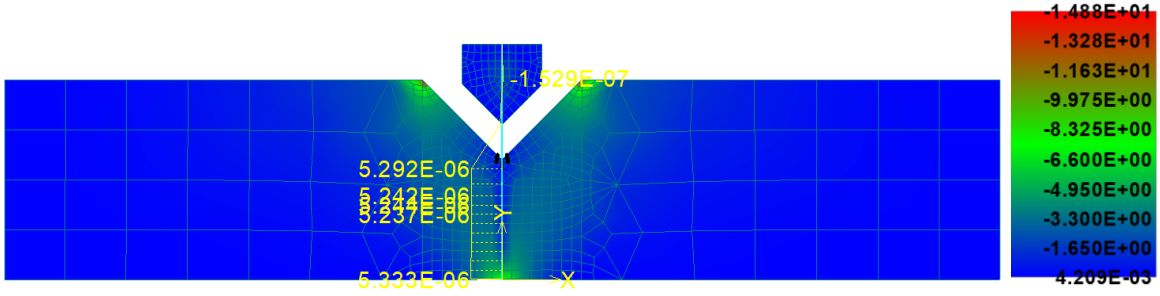

Fig. 67: Compressive principal stress [MPa] and reinforcement delta slip [m] (step 160).

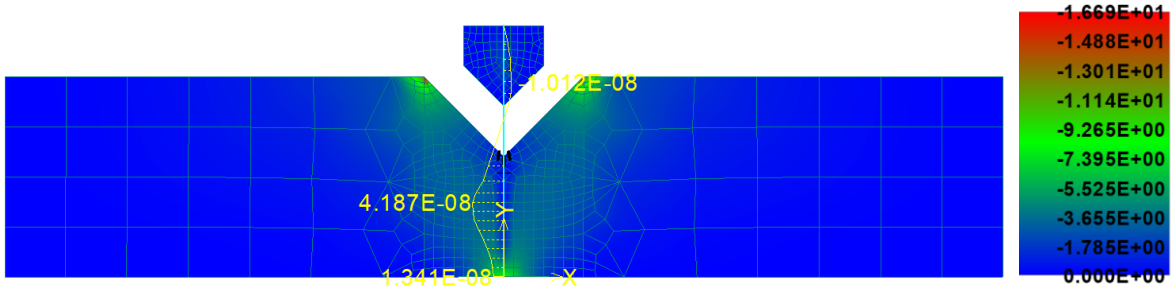

Fig. 68: Compressive principal stress [MPa] and reinforcement delta slip [m] (step 222).

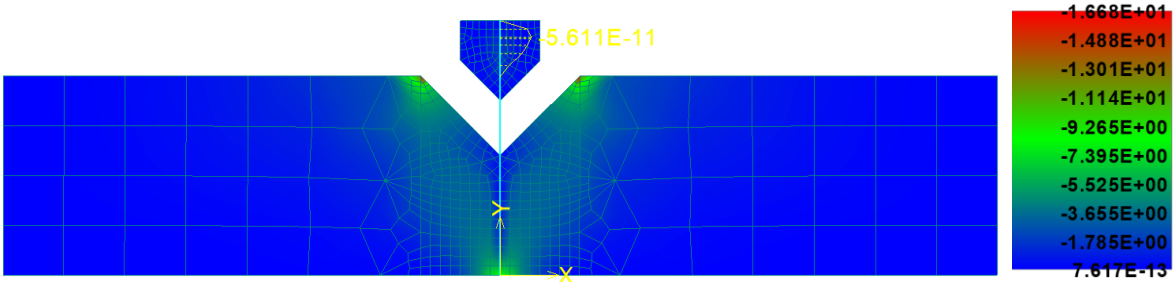

Fig. 69: Compressive principal stress [MPa] and reinforcement delta slip [m] (step 240).

In Fig. 70 is presented the reinforcement total slip, which is more important, with compressive principal stress. As visible total slip in model reached of value almost millimeter, which correspond with measured values.

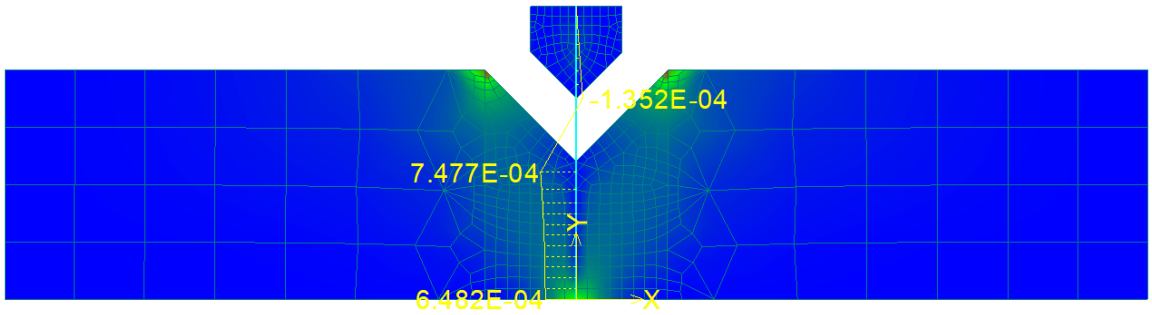

Fig. 70: Reinforcement total slip [m] (step 240).

In Fig. 71 and Fig. 72 are presented reinforcement parameters during the modeled loading process for more visible comparison of difference in loading steps. Presented parameters are contact stress in the bond area and tensile stress in the reinforcement. It is visible almost constant shape of contact stress in the concrete part, which suggests bad interaction conditions.

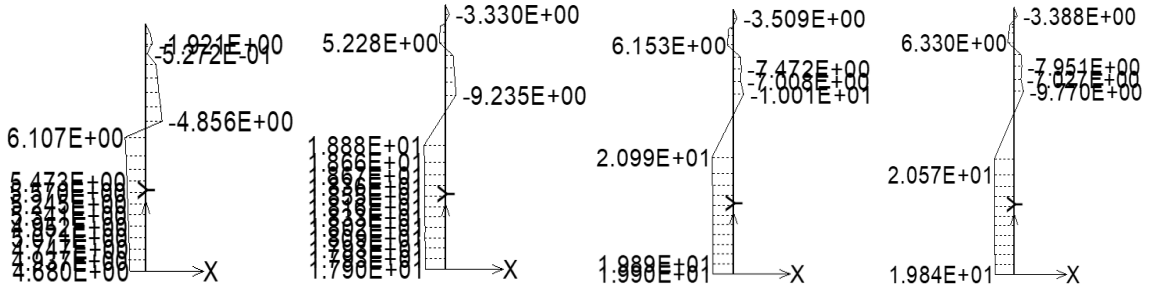

Step 35 Step 160 Step 222 Step 240

Fig. 71: Stress of bond during the loading.

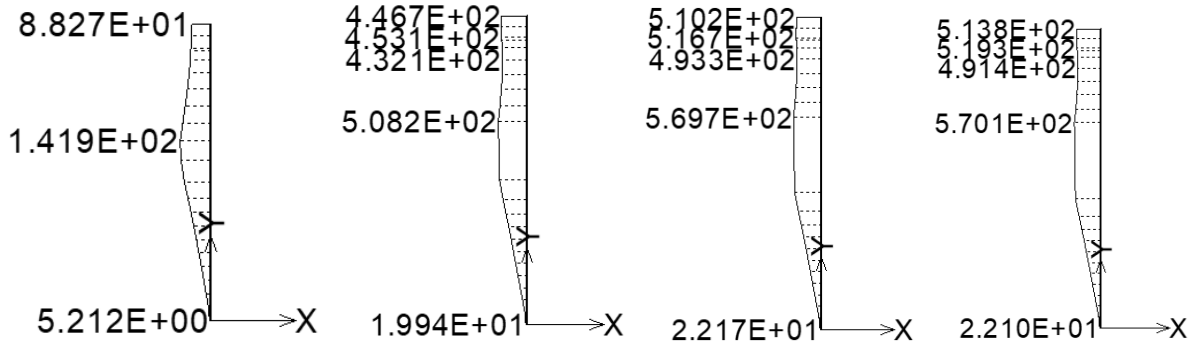

Step 35 Step 160 Step 222 Step 240

Fig. 72: Stress of reinforcement during the loading.

Next model in Fig. 73, Fig. 74, Fig. 75, Fig. 76 and Fig. 77 presents results of modeled reinforcement bond "sand", which represent the measured pull-out curve with the surface treatment using silica sand, see chapter 4.1.3. Similarly like in previous case, in are

presented gradually loading steps 40, 95, 100, 110 and 240. In all four figures are presented parameters compressive principal stress and reinforcement delta slip, in the last figure total slip. As visible in figures, reinforcement was again gradually activated with more and more steps. Pull-out of reinforcement is much lower in comparison with previous case of lower reinforcement bond. The model corresponds to the assumption.

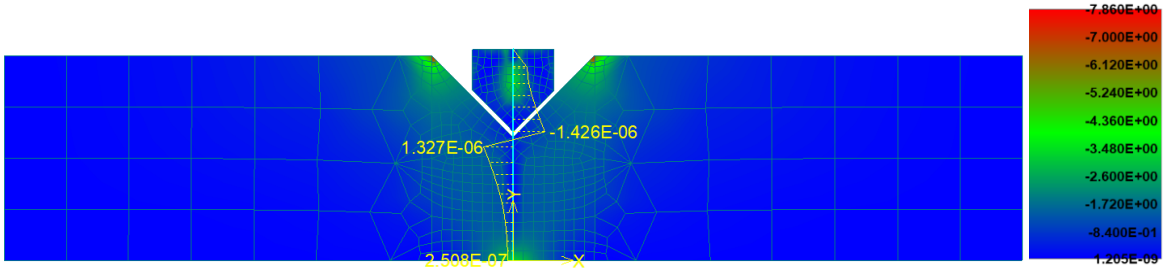

Fig. 73: Compressive principal stress [MPa] and reinforcement delta slip [m] (step 40).

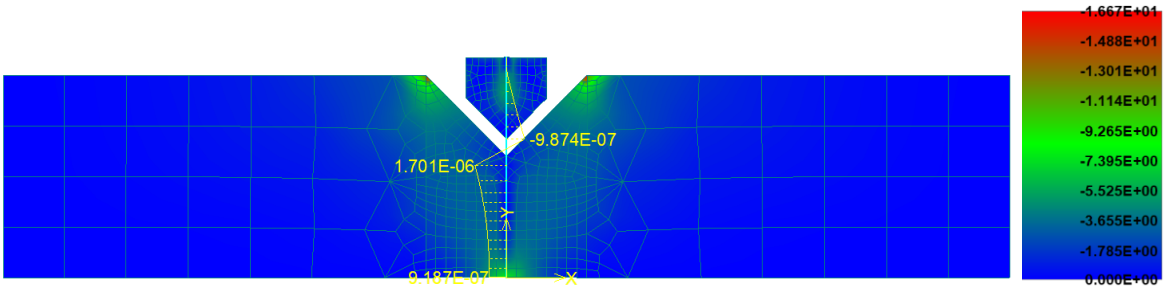

Fig. 74: Compressive principal stress [MPa] and reinforcement delta slip [m] (step 95).

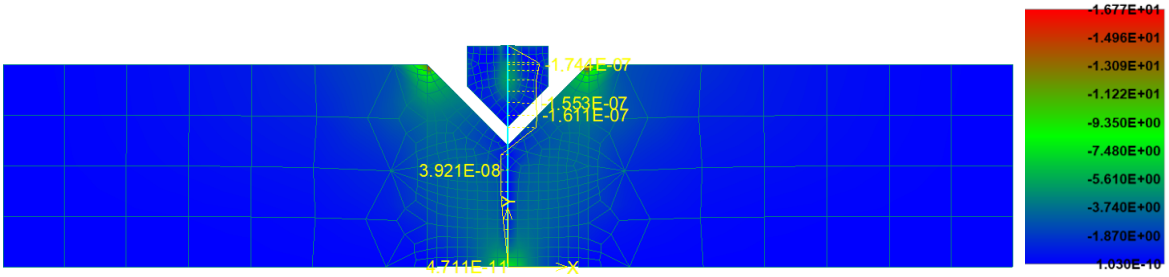

Fig. 75: Compressive principal stress [MPa] and reinforcement delta slip [m] (step 100).

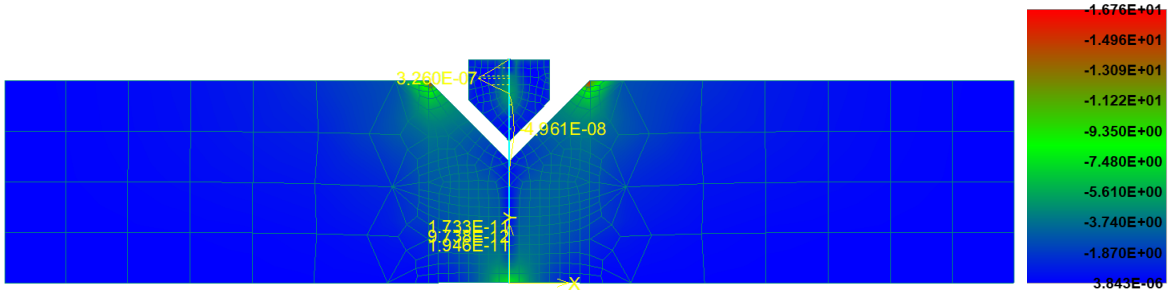

Fig. 76: Compressive principal stress [MPa] and reinforcement delta slip [m] (step 110).

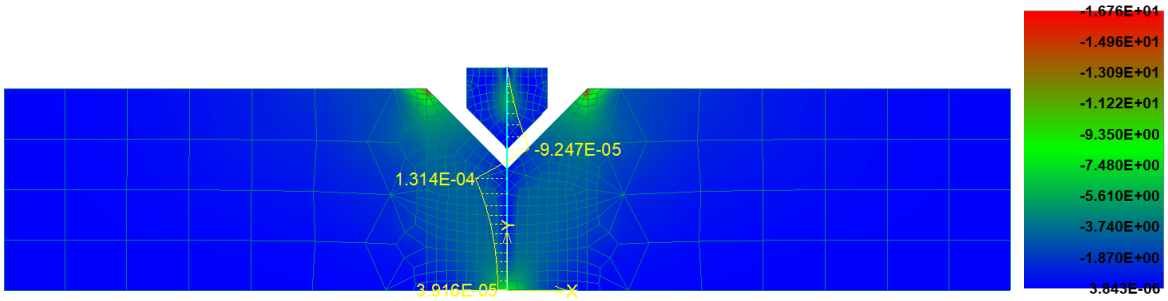

Fig. 77: Reinforcement total slip [m] in the last step (step 240).

In Fig. 78 and Fig. 79 are presented again reinforcement parameters during the modeled loading process for more visible comparison of difference in loading steps. Presented parameters are contact stress in the bond area and tensile stress in the reinforcement. It is visible not constant like in previous case, but almost linear shape of contact stress in the concrete part. It suggests the good interaction conditions.

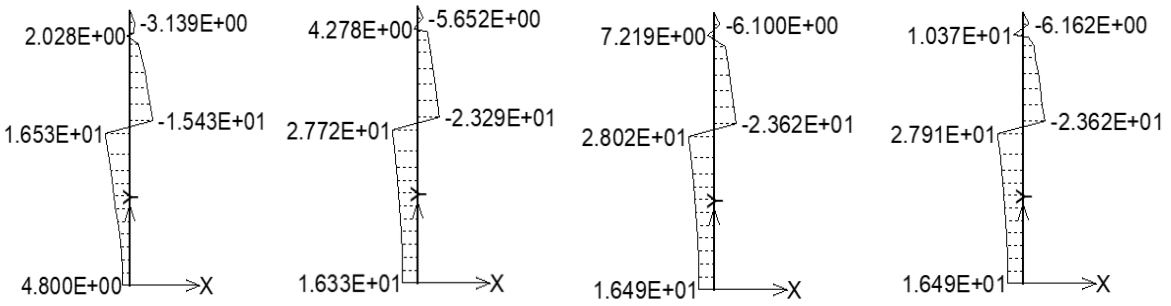

Step 40 Step 95 Step 100 Step 110

Fig. 78: Stress of bond during the loading.

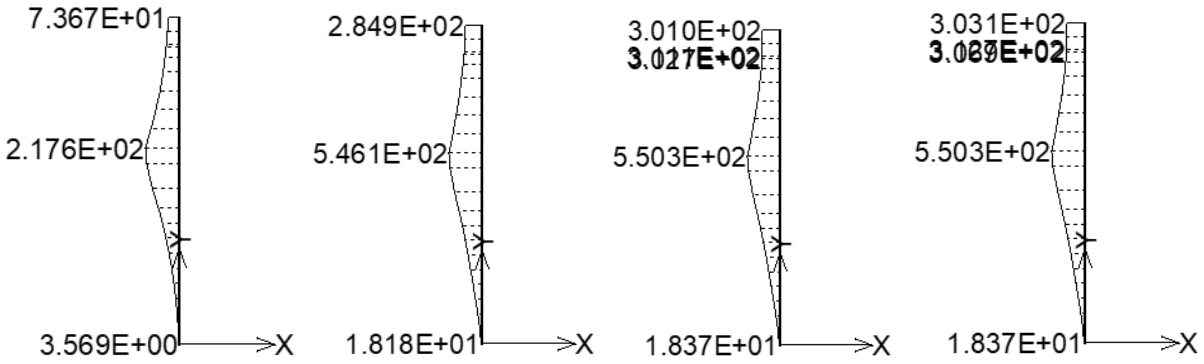

Step 35 Step 160 Step 222 Step 240

Fig. 79: Stress of reinforcement during the loading.

Finally, two resulted graphs are presented in the form of contact stress and pull-out curves during the process of loading and modeling for comparison of both results. Model and experiment in great accordance as presented in Fig. 80 and Fig. 81. Very interesting

is comparison of defined reinforcement bond (green lines) with modeled pull-out tests and it is necessary some description of curves. Atena 1 with corresponding green line represents the "Ultra-soft" reinforcement bond, Atena 2 with corresponding green line is the "Soft" reinforcement bond, Atena 3 with corresponding green line is the "Medium-soft" reinforcement bond, Atena 4 with corresponding green line is the "sand" reinforcement bond with the surface treatment. The last almost vertical green line and Atena model 5 represent the primitive reinforcement bond definition using two points, almost perfect bonding.

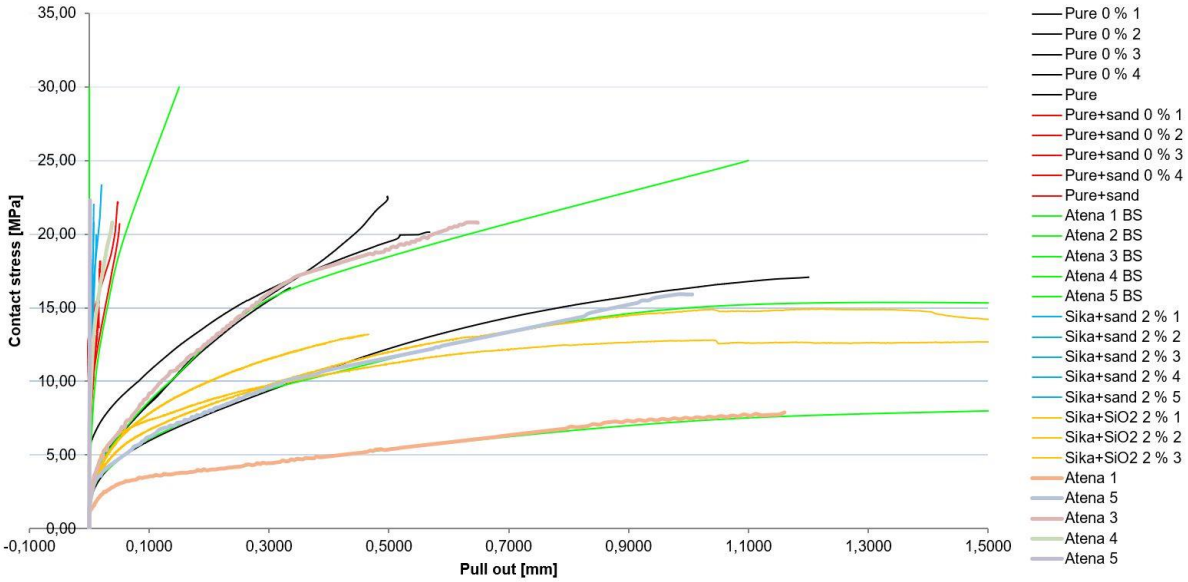

Fig. 80: Contact stress and pull out curves during the loading and modeling for comparison of both results. Model and experiment in accordance.

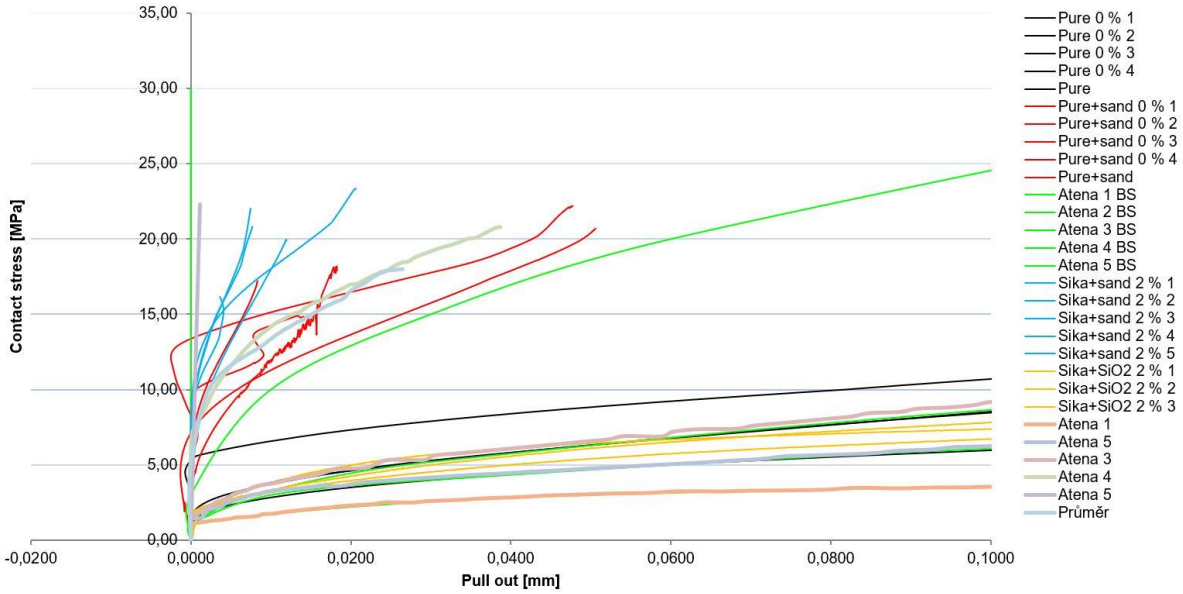

Fig. 81: Contact stress during the loading and modeling in comparison, pull out is limited by value 0,1 for more visible results of specimens with surface modification.

In Fig. 81 is presented the same graph, only x axis is limited to the value only 0.1 mm. Than results of models and experiments of specimens with the surface treatment are more visible. In this case is also presented good accuracy of the result and model with material parameters. It is possible to say that the model was calibrated with defined material parameters of concrete and reinforcement and various defined parameters of reinforcement bond.

4.3.3 Support modelling

It has already been explained above why the knowledge of interaction and bond behavior is so important. If the amount of reinforcement with similar elastic modulus like concrete part is lower in cross sectional area, the accurately modelling of crack propagation and opening is very important with precise locations of the first crack. This is especially the problem of slightly reinforced TRC elements with only two or one layer of TR with small amount of rovings in cross sectional area. It is a reason of plastic joints initiation under the loading supports. For slightly reinforced concrete elements are monitored parameters better visible especially interaction between reinforcement and used cementitious composite. The load transfer to the concrete element from the testing machine is typically modeled using some small steel plate with perfect bonding in contact area. But this small steel plate can adversely affect the location of the first initiated crack in the four-point bend test. This chapter presents the difference in results if we insert another flexible plate in model between the steel plate and the concrete element with a small defined stiffness [31].

The task was modeled using symmetry of four-point bending test in 2D surface of ATENA software for its size reducing. HPC was modeled using topology tool Macro-element and the textile reinforcement was modeled using topology tool Bar reinforcement as mentioned also with all next material parameters in chapter 4.1. The thickness of concrete macro-element in the Z-axis direction was defined 100 mm respected the real size of samples and the reinforcement cross-sectional area was defined 8.8 mm^2 for one layer both according to the experimental specimens. The support was modeled in two versions. The first one was modeled as a steel plate with defined cross-sectional area 4 x 8 mm in the Z direction with the same thickness 100 mm. This version represented traditional model for load transmission to the concrete part. The second one was also modeled as a steel plate with defined cross-sectional area only 2 x 8 mm and same thickness in Z direction but also with a second elastic plate with identical dimensions inserted between steel plate and concrete specimen. The elasticity modulus of elastic soft plate was defined only 1.0 GPa [31]. Numerical model, axis orientation and details of supports are closer present in Fig. 82.

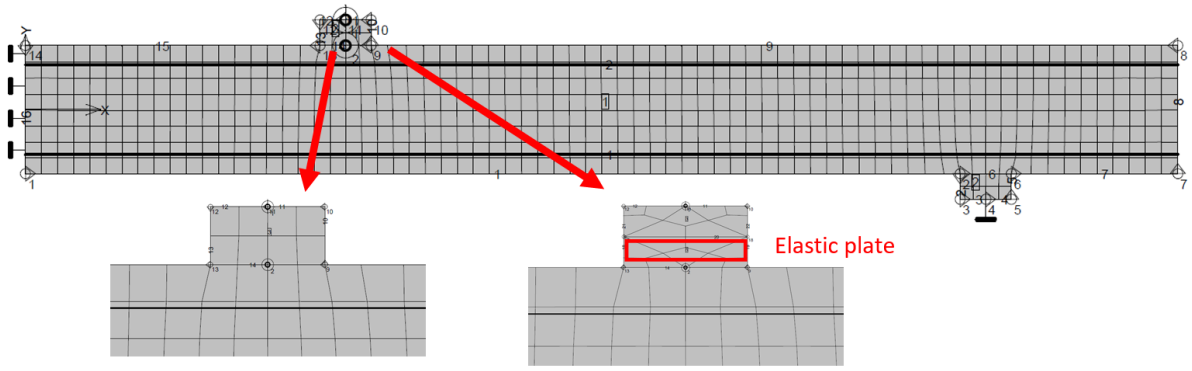

Fig. 82: View on geometry of model included generated finite element grid, detailed view on the steel plate (left) and steel plate with inserted soft elastic plate (right) [31].

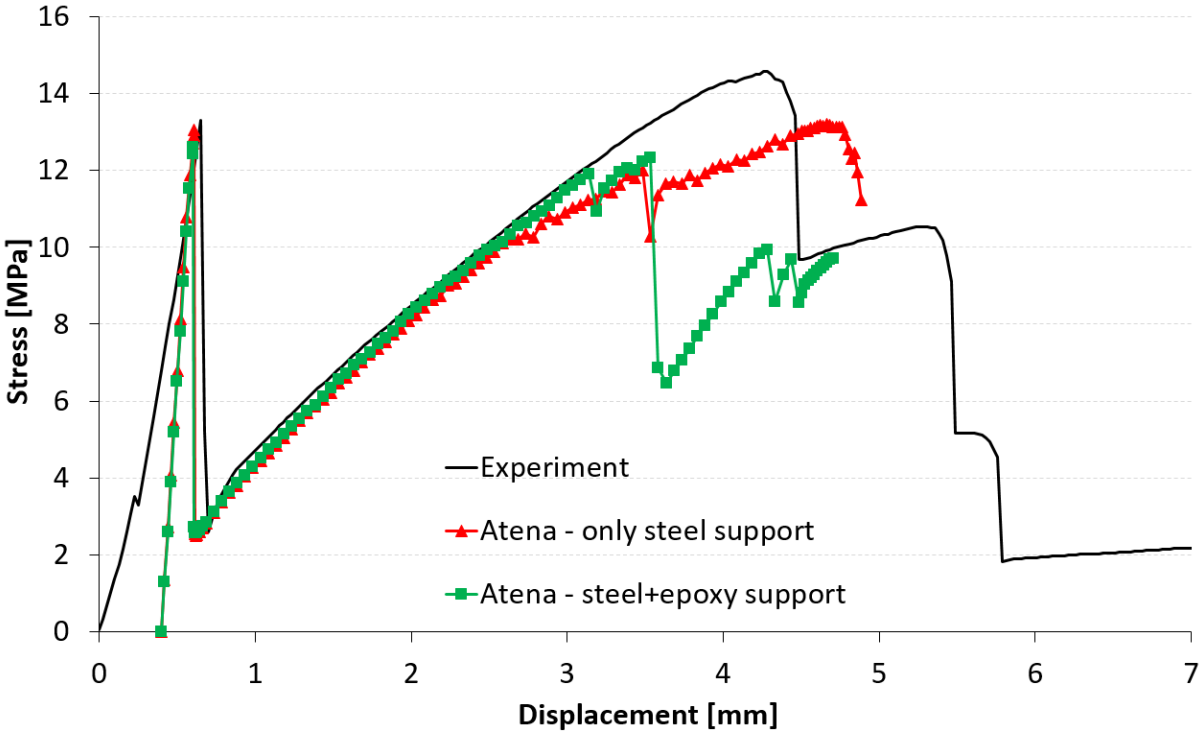

Fig. 83: Results of four point bending test. Comparison of experimental results with two variants of supports used in numerical model, pure steel and with inserted soft plate [31].

Both experimental results of four-point bending test and results of numerical modelling with two variants are presented in Fig. 2. For experimental results are characteristic two cracks under the loading supports and their opening until the specimen collapses. Sometimes only one crack can be initiated as presented also in Fig. 2. This happened due to more facts: incorrect position of reinforcement and different concrete cover, variable thickness of specimen, very bad interaction between composite reinforcement and cementitious matrix and small amount of reinforcement in cross-sectional area of specimen. On the other side especially in the case of good materials interaction reinforcement pulling out is not so significant and it leads to the third crack initiation in

the middle of specimen before its collapse. The case of third crack is not presented in Fig. 2. It is clear especially material interaction conditions are not constant for this type of impregnated textile reinforcement and crack initiation and opening is also slightly different. Fig. 2 presents great precision of numerical model during the crack opening of the slightly reinforced HPC and thus confirming the correctness of specified material parameters. The curves obtained from ATENA Engineering program are only shifted to the point of the first crack initiation because it is not possible to easily model the starting process of loading and all imperfections. The first crack initiation and its opening does not affect the simplification of the model using symmetry of four-point bending test [31].

In Fig. 83 is also presented that inserted soft elastic plate between steel plate and HPC specimen has no effect on the crack opening because the displacement monitor is located on the top surface of textile reinforced concrete specimen. Support modification did not affect the displacement and size of reaction, but it significantly influences the first crack location and further principal stresses development as seen in the various model damaging at the end of the loading process in Fig. 83. This effect is better presented in Fig. 84 with detailed view of the horizontal deformation around the area of loading support for both variant. Rigid joint of steel plate and HPC specimen (a) prevents natural deformation of the specimen during four-point bending test procedure and it leads to slight increase of bending stress in the middle area of specimens and due to increase the likelihood of bad location of the first crack. Simply designed and modeled modification wit inserted soft elastic plate (b) has no problem with both horizontal and vertical deformation and cross-sectional area is without any additional bending stress. The first crack is in numerical model always located just under the loading support exactly like during experiment [31].

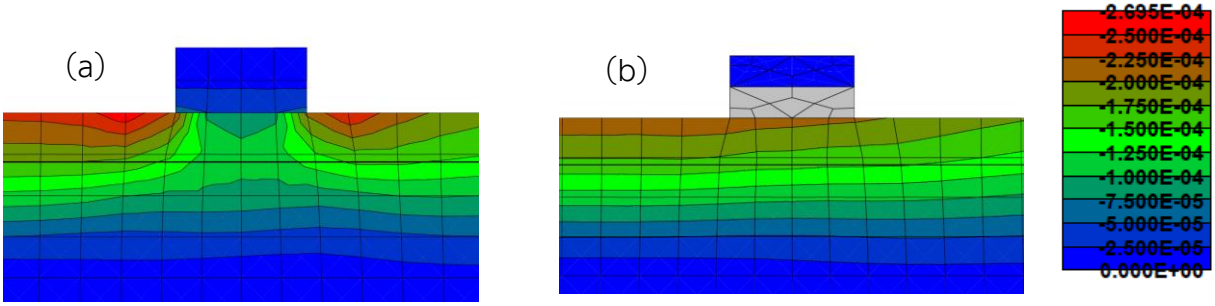

Fig. 84: Detailed view of the horizontal deformation around the loading support for the same reaction just before the first crack initiation for pure steel plate (a) and steel plate with inserted soft elastic plate (b) [31].

The first crack localization in models with different types of supports is presented in Fig. 85 with principal stresses and drawn cracks development. Invisible micro cracks begin to form in the part with tensile stresses (a) just before the first crack initiation is initiated at the first sight similarly for both modeled supports. For the pure steel support (b) the first crack is initiated depending on the mesh density and on the top support dimensions randomly and unrealistically somewhere in the area between the loading support and

the symmetry axis. Numbers around the crack (b), (c) represent debonding just after the first crack initiation. Simple modification using soft inserted elastic plate stabilize results and the first crack location also for different mesh density. As mentioned above the first crack is always located just under the area of loading support using soft inserted plate. In Fig. 86 is presented a picture of the real loading process of experimental panel where two typical open cracks are visible in the area of the loading supports and creation of plastic joints [31].

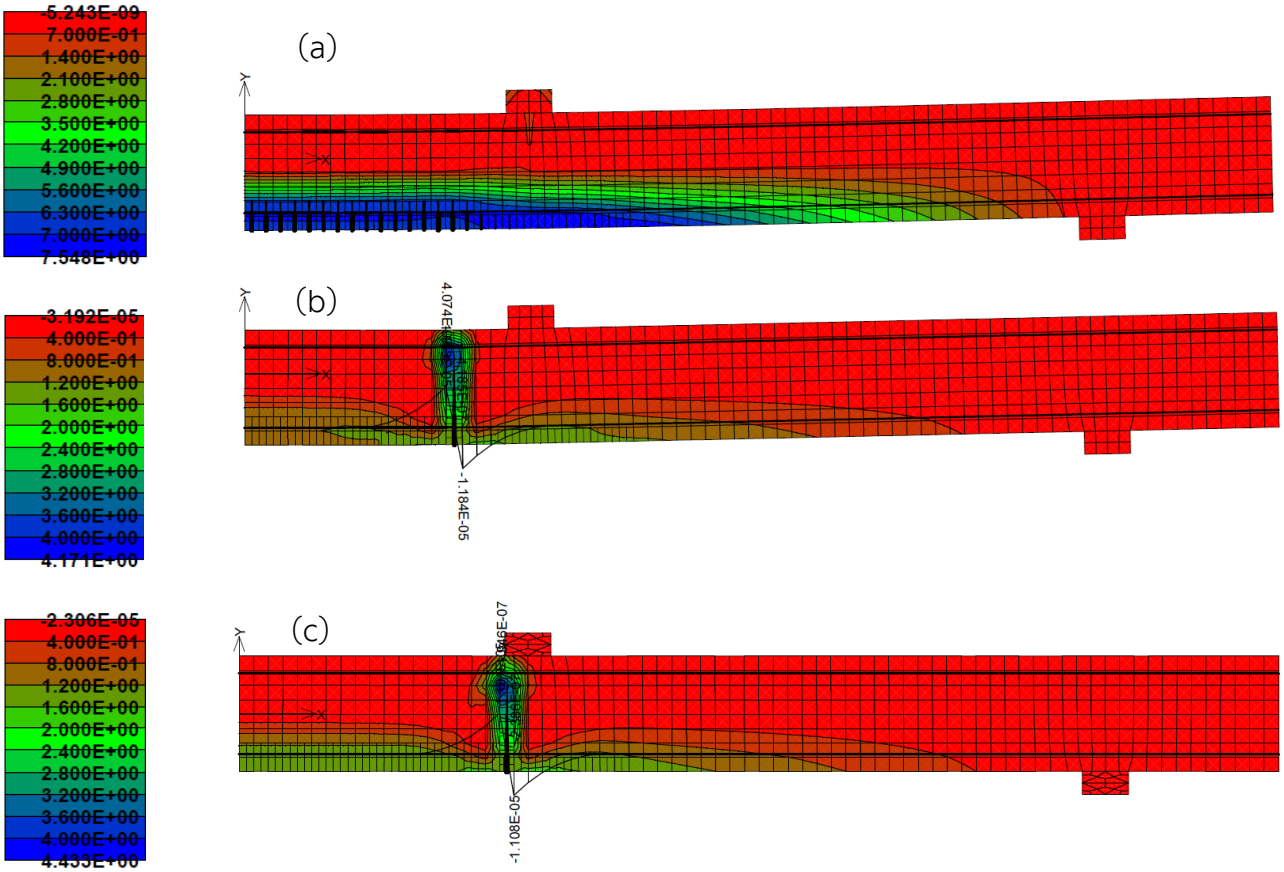

Fig. 85: View of the model with principal stresses before the first crack initiation (a), after the first crack initiation outside of the support area in the case of pure steel support (b) and under the loading support in the case of steel plate with inserted soft elastic plate (c) [31].

It is also necessary to mention inaccuracies of presented model. In the case of slightly reinforced concrete in the plastic joint area the collapse was not precisely modeled even though using of elastic plate inserted under the dispensing steel plate improved the results. The reinforcement was broken in the experiment but in the numerical model was previously damaged the concrete part. During the plastic joint opening the angle is large because of the thickness and HPC compression part is thus extremely low compared to the traditional concrete. The upper edge is crushed but the cross section was able to continue in the load transfer. This phenomenon is not captured in presented model. The

purpose of this experiment and its numerical model with slightly reinforced HPC was to validation of material parameters for further research. The aim is efficiently design of the reinforcement so that after the first crack initiation there is no reaction reduction and with increasing deformation occurred multiple cracking. Plastic joints in final applications are not desirable [31].

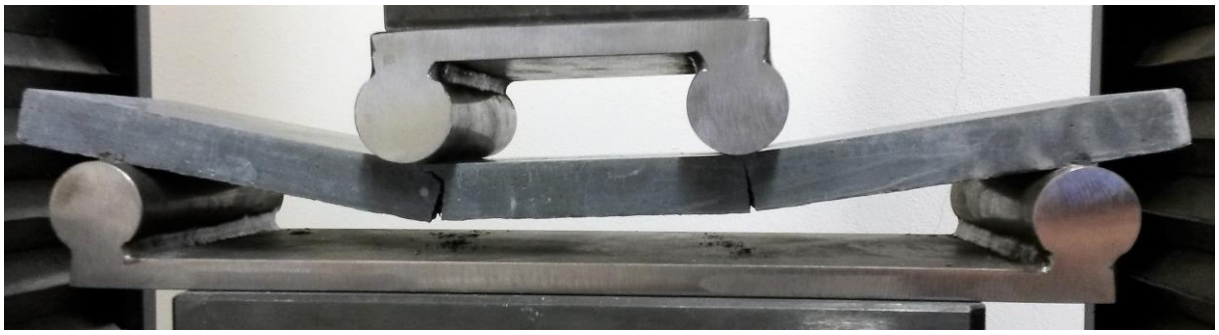

Fig. 86: View of the formed plastic joints under the loading support during mechanical experiment of slightly textile reinforced concrete slab [31].

4.4 Validation of model parameters on four-point bending test

In particular, the basic strength properties of both considered materials and interaction conditions between technical fabric and HPC were studied using most often direct uniaxial tensile test.

4.4.1 Model with 5 roving, considered "Medium soft" reinforcement bond

Model presented in previous chapter for calibration of four-point bending test was also used for the validation of material parameters and parameters of defined reinforcement bond curves based on the experimental results of pull-out test. The grid was gradually chosen so that it is a total of 13 points per sample thickness approximately 18 mm. This ensured sufficient accuracy of the results even with accurate micro cracks and cracks development. The model was created using symmetry of four-point bending test. For all material options presented in next chapters will be the model same. Soft insert under the loading support was also created for better results. Model is visible in Fig. 87.

In this first presented model of four-point bending test was considered two layers of reinforcement with five roving in each layer. As a reinforcement bond for this presented option was selected "Medium soft" curve presented in previous chapter about the material parameters – cohesion – reinforcement bond.

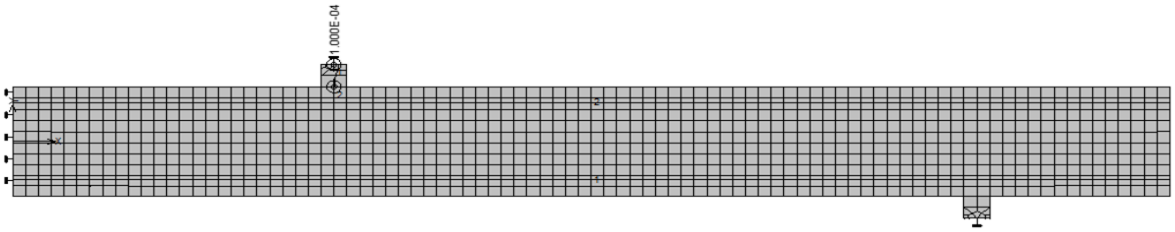

Fig. 87: Model of four-point bending test using symmetry. FEM, boundary conditions, monitors and loading are presented.

Next figures Fig. 88 - Fig. 95 present interesting model moments with short descriptions. These are always the steps around the initiation of the first crack and the activation of the reinforcement, it is also the development and opening of cracks, the capture of the moment around the modeled failure of the sample. Usually presented parameters are tensile stress in the reinforcement, slip of the reinforcement, total slip of the reinforcement, principal stress and principal strain of concrete, Eq plastic strain of concrete and cracks width.

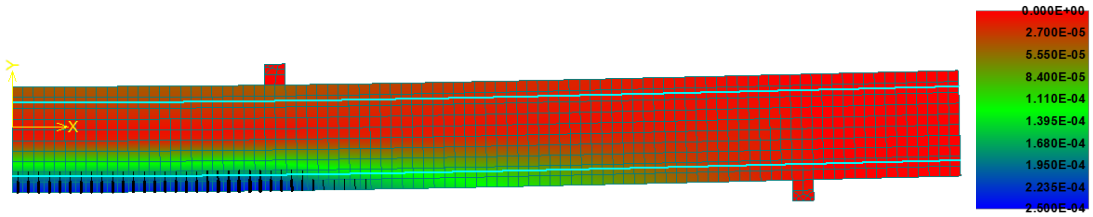

Fig. 88: Principal strain before first crack opening (step 12).

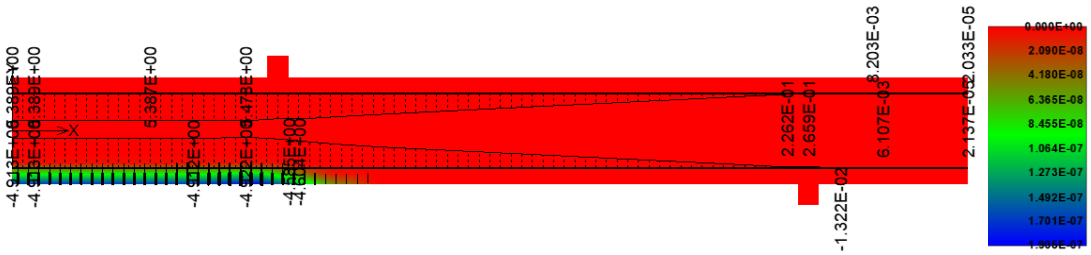

Fig. 89: Stress in the reinforcement and crack width (step 12).

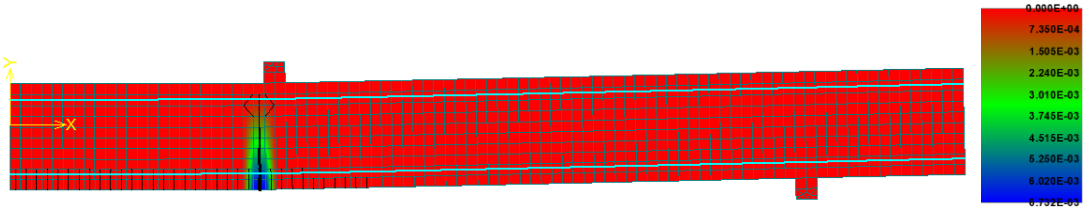

Fig. 90: Principal strain after first crack opening (step 13).

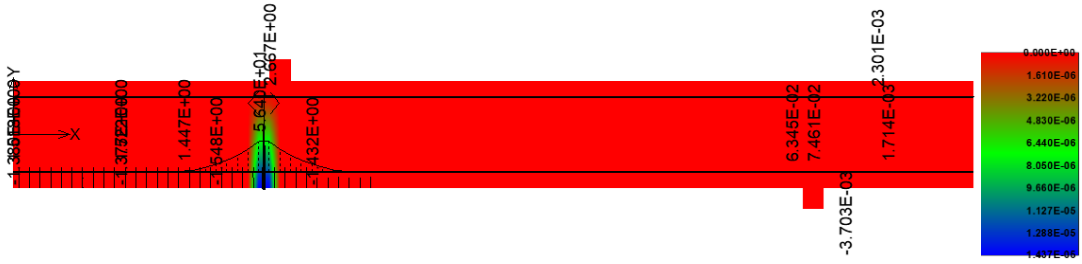

Fig. 91: Stress in the reinforcement after first crack opening and crack width (step 13).

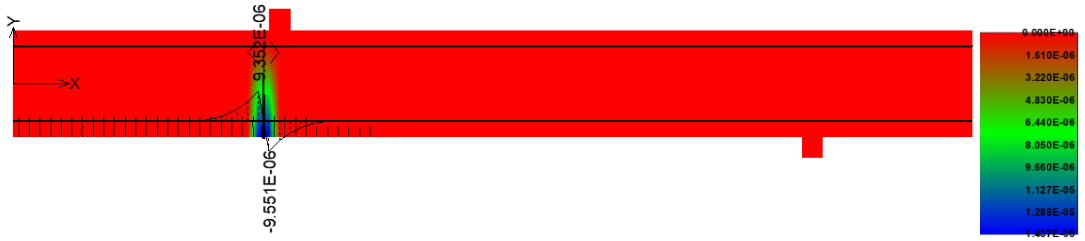

Fig. 92: Slip of the reinforcement after first crack opening and crack width (step 13).

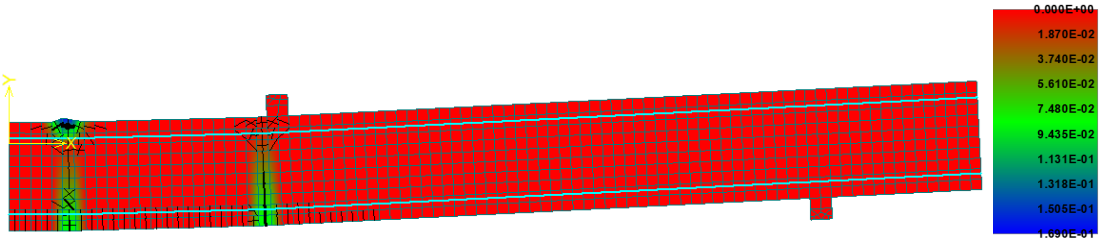

Fig. 93: Principal strain during the failure of structure (step 210).

Fig. 94: Principal stress of concrete and reinforcement during the failure (step 210).

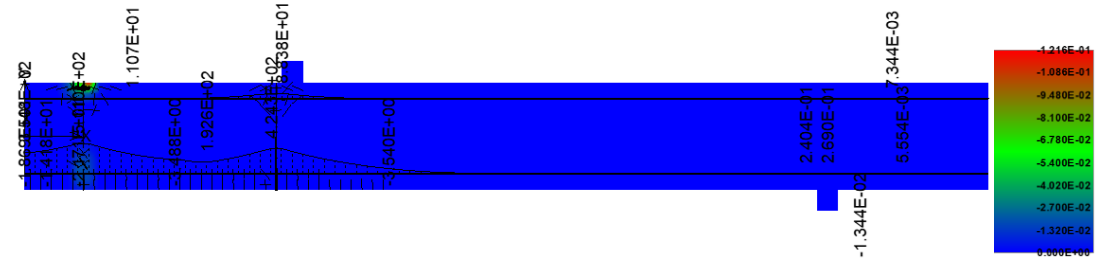

Fig. 95: Eq plastic strain of concrete and stress of reinforcement during the failure (step 210).

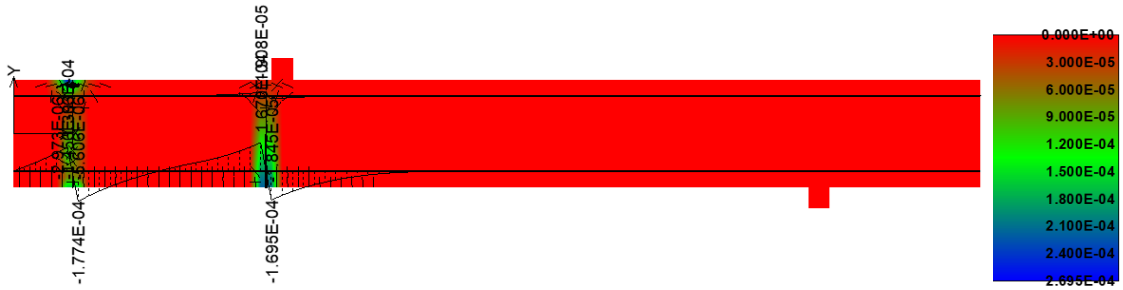

Fig. 96: Bond slip of the reinforcement and crack width (step 210).

4.4.2 Model with 5 rovings, considered "Sand" reinforcement bond

Model presented in previous chapter and in this chapter, also for next variants is the same and will not be more presented. The model was created using symmetry of four-point bending test. Soft insert under the loading support was also created for better results. Model is visible in Fig. 97Fig. 87.

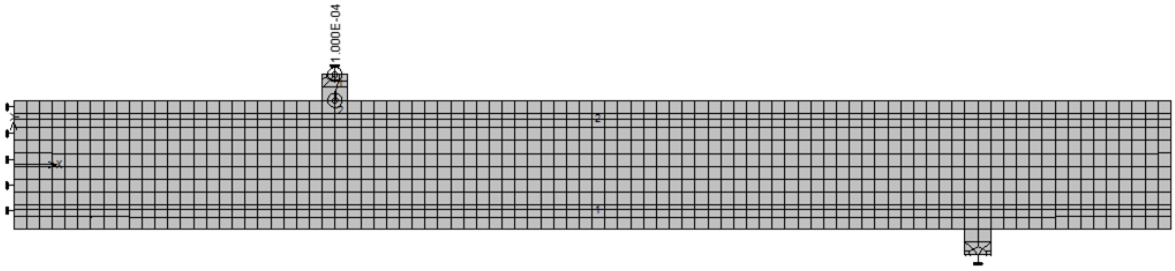

Fig. 97: Model of four-point bending test using symmetry. FEM, boundary conditions, monitors and loading are presented.

In this second presented model of four-point bending test was considered also two layers of reinforcement with five roving in each layer. As a reinforcement bond for this presented option was selected "Sand" curve presented in previous chapter about the material parameters – cohesion – reinforcement bond. So, it means the reinforcement bond curve with the highest stiffness.

Next figures Fig. 98 - Fig. 106 present interesting model moments with short descriptions. These are always the steps around the initiation of the first crack and the activation of the reinforcement, it is also the development and opening of cracks, the capture of the moment around the modeled failure of the sample. Usually presented parameters are tensile stress in the reinforcement, slip of the reinforcement, total slip of the reinforcement, principal stress and principal strain of concrete, Eq plastic strain of concrete and cracks width.

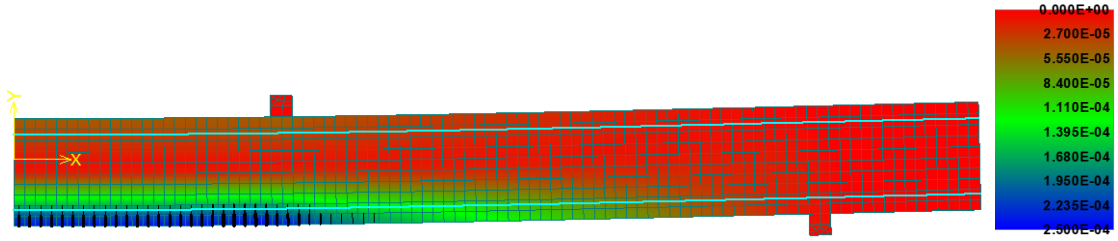

Fig. 98: Principal strain before first crack opening (step 12).

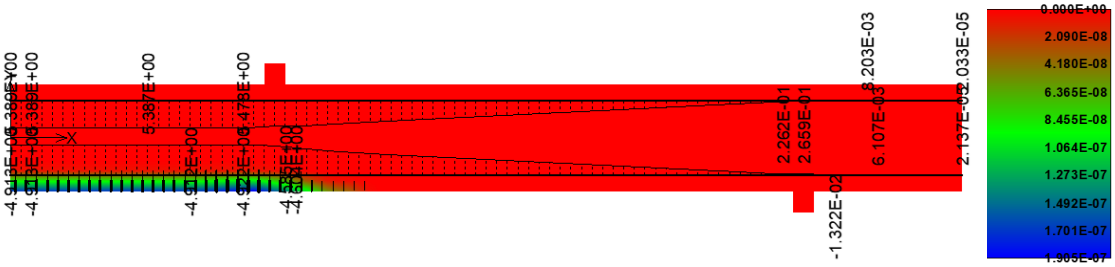

Fig. 99: Stress in the reinforcement and crack width (step 12).

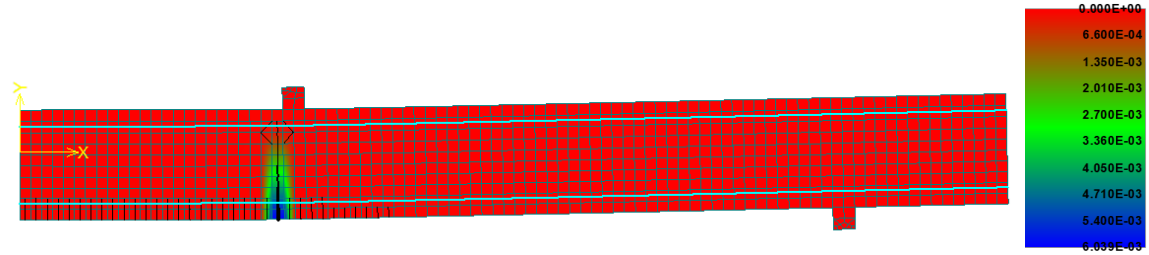

Fig. 100: Principal strain after first crack opening (step 13).

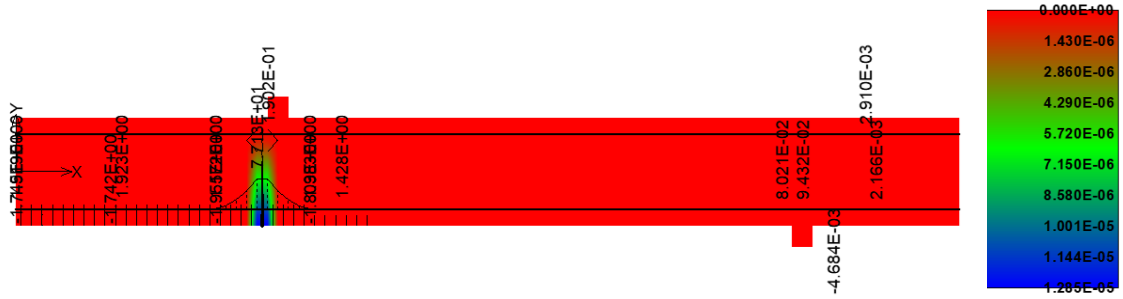

Fig. 101: Stress in the reinforcement after first crack opening and crack width (step 13).

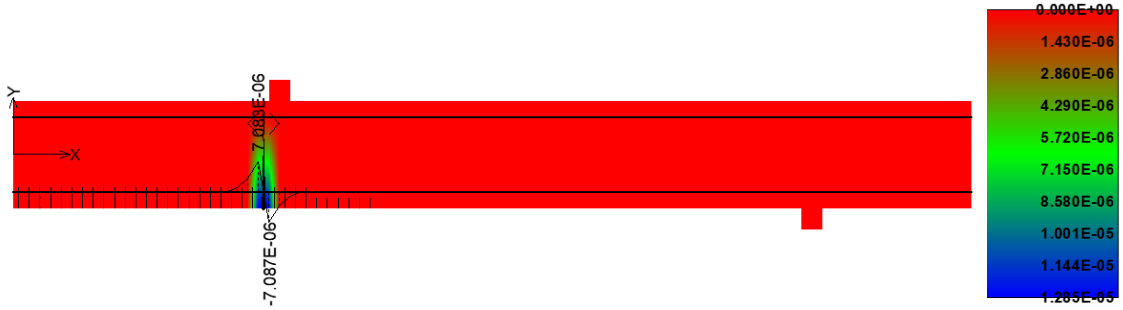

Fig. 102: Slip of the reinforcement after first crack opening and crack width (step 13).

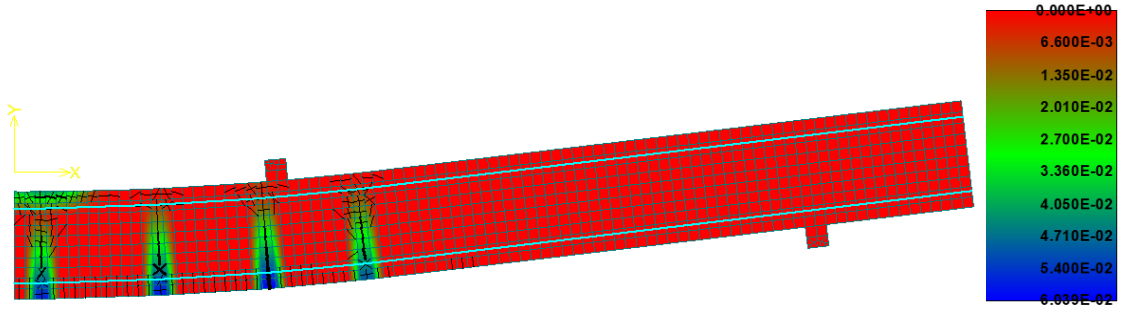

Fig. 103: Principal strain during the failure of structure (step 120).

In comparison with previous model with "Medium soft" bond curve, this model presents better interaction conditions and it perfectly correspond with mechanical experiments presented in previous chapters. More cracks is visible and from the reinforcement outputs logically faster activation is visible. Maximal concrete stress was usually achieved around 50 MPa. It shows that there is a sufficient reserve in the compression strength of concrete.

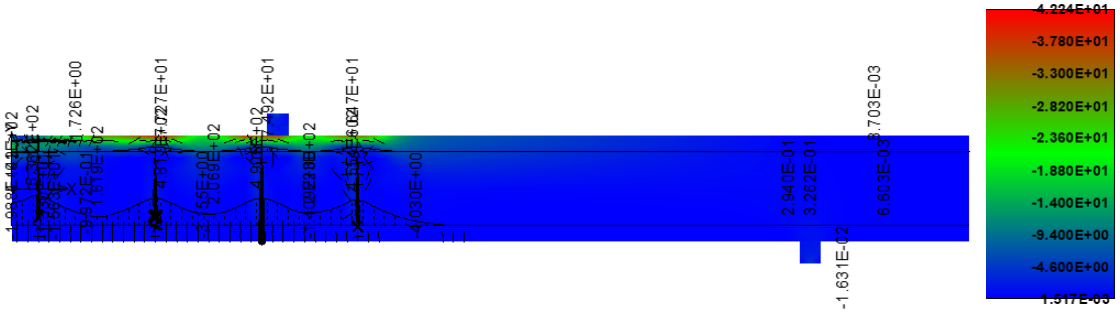

Fig. 104: Principal stress of concrete and reinforcement during the failure (step 120).

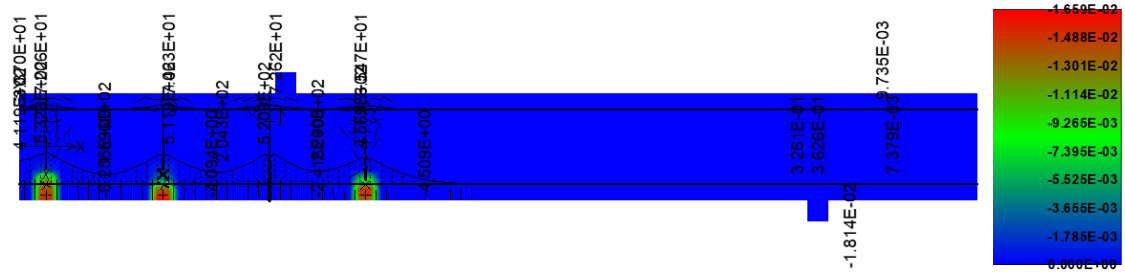

Fig. 105: Eq plastic strain of concrete and stress of reinforcement during the failure (step 120).

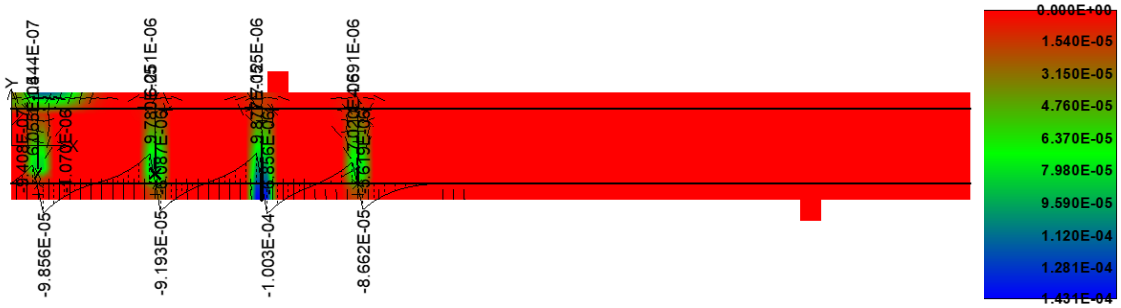

Fig. 106: Bond slip (total) of the reinforcement and crack width (step 120).

4.4.3 Model with 10 roving, considered "Soft" reinforcement bond

In this presented model of four-point bending test was considered also two layers of reinforcement with ten roving in each layer. As a reinforcement bond for this presented option was selected "Soft" curve.

Next figures Fig. 107- Fig. 115 present interesting model moments with short descriptions. These are always the steps around the initiation of the first crack and the activation of the reinforcement, it is also the development and opening of cracks, the capture of the moment around the modeled failure of the sample. Usually presented parameters are tensile stress in the reinforcement, slip of the reinforcement, total slip of the reinforcement, principal stress and principal strain of concrete, Eq plastic strain of concrete and cracks width.

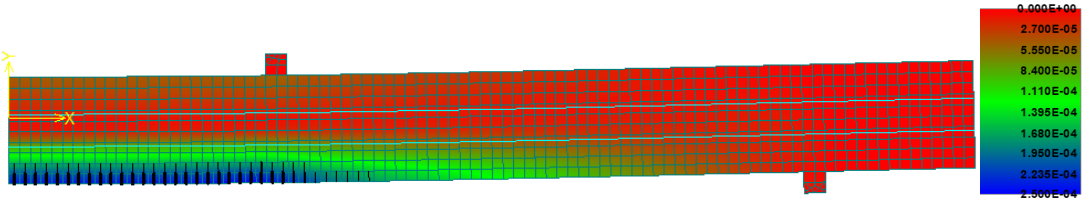

Fig. 107: Principal strain before first crack opening (step 12).

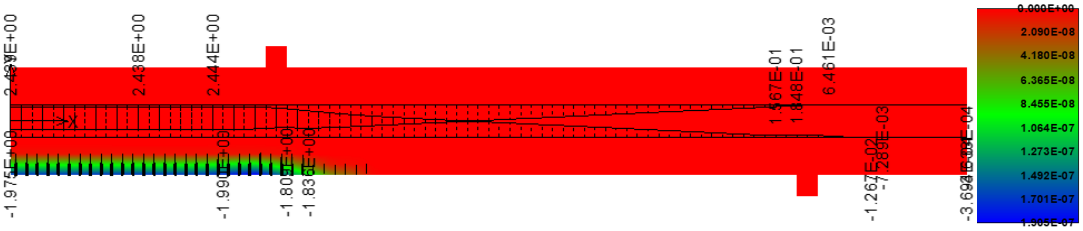

Fig. 108: Stress in the reinforcement and crack width (step 12).

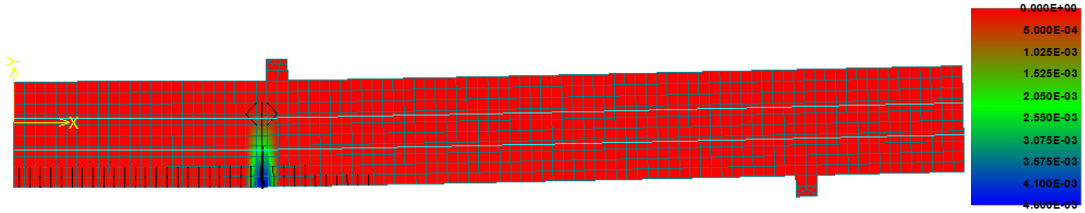

Fig. 109: Principal strain after first crack opening (step 13).

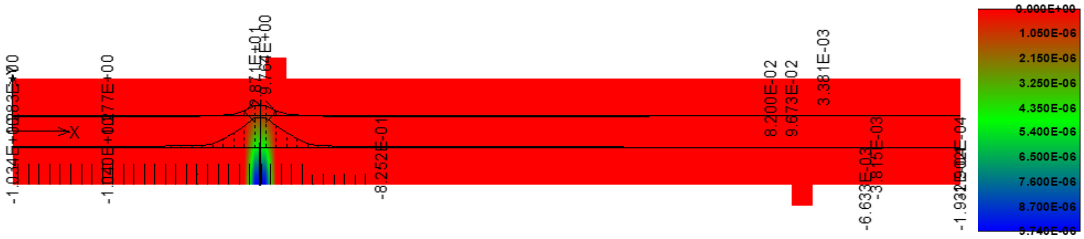

Fig. 110: Stress in the reinforcement after first crack opening and crack width (step 13).

Fig. 111: Slip of the reinforcement after first crack opening and crack width (step 13).

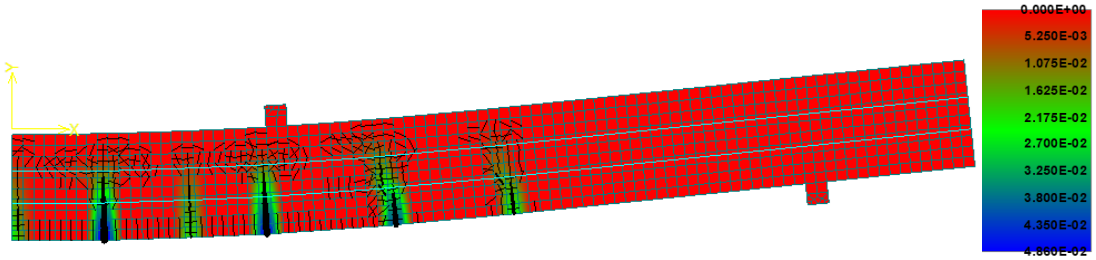

Fig. 112: Principal strain during the failure of structure (step 240).

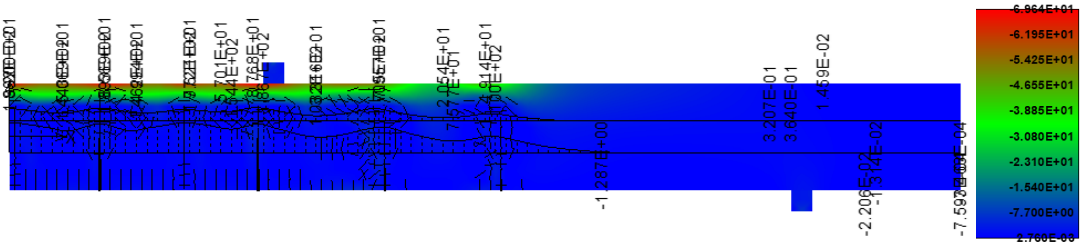

Fig. 113: Principal stress of concrete and reinforcement during the failure (step 240).

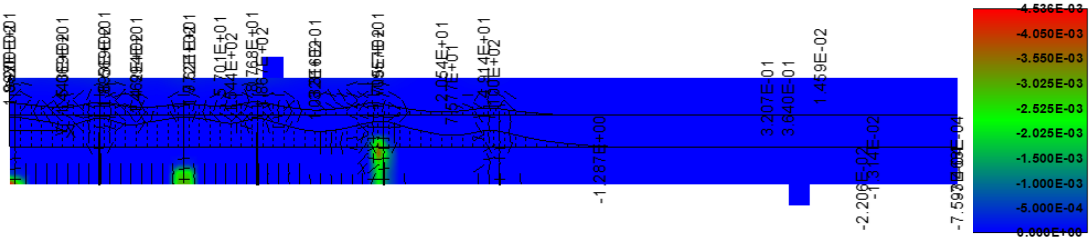

Fig. 114: Eq plastic strain of concrete and stress of reinforcement during the failure (step 240).

These results were expected thanks to the previous experience from modeling, and also experience with many mechanical experiments. Two time more composite reinforcements in cross-sectional area without any surface treatment gave similar results with the reinforcement with silica fine grain sand on the surface. It approximately corresponds with presented results of numerical model. Also model in comparison with picture from the real measurement is presented in Fig. 115. Other pictures were presented in chapter 3.3.3.3 Four-point bending test.

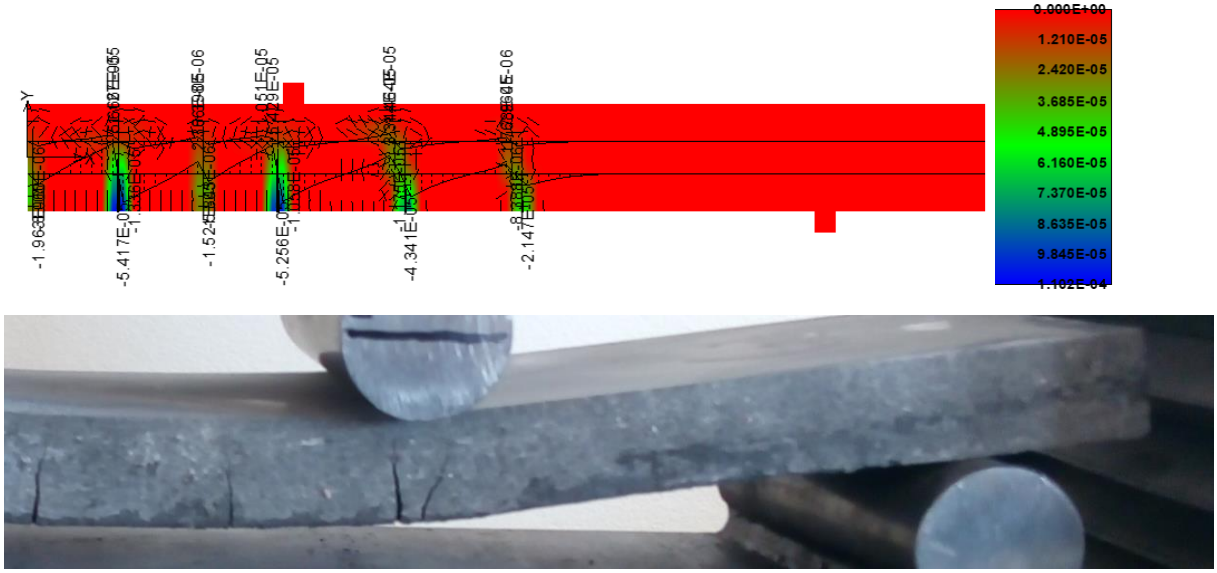

Fig. 115: Bond slip (total) of the reinforcement and crack width (step 240) and below comparison with picture from the measurement.

4.4.4 Model with 20 roving, considered "Soft" reinforcement bond

In this presented model of four-point bending test was considered also more easily only two layers of reinforcement with twenty roving in each layer. More exact is four layers like in the real experiment and it was also modeled, but results were almost the same so more easy method was selected. As a reinforcement bond for this presented option was selected again "Soft" curve. This is the highest amount of the reinforcement.

Next figures Fig. 116 - Fig. 125 present interesting model moments with short descriptions. These are always the steps around the initiation of the first crack and the activation of the reinforcement, it is also the development and opening of cracks, the capture of the moment around the modeled failure of the sample. Usually presented parameters are tensile stress in the reinforcement, slip of the reinforcement, total slip of the reinforcement, principal stress and principal strain of concrete, Eq plastic strain of concrete and cracks width.

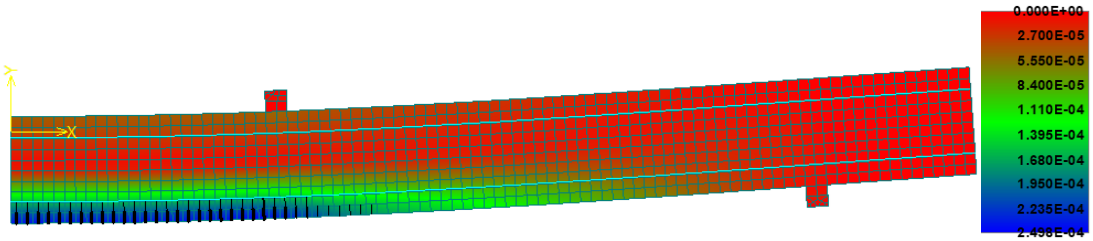

Fig. 116: Principal strain before first crack opening (step 12).

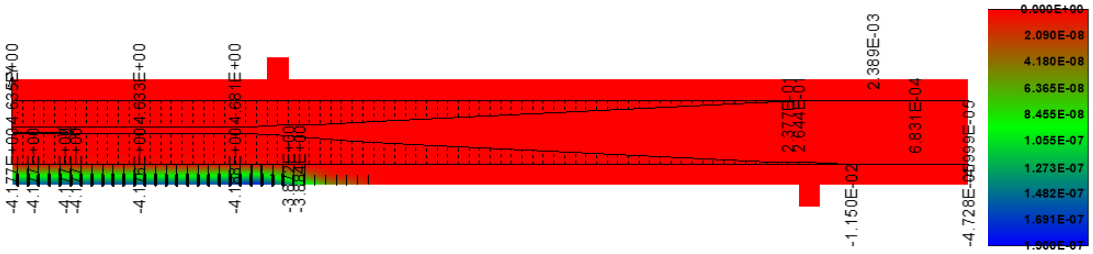

Fig. 117: Stress in the reinforcement and crack width (step 12).

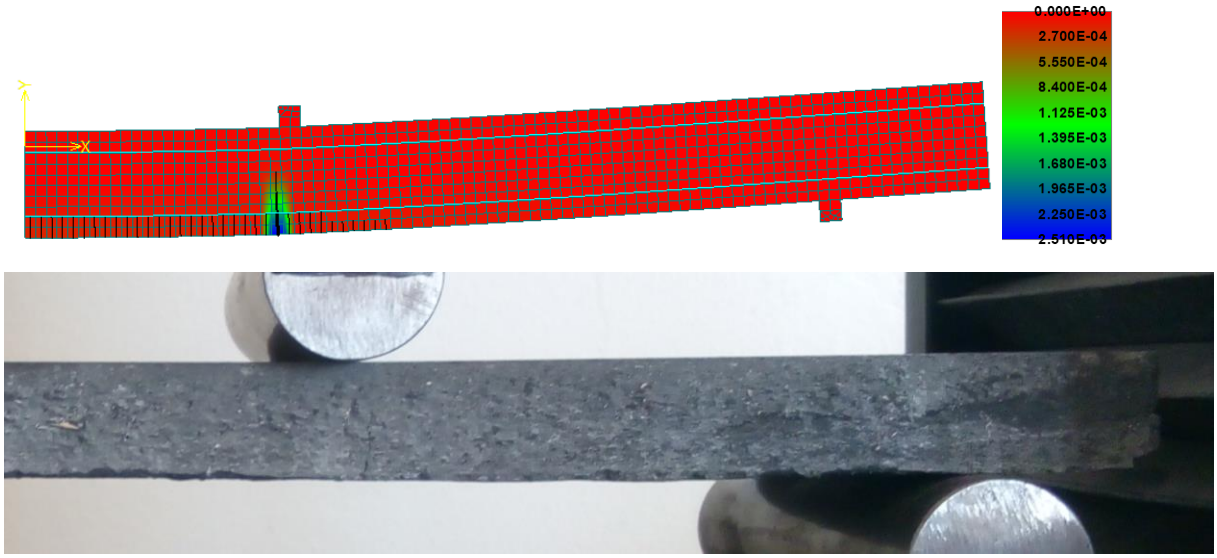

Fig. 118: Principal strain after first crack opening (step 13) and below comparison of model with picture from the measurement, visible the thin crack under the loading support.

Interesting point is again the moment of the first crack initiation, which is presented in Fig. 118. The model output is supplemented by the picture from the real process of measurement, and it approximately correspond. Of course, picture was taken little bit later after the first crack initiation when it was more opened and visible. In Fig. 119 is presented the stress of reinforcement just after the first crack initiation and it is visible low activation length of reinforcement and lower values of stress thanks to the higher amount of reinforcement.

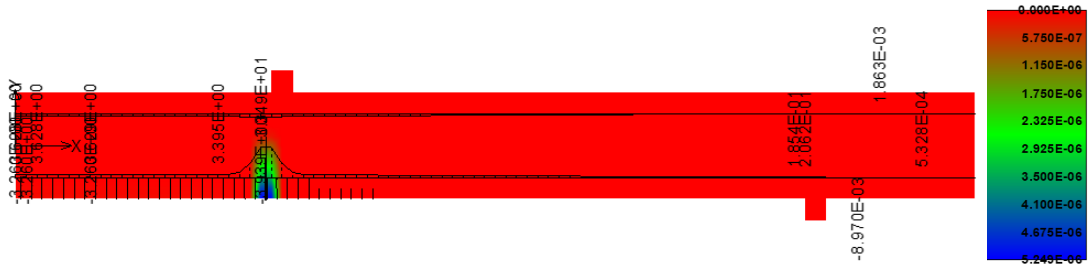

Fig. 119: Stress in the reinforcement after first crack opening and crack width (step 13).

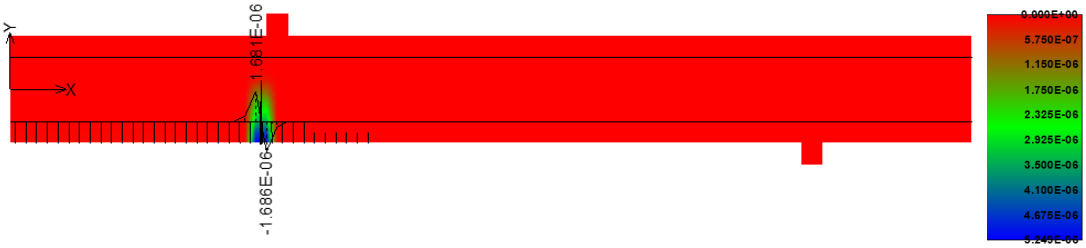

Fig. 120: Slip of the reinforcement after first crack opening and crack width (step 13).

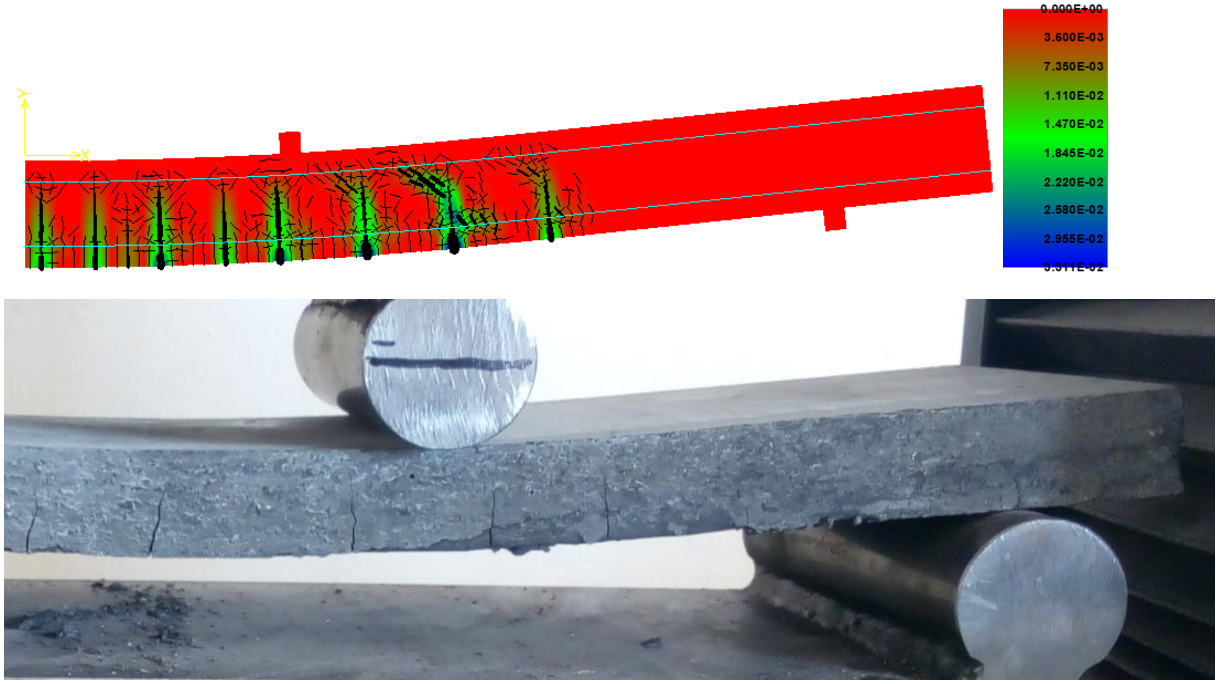

Fig. 121: Principal strain before failure of the structure (step 245) and below comparison of model with picture from the measurement, visible multiple cracking.

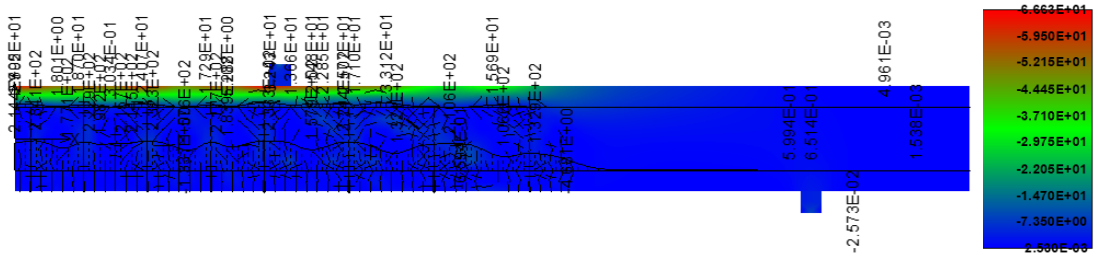

Fig. 122: Principal stress of concrete and reinforcement before the failure (step 245).

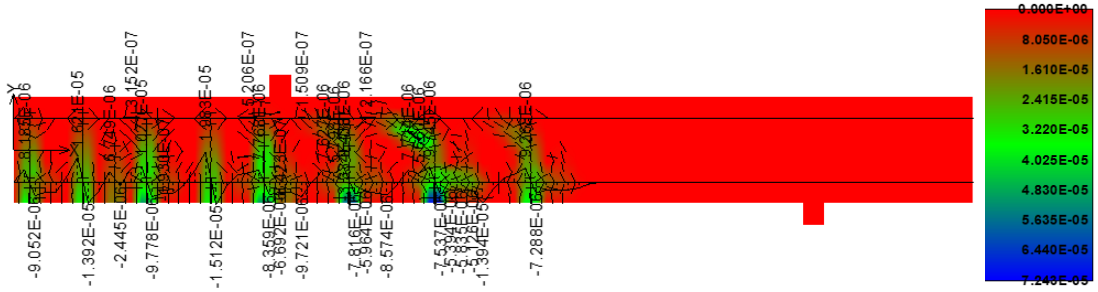

Fig. 123: Bond slip (total) of the reinforcement and crack width (step 245).

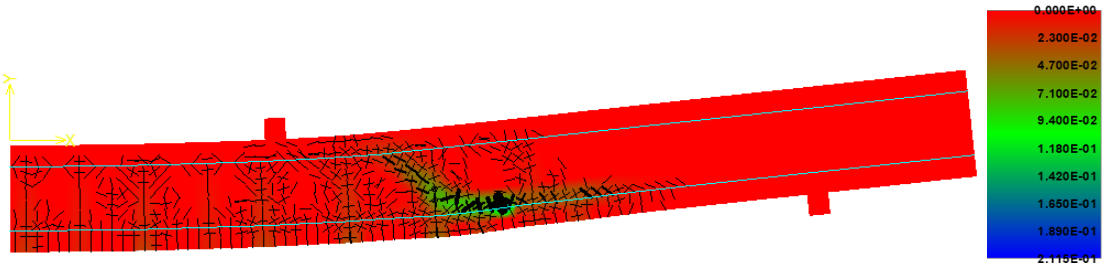

Fig. 124: Principal strain after failure of the structure (step 250).

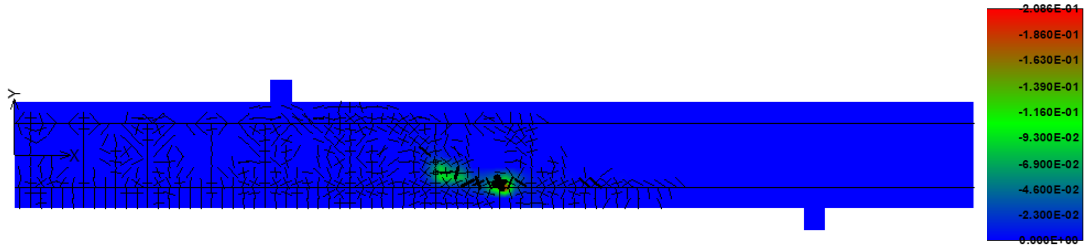

Fig. 125: Eq plastic strain of concrete and stress of reinforcement during the failure (step 250).

4.4.5 Model with 10 roving, considered "Soft" reinforcement bond and higher concrete cover

In this presented model of four-point bending test was considered also two layers of reinforcement with ten roving in each layer. As a reinforcement bond for this presented option was selected "Soft" curve. For this model was considered higher concrete cover 7 mm. Because after the experimental measurement was measured the real concrete cover and in some cases it was higher. Results of this model show the importance of exact concrete cover for thin TRC slabs.

Next figures Fig. 126- Fig. 134 present interesting model moments in the same way with short descriptions. These are always the steps around the initiation of the first crack and the activation of the reinforcement, it is also the development and opening of cracks, the capture of the moment around the modeled failure of the sample. Usually presented parameters are tensile stress in the reinforcement, slip of the reinforcement, total slip of the reinforcement, principal stress and principal strain of concrete, Eq plastic strain of concrete and cracks width.

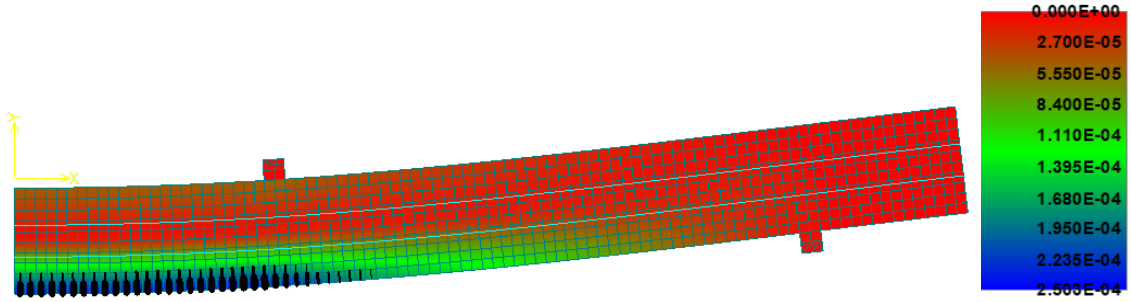

Fig. 126: Principal strain before first crack opening (step 12).

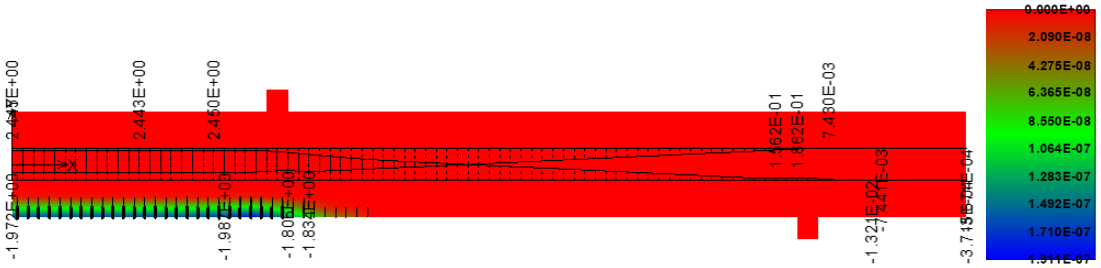

Fig. 127: Stress in the reinforcement and crack width (step 12).

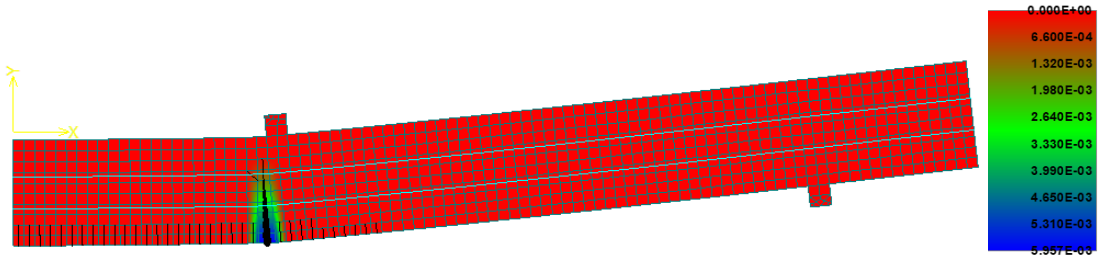

Fig. 128: Principal strain after first crack opening (step 13).

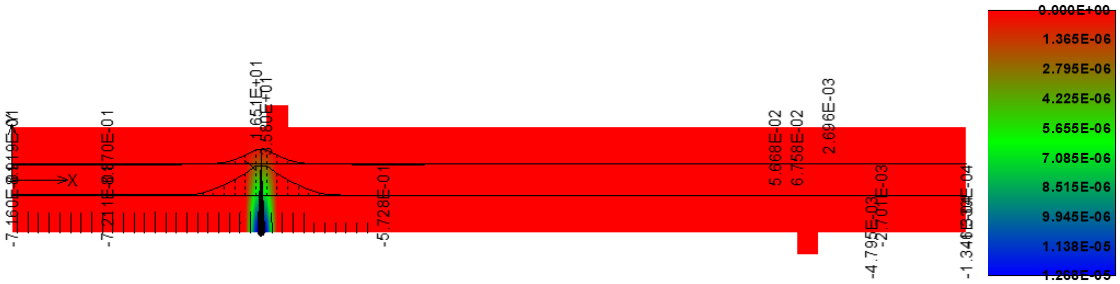

Fig. 129: Stress in the reinforcement after first crack opening and crack width (step 13).

Fig. 130: Slip of the reinforcement after first crack opening and crack width (step 13).

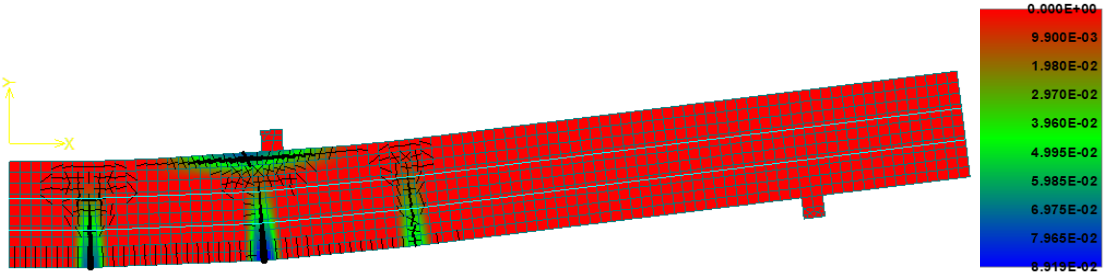

Fig. 131: Principal strain during the failure of structure (step 304).

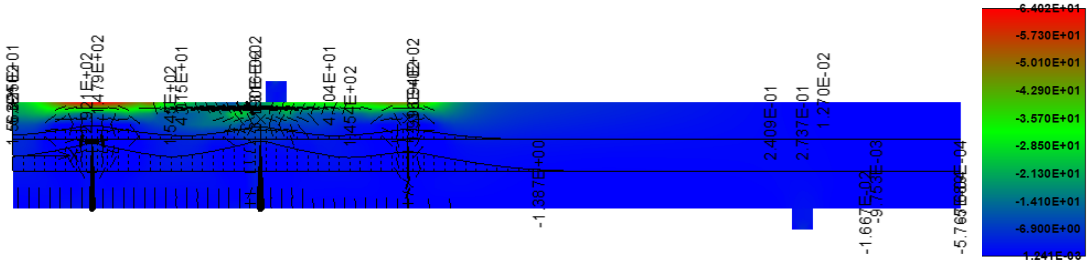

Fig. 132: Principal stress of concrete and reinforcement during the failure (step 304).

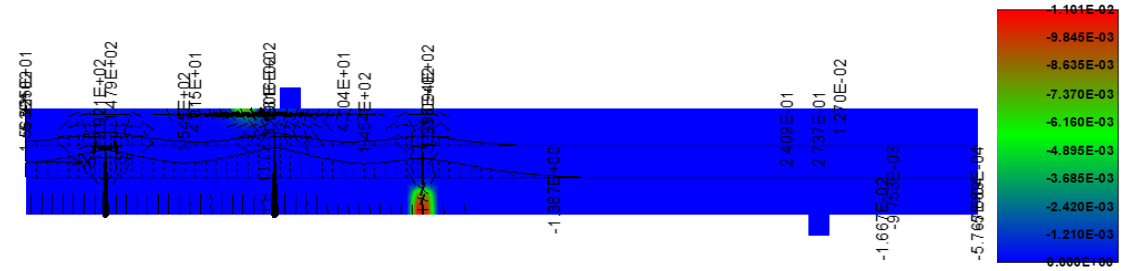

Fig. 133: Eq plastic strain of concrete and stress of reinforcement during the failure (step 304).

From results of numerical model is visible, that there is no rapid difference in results with different concrete cover in terms of the crack development. Difference was in numerical values. Reinforcement was activated more faster and displacement was logically higher for the same force in comparison with the same specimen with lower concrete cover and the same reinforcement bond curve.

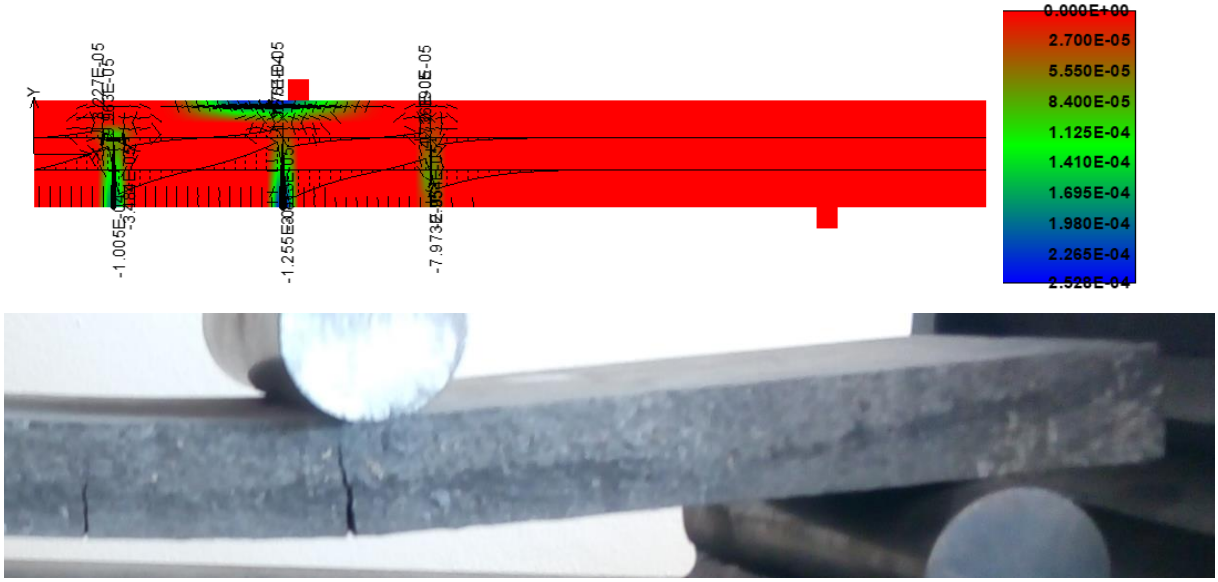

Fig. 134: Bond slip (total) of the reinforcement and crack width (step 304) and below comparison of model with picture from the measurement, visible wide crack under support similar amount and location of cracks.

4.4.6 Model with 10 roving, considered "Ultra-soft" reinforcement bond

In this last presented model of four-point bending test was considered also two layers of reinforcement with ten roving in each layer. As a reinforcement bond for this presented option was selected "Ultra-soft" curve. More models were created, but it is not necessary to mention all variants, only the representatives one.

Next figures Fig. 135- Fig. 142 present interesting model moments with short descriptions. These are always the steps around the initiation of the first crack and the activation of the reinforcement, it is also the development and opening of cracks, the capture of the moment around the modeled failure of the sample. Usually presented parameters are tensile stress in the reinforcement, slip of the reinforcement, total slip of the reinforcement, principal stress and principal strain of concrete, Eq plastic strain of concrete and cracks width.

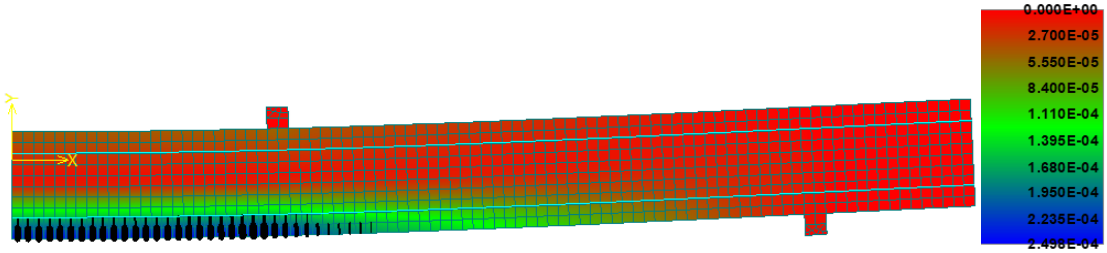

Fig. 135: Principal strain before first crack opening (step 12).

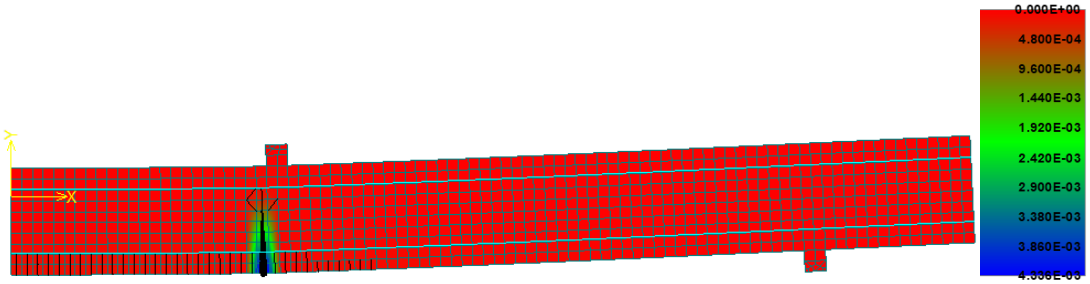

Fig. 136: Principal strain after first crack opening (step 13).

Fig. 137: Stress in the reinforcement after first crack opening and crack width (step 13).

Fig. 138: Slip of the reinforcement after first crack opening and crack width (step 13).

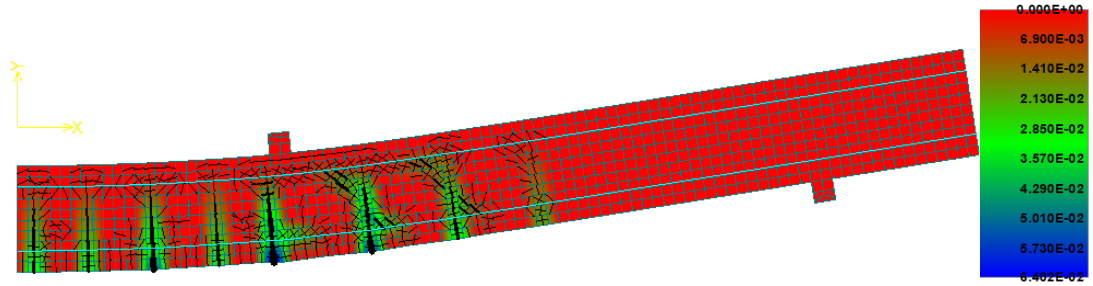

Fig. 139: Principal strain before failure of the structure (step 380).

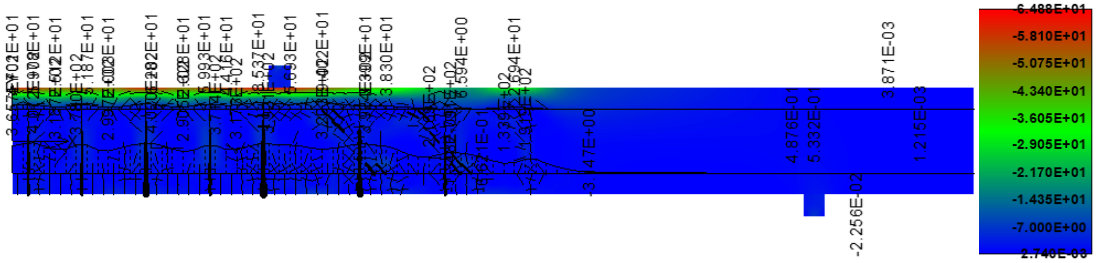

Fig. 140: Principal stress of concrete and reinforcement before the failure (step 380).

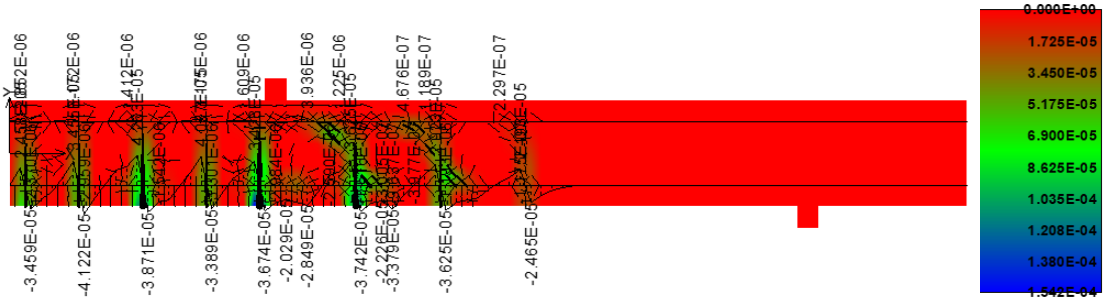

Fig. 141: Bond slip (total) of the reinforcement and crack width before the failure (step 380).

In presented Fig. 142 is visible crack width during the failure on model (step 400) and below this picture model is for comparison with picture from the real process of measurement. The collapse was due to the shear stress in combination with the bending stress. It is very difficult to model this situation after the shear crack opening. This is the situation, where the model calculations finished and loading of real specimens continue. So, on this real specimen we can see horizontal crack behind the support, which was modeled, but collapse of specimens was later in the middle part between loading supports.

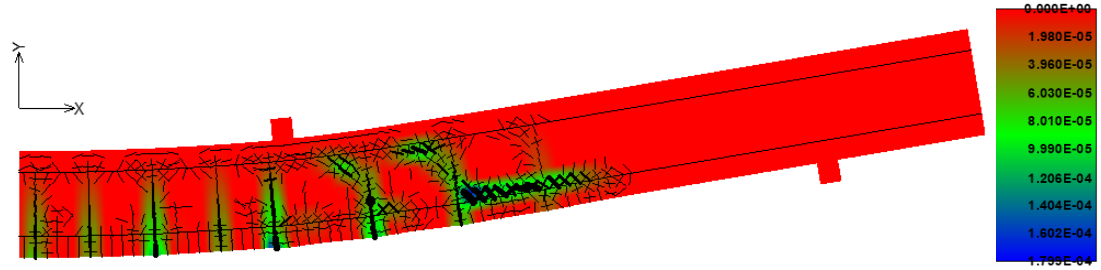

Fig. 142: Crack width during the failure (step 400) and below comparison with picture from the measurement, visible failure because of the shear forces like is visible in model before the crack opening.

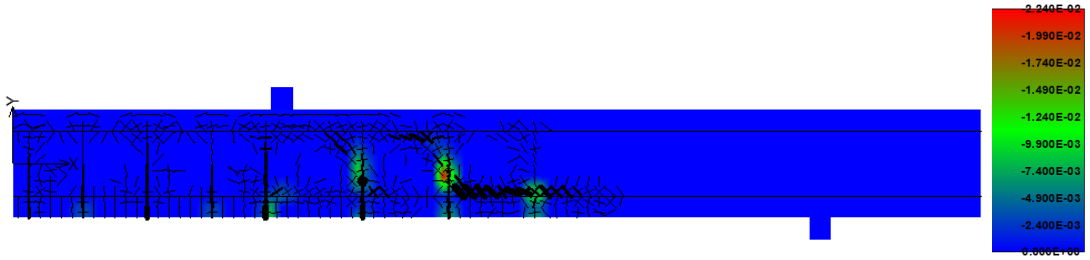

Fig. 143: Eq plastic strain of concrete during the failure (step 400).

4.4.7 Comparison of results of numerical model and experiment

First is presented figure mentioned in 2015 in [34]. This curve represents the be beginning of numerical modeling in ATENA Engineering. The four-point bending test of façade elements with different dimensions 300 x 700 x 25 mm was carried out according to standard ČSN EN 12390-5. The panel was reinforced with 2D AR glass technical textile on both surfaces with concrete cover 6 mm. The distance between centers of supports of facade elements was 600 mm and between loading supports on the opposite side 200 mm. The 30 mm radius of curvature was used as support. So, values presented in Fig. 144 are not so well comparable with other figures below. But crack development and mainly crack opening is very good visible, it is not exact. On the other side stiffness and maximal force of numerical model is very similar to the experimentally curve [34]. TRC specimens were slightly reinforced. Collapse was due to the reached maximal tensile strength of reinforcement without shear cracks like mentioned above with higher amount of reinforcement. In the model with more exact crack development is more difficult to model the final part of curve because of the massive crack opening.

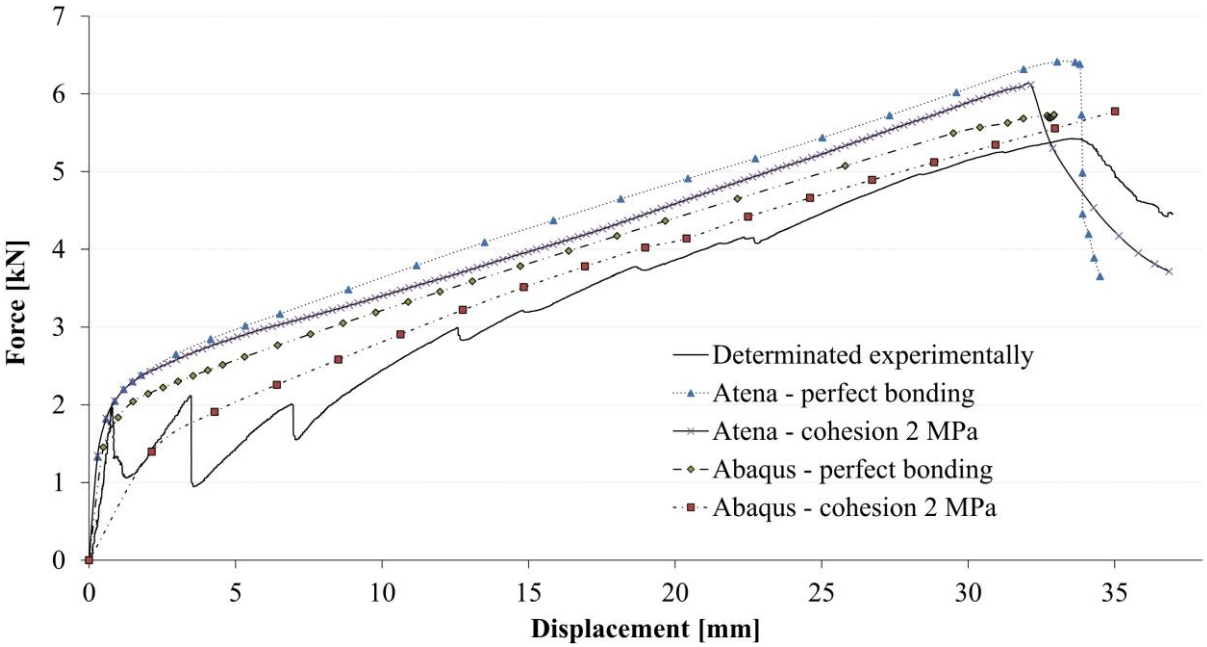

Fig. 144: Load-displacement curves of façade element from 4 point bending test, result of real measurement and results of the first numerical modeling in 2015. Model with bad crack opening for comparison with other models and its development [34].

In Fig. 145 are presented all curves presented also in experimental part in addition with resulted curves from the numerical modeling. Load-displacement (Force-displacement) curves of slabs 100 x 360 x 18 mm from four-point bending test are presented in all basic variants with three variants of reinforcement. 2x5 means 5 impregnated rovings in two layers of reinforcement as mentioned in previous chapter. So 2x10 are specimen with two layers and 10 rovings in each layer. 4x10 are specimen with four layers and 10 rovings in each layer. The collapse was usually due to the shear stress in combination with the bending stress, especially for good interaction conditions and higher amount od reinforcement. It is very difficult to model this situation after the shear crack opening and massive bending crack opening, so final parts of modeled curves are not exact. But this part of the curve is far beyond the applicability of the element. In that moment, the deflection (displacement) of the element is in the order of higher unity millimeters between the loading supports with distance 300 mm.

Fig. 146, Fig. 147 and Fig. 148 present the same graph, but separately for 2x5, 2x10 and 4x10 rovings – variants. In addition, it is presented only one representative curve for smooth variant and curve with the surface treatment with corresponding numerical models. Than are results of numerical models and experiment more comparable. Model reached the great results and it can be said that the chosen methods and procedures were correct.

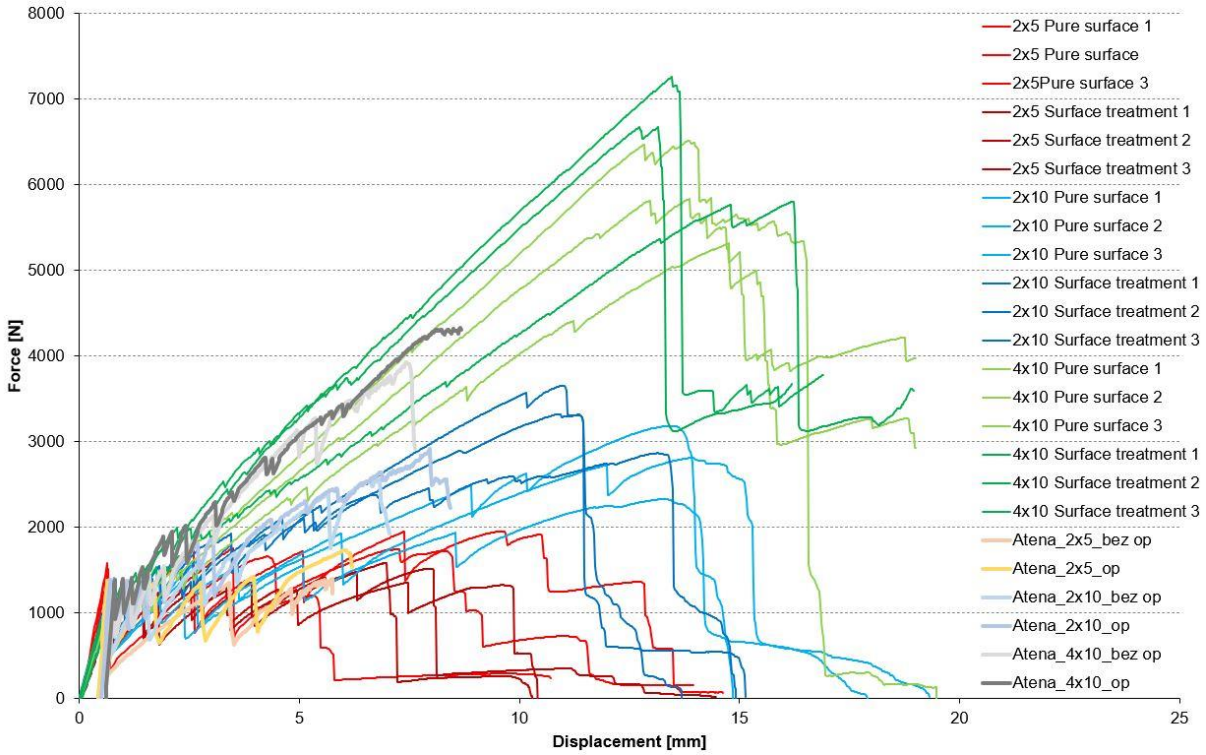

Fig. 145: Load-displacement curves of slabs 100 x 360 x 18 mm from 4 point bending test, all basic variants, result of real measurement and results of the numerical modeling.

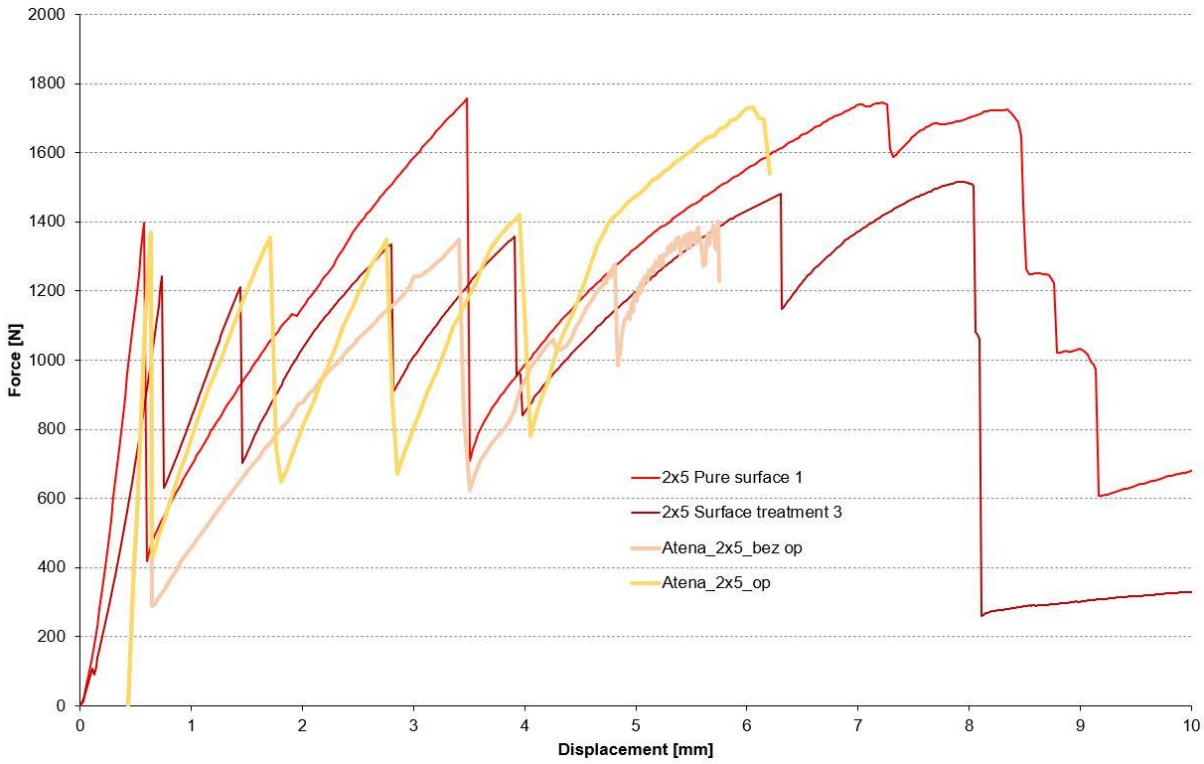

Fig. 146: Load-displacement curves as presented in Fig. 145, separately for more visible details 2x5 rovings with only one typical curve.

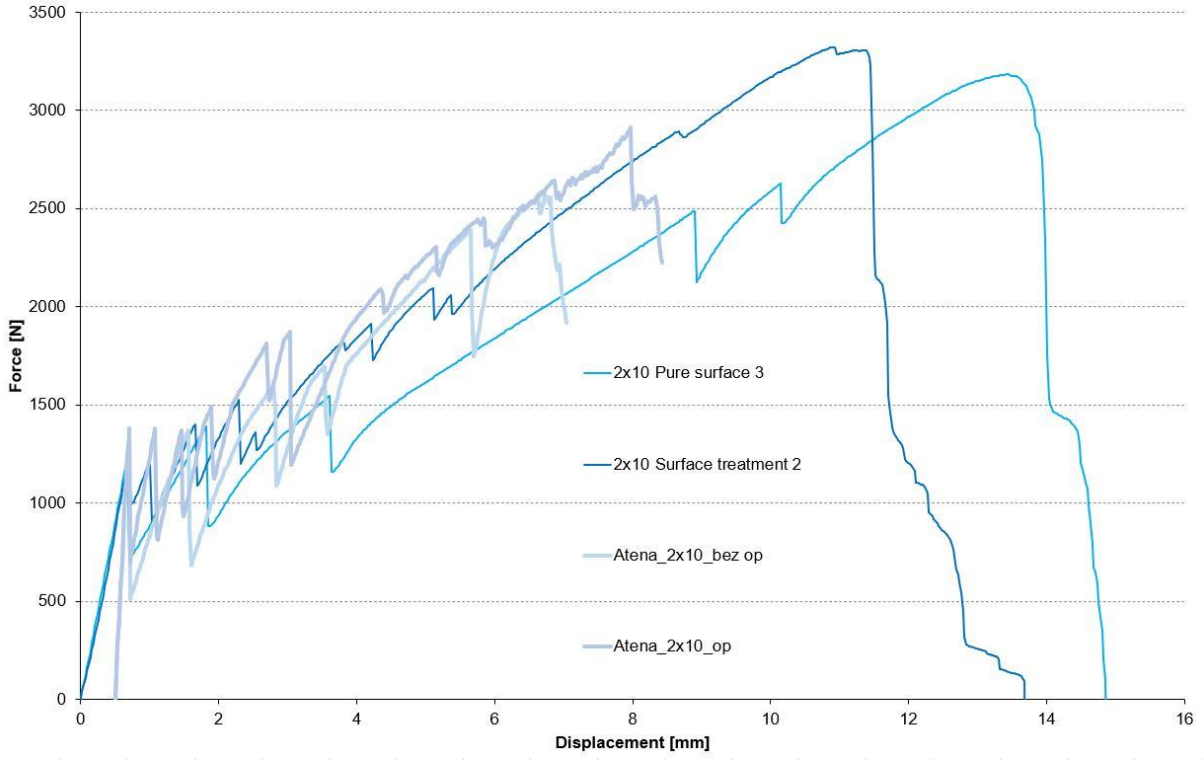

Fig. 147: Load-displacement curves as presented in Fig. 145, separately for more visible details 2x10 rovings with only one typical curve.

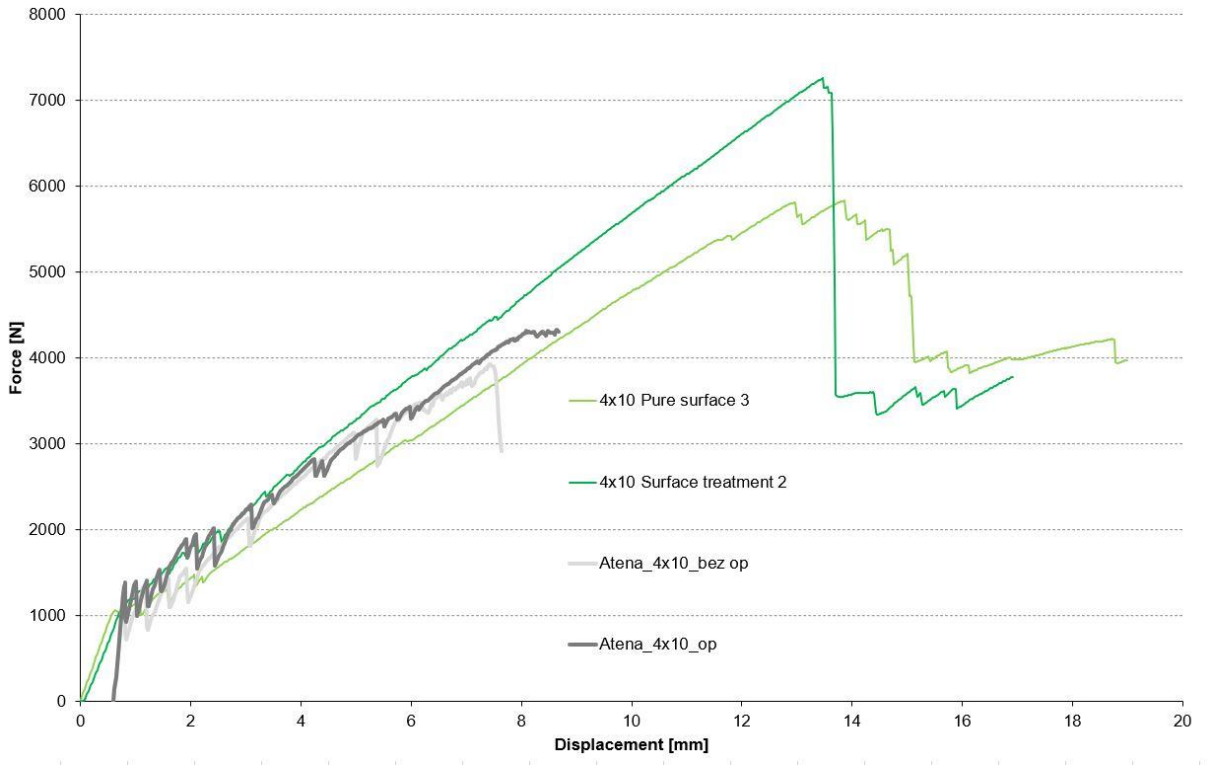

Fig. 148: Load-displacement curves as presented in Fig. 145, separately for more visible details 4x10 rovings with only one typical curve.

5 Example of application - subtle cantilever concrete bench

The shape and construction of subtle concrete bench was influenced by purpose of use. Presented bench is the basic body for the so-called solar bench. It was made of two parts firmly connected to each other. The first bottom part was concrete slab 60 mm below ground with thickness 100 mm and it was made from ordinary concrete with partial replacement of natural aggregate with recycled aggregate and with steel reinforcement. The material selection was because of its better price and its invisible placement underground. Upper visible part was made from modern carbon textile reinforced concrete (TRC). Upper part is more difficult construction of plate with thickness only 40 mm with its static scheme as L shaped cantilever with angle 35° and its length approximately 1.0 m. Its inclined part is intended for the photovoltaic panel. The holes in the invisible part of the base plate serve for storing batteries and all intelligent technologies. Both parts of the bench are guided by goosenecks for electrical connection of batteries, technology, panels and controls each other [13].

The original look of the thin concrete upper part of construction was created thanks to the modern carbon technical textiles as a reinforcement. Method of reinforcement of upper visible part, reinforcement shaping and connecting by overlapping has similar principles like for traditional steel reinforcement. Concrete frame corner reinforcement methods were also followed in the case of impregnated textile reinforcement, and it was the main reason of decision to create an advanced numerical model and mechanical

experiment. The aim was the determination of load bearing capacity of subtle concrete bench and the stress development and behavior around the area of concrete frame corner [13].

Bench length in previous study was designed 2.14 m, but for the experimental test, specimen length was only 0.6 m. The bottom slab dimension was 1.0 x 0.6 m with hole in its middle part 0.68 x 0.28 m for lightweighting. It leaded more to the system of beams in the sense of construction than one large slab as presented in Fig. 150 (b). So cross-sectional area of the ribs was 100 x 160 mm. Upper part of concrete bench was L shape with angle 35° and its highness 0.5 m and cantilever length 1.0 m. L shape part thickness was only 40 mm. View on cross-sectional drawing of bench with described and other dimensions is presented in Fig. 149 [13].

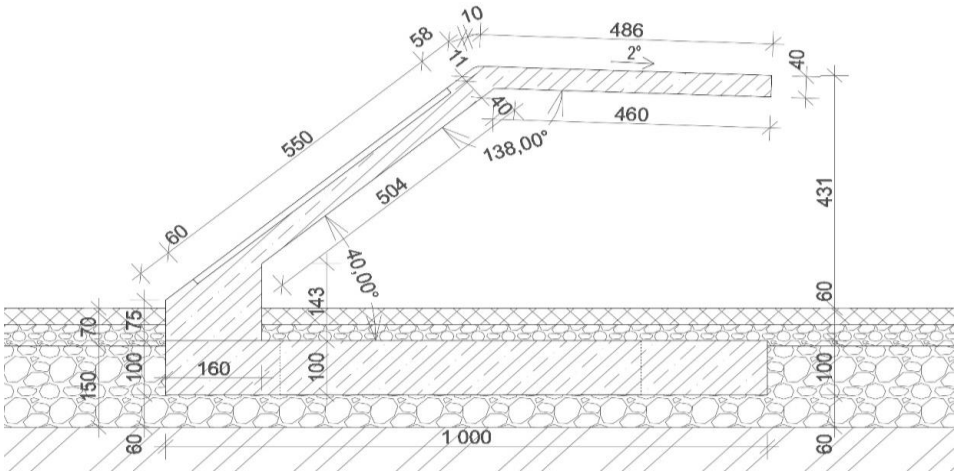

Fig. 149: View on cross-sectional drawing of bench with dimensions [13].

Fig. 150: Detailed view on the TT of upper part in the area of L shape (a), view on the complete concrete bench prepared for mechanical loading-bearing test (b) [13].

As mentioned above bottom part was made from ordinary concrete with traditional steel reinforcement. The reinforcement was manually shaped inside of wooden form before the concreting using 4 bars for each concrete beam part, 2 for upper surface and 2 for bottom surface with concrete cover 20 mm. Traditional reinforcement methods were followed. Steel anchors were included to this basement for subsequent joining of both bench parts. Upper visible part was made from carbon textile reinforced concrete. Mold was prepared using the combination of steel frame and wooden plates. 4 layers of carbon technical textiles were used, 2 for upper surface and 2 for bottom surface with concrete cover about 5 mm. Both ends and L break were reinforced by own made shaped pieces of reinforcement using the same reinforcement materials. It was in similar way to traditional methods of steel reinforcement, so shapes were U shape on both ends and one L shape on the outside of break in the middle of upper part. Detailed view on the carbon reinforcement in the break area is presented in Fig. 150. View on the complete concrete bench prepared for mechanical loading-bearing test is presented in Fig. 150. Principles of frame corner reinforcement were followed. The exact position of textile reinforcement in the mold was ensured by the supported small steel strips between upper and bottom reinforcement and by own made small plastic spacers produced by 3D printing machine. Plastic spacers were glued on the outside reinforcement surface. Stress transfer in the reinforcement provided the reinforcement overlapping. Steel supported strips were finished with steel plate with screw holes on the side of connecting with bottom bench part [13].

Numerical analysis was performed using ATENA Science GiD software. Model and its necessary material parameters was created based on the previous research experience. The same mesh size and the type of solver with loading speed were also used. Nine linear elements were adjusted along the height of the beam to correctly model and detect the cracks development. The reinforcement was modelled as a 1D member with defined cohesion. For easier modelling in the support area were modelled two screws, which do not correspond to reality. It prevents to a brittle fracture in the support area and tipping over the entire bench. Thanks to that model could be easily created in 2D surface. The support was considered perfectly anchored because it was assumed that anchoring in a massive concrete block provide sufficient rigidity to prevent unexpected rotation due to bead or screw bigger deformation. The place with load application is simulated using load plate with ideal elastic material corresponding with its parameters to steel. It was not necessary to create a soft layer under this load plate, because collapse was not expected in this area with minimal stress concentration. View on the numerical model is presented in Fig. 151 on the left side (a) and its comparison with picture of specimen from real experiment is presented in Fig. 151 on the right side (b) [13], [32].

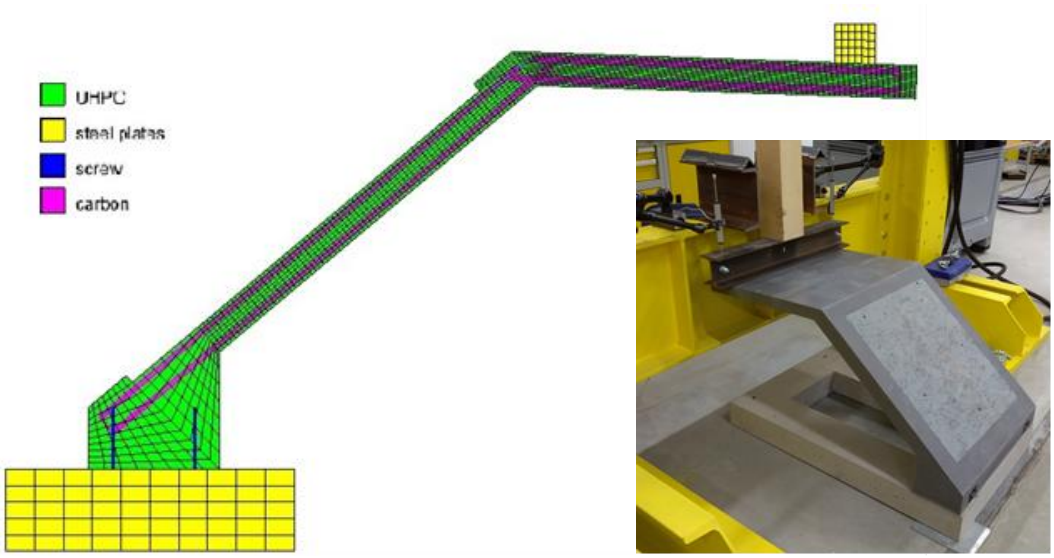

(a) (b)

Fig. 151: View on based numerical model and materials in ATENA Science GiD (a) included picture from the process of real measurement for comparison (b) [13].

Experimental destructive load-bearing test was executed due to the determination of load-bearing capacity and its comparison with numerical model before prototype realization. Testing set-up had to be similar to the real bench loading conditions with maximum internal force response after the loading force application. So uniaxial loading test in negative direction z axis (geotropically negative) was chosen for the testing procedure. The loading force application was in the middle of upper part of bench and on the end of cantilever, exactly 50 mm from the cantilever edge. The point loading force was applied over the steel distribution profile with higher stiffness for the linear loading simulation. On both ends were located potentiometers for the average deflection monitoring in the middle of bench. The testing set-up is evident in the Fig. 151 (b). Used measurement equipment was Inova linear actuators series, specifically AS 10/63 due to maximum expected reaction less than 50 kN. Testing procedure was performed with controlled load speed 2.0 mm per minute after 28 days of specimens hardening. The loading process continued until the specimen failure with constant speed of loading. Measured values were logically force, time and displacement [13].

Results of experimental verification in comparison with numerical model results are presented in graph in Fig. 152. The form of presented graph is traditionally force on y axis and displacement on x axis. One single experimental curve for only one realized specimen is presented. The maximal force reached in experiment was 11.6 kN/m with corresponding displacement 48 mm. This force was recalculated from the real bench length 0.6 m per linear meter. In same Fig. 152 are also presented results of numerical modeling. Curve with perfect bonding represent model without cohesion parameters defining. It means perfect interaction between reinforcement and cementitious matrix.

Curve with modeled cohesion represent model with exactly defined cohesion parameters in the contact area of reinforcement and concrete [13].

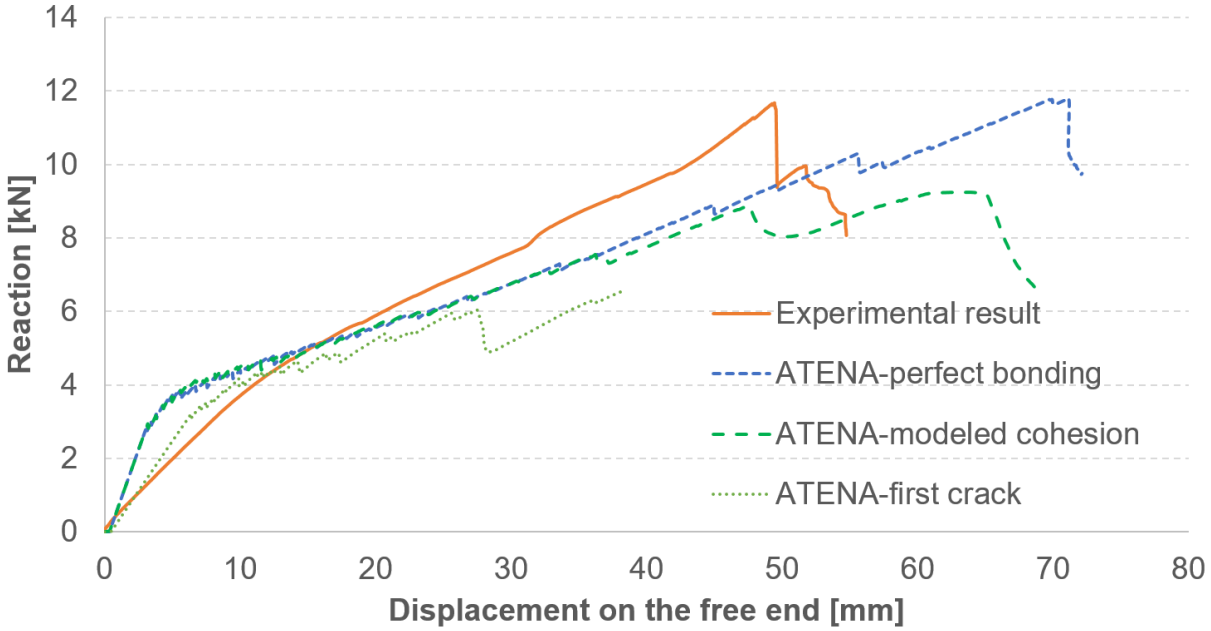

Fig. 152: Experimental test and numerical results presented in the form of force – displacement graph, numerical results – two options and one model with previous modeled first crack [13].

The last curve from numerical modeling in the same Fig. 152 present result of version with already initiated first crack modeled using the thin line of elastic material with lower stiffness. It is the answer for difference between curves slope in the first part, which represent the linear part before the first crack initiation, when the reinforcement is not yet activated. Next parts of curves are characterized by cracks development and crack opening. All numerical curves are very similar to experimental result in this part. Sometimes in the case of textile reinforced concrete, crack development is visible in the form of small jumps on the curves. In the case of presented bench its cross-section is strongly reinforced and therefore prevent significant opening of cracks immediately after their formation. The last part of curves is the loss of bearing capacity. Only curve ATENA-first crack was not exact, but it was solved mainly due to the verification of the first curve part. Other two curves are similar to experimental one. Curve ATENA-modeled crack has maximal force 9.3 kN/m with corresponding displacement 66 mm. Curve ATENA-perfect bonding has maximal force 11.7 kN/m with corresponding displacement 70 mm, so the force is almost the same in comparison with experimental one. FIGURE 5 presents representative numerical model outputs of curve ATENA-modeled cohesion around the point of maximal load-bearing capacity [13].

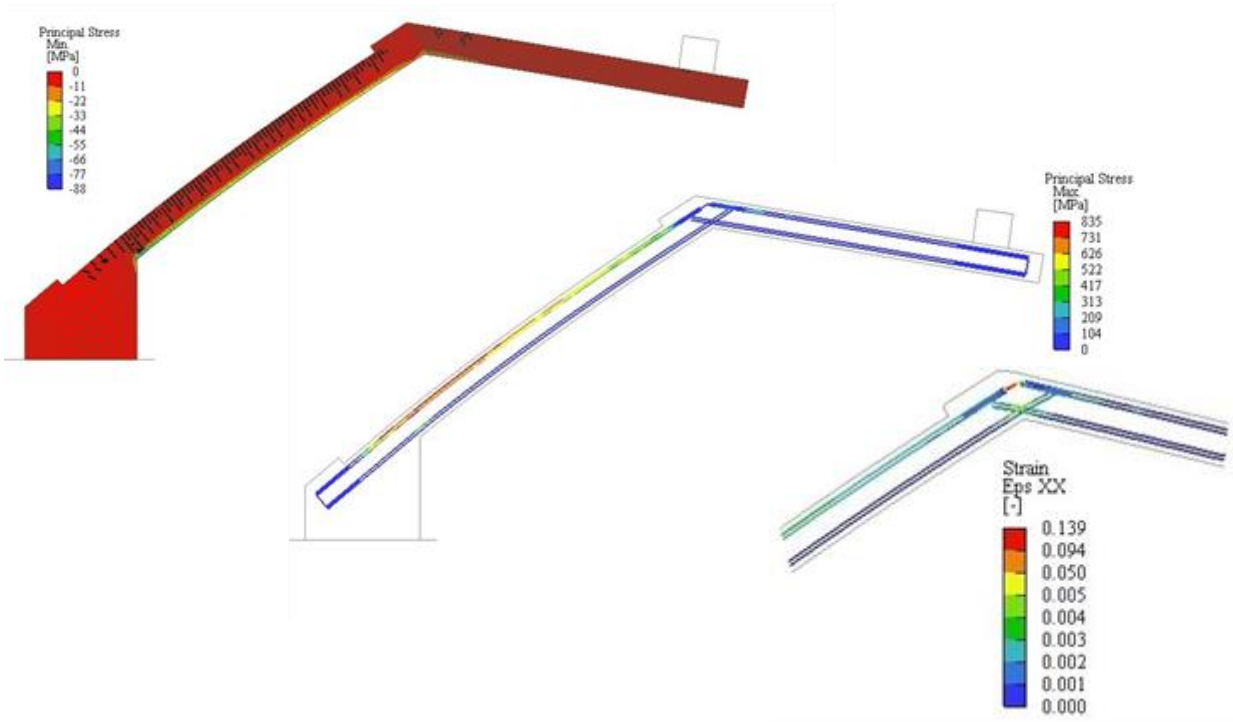

(a) (b) (c)

Fig. 153: Results of numerical model, principal minimal stress in concrete (a) and principal maximal stress in reinforcement just before the moment damage (b), detailed view on the reinforcement strain in frame corner after the moment of damage (c) [13].

6 Conclusion

Results show that method of determination of interaction conditions between single roving and HPC matrix inspired by Dresden university not suitable for this type of reinforcement.

During the testing procedure of the own developed pull-out test method inspired by ACI standard, the composite textile reinforcement in the form of a single impregnated roving with surface treatment made with fine-grained silica sand reached the maximum values of tensile stress in the composite reinforcement corresponding to the results of tensile test presented in a previous research. That means that the surface treatment using fine-grained silica sand has no significant negative effect on the tensile strength of the impregnated roving. The impregnated individual rovings were in most cases damaged (in the case of impregnated rovings with smooth surface after significant pull-out) where they were in contact with the surrounding HPC prism due to the fact, that the reinforcement was pressed by the irregular contact area of the HPC during the process of reinforcement activation. The fibers near the surface of the textile reinforcement were therefore subjected to higher tensile stress, which lead to the weakening of the reinforcement and subsequent breaking of the roving in this area. Epoxy resin impregnation of the individual rovings however provides sufficient protection of AR-glass fibers in HPC matrix from premature damage for both smooth and modified reinforcement. The HPC part of tested specimens showed no signs of damage [5].

The difference between specimens with and without surface treatment is also clearly visible. The curves representing typical samples with smooth surfaces show a rapid pull-out of the reinforcement from the part of the HPC sample with higher pull-out values and lower corresponding force. After activation of the reinforcement in its full length, there is a very slow increase in force during the loading process due to poor interaction of both materials. This result signifies the need of large anchorage length of the smooth composite reinforcement required for the load transfer in the actual TRC element. The curves representing typical samples with surface modification provide much better results with higher contact stiffness. Grains of fine silica sand allow almost no slipping due to the high surface roughness [5].

The contact area of the reinforcement and cementitious matrix is constant in this method, due to the composite reinforcement passing completely trough the HPC prism. The pull-out is measured by a potentiometer placed on the free end of the reinforcement protruding from the HPC prism which ensures activation of the reinforcement in its whole length [5].

Textile reinforcement with surface treatment provides significantly better results regarding the crack formation and development as was also demonstrated by flexural bending test performed on small slabs using different variants and amounts of composite textile reinforcement. Better bonding conditions lead to a very short anchorage length for reinforcement activation without a significant loss of force due to the loading process controlled by constant increment of displacement. The ultimate bending strength was also a little higher. The most visible difference in the results is at

the beginning of the curve during the process of reinforcement activation in the case of 2x10 impregnated rovings with smooth surface and with surface treatment. The surface treatment is therefore very effective and can also have economic benefits by saving reinforcement material [5].

It is also obvious from the presented figures that with a higher amount of textile reinforcement with relatively low E modulus a bending behavior similar to that of elements made of traditional materials and with traditional diameters of reinforcement can be achieved. This means that after the first initiation of cracks, there is no massive opening of cracks. This effect was achieved with a roving material made of alkali-resistant glass, which has a modulus of elasticity slightly higher than the HPC used. After impregnation with epoxy resin, the composite reinforcement as a whole even has a similar modulus of elasticity. It explains why such a large amount of composite reinforcement was needed to achieve those results during the bending test [5].

In this work, the author dealt only with roving from glass for a better understanding of the issue and a because of large amount of measured data and material options. Later, this procedure and assumptions were repeated in the final works of Jiří Žalský. He dealt with the same problem for carbon impregnated roving, respectively according to the defined procedure in this thesis and under the supervision of the author of this thesis he repeated the procedure for carbon roving with fewer variants of reinforcement and came to the same conclusions [35]–[37]. These results also confirm the correctness and suitability of the chosen procedure for impregnated roving.

It is also important to mention the pitfalls of the solution. Roving impregnated by epoxy resin and essentially perfectly homogenized is used in the HPC matrix to 100% of its loading capacity potential. The positive effect of the surface treatment was also demonstrated and proved. In the plot diagram, however, the behavior of the reinforcement is ideally elastic until the moment of failure. This means that the reinforcement breaks suddenly without much warning, without any plastic deformation. This is a fragile way of breaking with no ductility. Due to the fact that thin specimens were used and that the elastic elongation of the used reinforcement is large, extreme deflections occur before the specimens collapse, which warn themselves. it would be good, and I recommend continue focusing to this issue - ductility. The solution can be for example hybrid reinforcement, where an advantageous combination of more materials occurs. This solution was already outlined in the bachelor's thesis of Eliška Kafková in 2021 [38], which was conducted under the supervision of the author of this thesis. The combination of homogenized carbon technical textiles with surface treatment using silica fine grain sand and various dispersed fibers was tested and excellent results were achieved in terms of load-bearing capacity and also in terms of ductile behavior.

List of Figures

List of Tables

References

[1] T. Vlach, M. Novotná, C. Fiala, L. Laiblová, and P. Hájek, "Cohesion of Composite Reinforcement Produced from Rovings with High Performance Concrete," *Appl. Mech. Mater.*, vol. 732, pp. 397–402, 2015, doi: 10.4028/www.scientific.net/AMM.732.397.

[2] T. Vlach, A. Chira, L. Laiblová, C. Fiala, M. Novotná, and P. Hájek, "Numerical Simulation of Cohesion Influence of Textile Reinforcement on Bending Performance of Plates Prepared from High Performance Concrete (HPC)," *Adv. Mater. Res.*, no. 1106, 2015.

[3] "Handbook of Technical Textiles - 1st Edition." https://www.elsevier.com/books/handbook-of-technical-textiles/horrocks/978-1-85573-385-5 (accessed Aug. 31, 2017).

[4] P.-C. Aïtcin, *High Performance Concrete*. CRC Press, 2011.

[5] T. Vlach, J. Řepka, J. Hájek, R. Fürst, Z. Jirkalová, and P. Hájek, "COHESION TEST OF A SINGLE IMPREGNATED AR-GLASS ROVING IN HIGH-PERFORMANCE CONCRETE," *Staveb. Obz. - Civ. Eng. J.*, vol. 29, no. 03, pp. 358–369, 2020, doi: 10.14311/CEJ.2020.03.0032.

[6] Brameshuber, *Report rep036 : Textile Reinforced Concrete - State-of-the-Art Report of RILEM TC 201-TRC> RILEM*. Germany: RILEM, 2006. Accessed: Feb. 25, 2017. [Online]. Available: http://rilem.net/gene/main.php?base=500219&id_publication=100

[7] P. .R and A. Muthadhi, "Structure and Mechanical Properties of Textile Reinforced Concrete: Review," vol. 7, pp. 1–12, Jul. 2021.

[8] N. Williams Portal, I. Fernandez Perez, L. Nyholm Thrane, and K. Lundgren, "Pull-out of textile reinforcement in concrete," *Constr. Build. Mater.*, vol. 71, pp. 63–71, Nov. 2014, doi: 10.1016/j.conbuildmat.2014.08.014.

[9] M. Krüger, "Vorgespannter textilbewehrter Beton," *Prestressed textile reinforced concrete*, 2004, doi: http://dx.doi.org/10.18419/opus-192.

[10] E. Lorenz and R. Ortlepp, "Bond Behavior of Textile Reinforcements - Development of a Pull-Out Test and Modeling of the Respective Bond versus Slip Relation," in *High Performance Fiber Reinforced Cement Composites 6*, G. J. Parra-Montesinos, H. W. Reinhardt, and A. E. Naaman, Eds. Springer Netherlands, 2012, pp. 479–486. Accessed: Mar. 17, 2017. [Online]. Available: http://link.springer.com/chapter/10.1007/978-94-007-2436-5_58

[11] B. Banholzer, "Bond behaviour of a multi-filament yarn embedded in a cementitious matrix," Bibliothek der RWTH Aachen, 2004. Accessed: Sep. 06, 2017. [Online]. Available: http://sylvester.bth.rwth-aachen.de/dissertationen/2005/028/

[12] T. Vlach, L. Laiblová, J. Řepka, Z. Jirkalová, and P. Hájek, "Experimental Verification of Impregnated Textile Reinforcement Splicing by Overlapping," *Acta Polytech. CTU Proc.*, vol. 22, pp. 128–132, 2019.

[13] T. Vlach, J. Řepka, T. Blažek, Z. Jirkalová, and P. Hájek, "Subtle cantilever concrete bench with shaped plate," *AIP Conf. Proc.*, vol. 2210, no. 1, p. 020028, Feb. 2020, doi: 10.1063/5.0000387.

[14] M. Kynclova, "Environmentally effective waffle floor structures from fibre concrete," presented at the International PhD Symposium in Civil Engineering, Technical University of Denmark, Lyngby, 2010.

[15]T. Vlach, P. Hájek, C. Fiala, L. Laiblová, J. Řepka, and P. Kokeš, "Waffle Facade Elements from Textile Reinforced High Performance Concrete," *Proc. HiPerMat 2016 - 4th Int. Symp. Ultra-High Perform. Concr. High Perform. Constr. Mater.*, vol. 2016, p. 10.

[16]C. Fiala *et al.*, "Construction and Static Loading Tests of Experimental Subtle Frame from High Performance Concrete for Energy Efficient Buildings," *Solid State Phenom.*, vol. 259, pp. 275–279, 2017, doi: 10.4028/www.scientific.net/SSP.259.275.

[17]A. Chira, A. Kumar, T. Vlach, L. Laiblová, and P. Hajek, "Textile-reinforced concrete facade panels with rigid foam core prisms," *J. Sandw. Struct. Mater.*, vol. 18, no. 2, pp. 200–214, Mar. 2016, doi: 10.1177/1099636215613488.

[18]A. Chira, A. Kumar, T. Vlach, L. Laiblová, A. S. Škapin, and P. Hájek, "Property improvements of alkali resistant glass fibres/epoxy composite with nanosilica for textile reinforced concrete applications," *Mater. Des.*, vol. 89, pp. 146–155, Jan. 2016, doi: 10.1016/j.matdes.2015.09.122.

[19]T. Vlach, L. Laiblová, and P. Hájek, "Influence of Different Fillers in Polymer Matrix of Single Roving on the Tensile Properties," *Key Eng. Mater.*, vol. 731, pp. 86–91, 2017, doi: 10.4028/www.scientific.net/KEM.731.86.

[20]R. Rypl, R. Chudoba, U. Mörschel, S. E. Stapleton, T. Gries, and G. Sommer, "A novel tensile test device for effective testing of high-modulus multi-filament yarns," *J. Ind. Text.*, vol. 44, no. 6, pp. 934–947, 2015.

[21]T. Vlach, L. Laiblova, M. Zenisek, P. Kokes, and P. Hajek, "Comparison of two approaches for the tensile test of single roving in polymer matrix," presented at the EAN 2016 - 54th International Conference on Experimental Stress Analysis, 2016.

[22]T. Vlach, M. Novotná, C. Fiala, L. Laiblová, and P. Hájek, "Cohesion of Composite Reinforcement Produced from Rovings with High Performance Concrete," *Appl. Mech. Mater.*, vol. 732, pp. 397–402, 2015, doi: 10.4028/www.scientific.net/AMM.732.397.

[23]T. Pavlů and M. Šefflová, "The Static and the Dynamic Modulus of Elasticity of Recycled Aggregate Concrete," *Adv. Mater. Res.*, vol. 1054, pp. 221–226, 2014, doi: 10.4028/www.scientific.net/AMR.1054.221.

[24]P. Cikrle and V. Bílek, "Modulus of elasticity of high strength concretes," *Beton TKS*, vol. 5, pp. 40–44, 2010.

[25]T. Vlach *et al.*, "Comparison of Different Methods for Determination of Modulus of Elasticity of Composite Reinforcement Produced from Roving," *Adv. Mater. Res.*, no. 1054, 2014, Accessed: Feb. 27, 2017. [Online]. Available: https://www.researchgate.net/profile/Chira_Alexandru/publication/269275747_Comparison_of_Different_Methods_for_Determination_of_Modulus_of_Elasticity_of_Composite_Reinforcement_Produced_from_Roving/links/548ec3ca0cf225bf66a628e8.pdf

[26]A. Kumar *et al.*, "Nanocoating on alkali-resistant glass fibers by octadecyltrichlorosilane to improve the mechanical strength of fibers and fibers/epoxy composites," *Text. Res. J.*, p. 0040517517693977, Feb. 2017, doi: 10.1177/0040517517693977.

[27]R. Chudoba, M. Vořechovský, V. Eckers, and T. Gries, "Effect of Twist, Fineness, Loading Rate and Length on Tensile Behavior of Multifilament Yarns (A Multivariate Study)," *Text. Res. J.*, vol. 77, no. 11, pp. 880–891, Nov. 2007, doi: 10.1177/0040517507081280.

[28]T. Bittner, P. Bouška, M. Kostelecká, and M. Vokáč, "Experimental Investigation of Mechanical Properties of Textile Glass Reinforcement," in *Applied Mechanics and Materials*, 2015, vol. 732, pp. 45–48. Accessed: Feb. 27, 2017. [Online]. Available: http://www.scientific.net/AMM.732.45

[29]T. Vlach, L. Laiblová, M. Ženíšek, A. Chira, A. Kumar, and P. Hájek, "The Effect of Surface Treatments of Textile Reinforcement on Mechanical Parameters of HPC Facade Elements," in *Key Engineering Materials*, 2016, vol. 677, pp. 203–206. Accessed: Feb. 27, 2017. [Online]. Available: http://www.scientific.net/KEM.677.203

[30]L. Laiblová, T. Vlach, M. Ženíšek, A. Kumar, and P. Hájek, "Comparison of Different Types of Glass Reinforcement for HPC Facade Elements from Mechanical and Economical Aspects," *Key Eng. Mater.*, vol. 722, pp. 286–291, 2017, doi: 10.4028/www.scientific.net/KEM.722.286.

[31]T. Vlach, L. Laiblová, M. Ženíšek, J. Řepka, and P. Hájek, "Soft Insert for Support Modeling of Slightly Textile Reinforced Concrete," *Key Eng. Mater.*, vol. 760, pp. 158–163, 2018, doi: 10.4028/www.scientific.net/KEM.760.158.

[32]V. Cervenka, J. Cervenka, and R. Pukl, "ATENA — A tool for engineering analysis of fracture in concrete," *Sadhana*, vol. 27, no. 4, pp. 485–492, Aug. 2002, doi: 10.1007/BF02706996.

[33]N. Hrebenkach, "ATENA Program Documentation Part," p. 350.

[34]T. Vlach, A. Chira, L. Laiblová, C. Fiala, M. Novotná, and P. Hájek, "Numerical Simulation of Cohesion Influence of Textile Reinforcement on Bending Performance of Plates Prepared from High Performance Concrete (HPC)," *Adv. Mater. Res.*, no. 1106, Art. no. 1106, 2015.

[35]J. Žalský, "Rámový roh z textilního betonu," Feb. 2020, Accessed: Aug. 13, 2021. [Online]. Available: https://dspace.cvut.cz/handle/10467/86787

[36]J. Žalský, T. Vlach, L. Laiblová, Z. Jirkalová, J. Řepka, and P. Hájek, "Numerical Analysis of Rigid Frame Joint with Textile Carbon Reinforcement," *Solid State Phenom.*, vol. 292, pp. 159–163, 2019, doi: 10.4028/www.scientific.net/SSP.292.159.

[37]Ž. Jiří, "Numerická analýza rámového rohu vyztuženého textilní uhlíkovou výztuží," Jun. 2018, Accessed: Aug. 13, 2021. [Online]. Available: https://dspace.cvut.cz/handle/10467/78200

[38]K. Eliška, "vliv r\uuzných výztužných vláken na zp\uusob porušení textilního betonu," B.S. thesis, České vysoké učení technické v Praze. Vypočetní a informační centrum., 2021.